THERMAL MODELLING OF GAS METAL ARC WELDING USING FINITE ELEMENT ANALYSIS

Allan J. Smailes
B.E. (Mech) Hons, Adelaide, 1992

Department of Mechanical Engineering
The University of Adelaide
South Australia 5005

Submitted for the degree of Master of Engineering Science, January 1999

CONTENTS

LIST OF TABLES

LIST OF FIGURES

THERMAL MODELLING OF GAS METAL ARC WELDING USING FINITE ELEMENT ANALYSIS

ABSTRACT

Finite element models are produced to predict how a weld piece changes thermally in response to gas metal arc welds. The weld is represented by a heat source applied to the model. The modelling regime selected for this work is 3-dimensional (3D), quasi-steady-state (QSS) and conduction based. The QSS assumption is justified as a useful and valid simplification for the welds modelled in this work. Conduction based analysis is a further simplification, bringing the computational complexity of the models down to a level that is industrially attractive. It acts on the very significant simplification that the flow of molten metal within the weld pool is not modelled and heat transfer within the weld piece is governed purely by conduction. The transfer of heat that would have occurred in the flow of molten metal is compensated for in the definition of the heat source and enhancement of the thermal conductivity. Developing heat sources that can do this effectively is a major objective of this thesis. The emerging idea of using a "split heat source" was defined and adopted. In the split heat source system, the heat is divided into two parts, attributed to the arc and the droplet respectively. The arc component is applied at or near the weld surface and the droplet heat at a depth to reflect the dominant downward flow pattern. Predicted weld fusion profiles using this type of heat source are shown to be extremely effective over a range of welding conditions. The deformation of the weld pool surface is shown to significantly affect the distribution of heat from the arc. It alters the commonly accepted Gaussian form of the arc heat delivering considerably more heat away from the centre line of the welding electrode. This has explained under prediction of pool width observed in some models. The deformed pool surface heat distribution appears to be a significant oversight in almost all observed weld models and it is recommended that it be used as a standard practice.

The weld models are applied to V-joint and T-joint weld preparations, demonstrating the effectiveness of the modelling approach and the split heat source. Weaving welds are modelled perhaps for the first time, using a split heat source integrated over one weld cycle which shows much promise. The novel application of QSS in modelling multi-pass and preheat models was also developed and tested against experiment.

STATEMENT OF ORIGINALITY

The following thesis contains no material which has been accepted for the award of any other degree or diploma in any university or other tertiary institution, and to the best of my knowledge, contains no material previously published or written by another person, except where due reference has been made in the text.

I give consent for this copy of my thesis, when deposited in the University Library, to be made available for loan and photocopying.

Allan John Smailes, January 1999

ACKNOWLEDGMENTS

I gratefully acknowledge the Cooperative Research Centre for Materials Welding and Joining for making this work possible through their generous provision of research funding.

The staff of the CSIRO division of Manufacturing Science and Technology have been helpful in every way, providing the research facilities and technical support and making the environment friendly, enjoyable and effective.

I thank both my supervisors, Dr. Mike Painter and Dr. M. Wahab, for their guidance, encouragement, and of course, patience. Also for sharing their wealth of experience with me in the many hours of discussion which sparked ideas and gave direction to this work.

I gratefully acknowledge the University of Adelaide and the staff who work so hard to provide such a high quality of service and education.

I would like to thank all the lads who persistently interrogated me on the progress of my thesis and offered me bribes and rewards in a vain attempt to help speed things along.

Thanks to my family and to God for their unconditional support & encouragement.

Chapter 1

INTRODUCTION

1.1 OBJECTIVES

The core techniques of computational weld mechanics: heat transfer, computational fluid dynamics, stress analysis are available but developing techniques of applying these to make industrially useful welding models remains a significant challenge with great potential benefit. This thesis aims to establish the current state of numerical weld modelling and extend this work to develop efficient and effective thermal finite element models for real and useful welding applications.

The objectives of this thesis are to:

- Review the status of thermal modelling of gas metal arc welding of steel.
- Optimise heat sources, which represent the welding heat input, for V-joint and T-joint weld configurations. This is in contrast to most work to date which has focused on "bead on plate" models, or taken heat sources developed for bead on plate models and applied them to joints for which they are not necessarily optimal.
- Previous work has generally produced models tuned and applicable to only one welding condition. An objective of this work is to tie the heat source to the primary welding parameters so it is valid over a range of conditions.
- Develop efficient models using the above heat sources and weld configurations to predict the thermal output.
- Develop the model's applicability to multi-pass and preheat welding. Transient multi-pass models are common, but almost exclusively 2-dimensional, due to high costs in analysis time. This work aims to demonstrate the suitability of 3-dimensional quasi-steady-state models for multi-pass welds.
- Model "weave welding" which is an area for which no previous research work has been observed.
- Experimentally verify the generated models.

1.2 WHY THERMAL MODELLING OF GAS METAL ARC WELDING?

Welding is a joining process that is being applied to an ever widening range of fabrication activities. From underwater to outer space; in transport, manufacturing, construction and mining, pipelines and tanks, welding is essential. According to Jeffus (1993), Shielded Metal Arc Welding (SMAW) is the most common method of joining metals and thus is a logical choice for the focus of this work. The specific type of SMAW to be considered is Gas Metal Arc Welding (GMAW) in which shielding is achieved by the flow of inert gas around the arc and molten metal to prevent reaction with oxygen and nitrogen in the air.

Thermal problems which are associated with GMAW are: induced residual stress and distortion; and altered microstructural properties which stem from the intense localised heat applied to the structure at the weld location. Mathematical analysis of welding to predict these effects is referred to as Computational Weld Mechanics (CWM). Thermal analysis seeks to calculate the changing temperatures during welding which is key input in CWM as indicated in Figure 1.1. Thus thermal modelling is a vital area of research for mathematical analysis of welding.

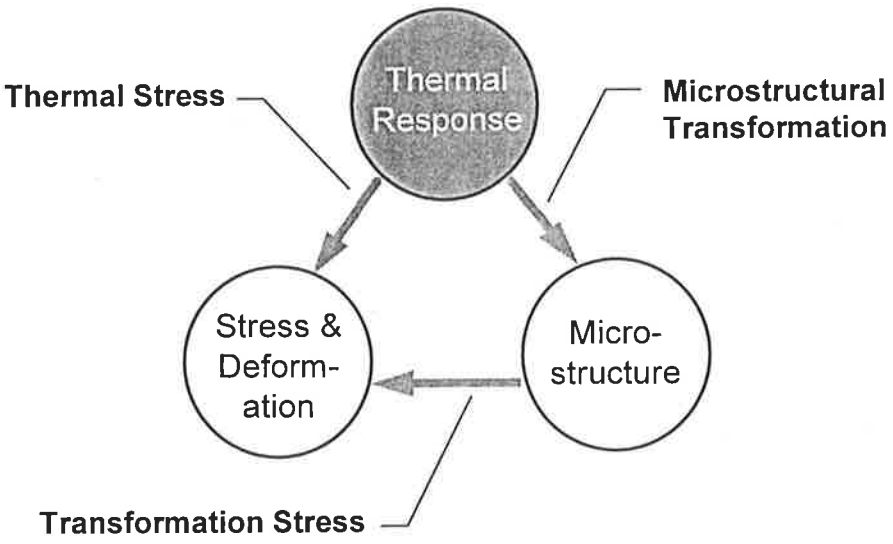

Figure 1.1 Weld thermal response as primary input for CWM (after Karlsson 1986).

Note that there is a minor feed back opposing each of the arrows in Figure 1.1 and this will be discussed later in Section 1.4.3.

Thermal modelling can yield the following information, either as direct output from the model, or using the thermal results for further calculations as shown in the flow diagram in Figure 1.1:

- Thermal field prediction - gives the weld bead width and penetration from the fusion isotherm. Also, the peak temperature at any point in the weld piece can be monitored as this is often a design constraint.

- Microstructure prediction - this is useful because of its effect on the creep behaviour, fatigue crack initiation, and material toughness and yield strength. Microstructure predictions can be used to determine suitable weld material, electrode material, and pre and post-heat treatment of welded parts.

- Hardness prediction – can be derived using the material's carbon equivalent and the predicted cooling curve.

- Distortion prediction - both residual and during welding can be found. This is especially relevant when welding large structures such as in the ship and submarine building industries. Modelling is particularly suited for investigating different welding sequences which can be used to minimise the distortion.

- Residual stress prediction - peak values can be monitored; also, the level of prestress that will negate the welding residual stress can be calculated (eg. Michaleris *et al.* 1997).

A further value of modelling the welding process is that insight has been gained into the processes and driving forces within the arc and pool, which ultimately determine the quality of the weld. The models give a glimpse of the vigorous flow fields within the molten weld pool which are currently impossible to visualise experimentally.

Doumanidis (1992) shows how modelling can be used to give real time indication of weld bead penetration for control purposes. Ohji *et al.* (1990) in a series of papers have shown how a model can be used "in-process", with continuous feed back, to find the welding parameters which achieve a desired weld width. The model is impressive in quickly finding and modifying welding parameters to achieve and maintain the specified width.

Radaj (1995) has conducted a review of the potential of numerical analysis of welding in the design process. Radaj lists potential applications of numerical analysis for metallurgists, design engineers and production engineers. He concludes that there is clear potential for numerical welding analysis to become integrated into the development process. Radaj also includes examples from Deutsche Aerospace and Mercedes Benz for potential applications of numerical weld modelling.

Closer to home, the Gas Transmission industry in Australia is funding the CSIRO to conduct modelling research to improve in service welding procedures. The potential value to the industry is estimated by Venton (1997) at 2 to 4 million dollars between 1998 and 2002.

It is anticipated that as techniques of modelling fusion welding processes are further refined, software improved and industry becomes aware of computational modelling in GMAW, many new areas of application will be discovered as needs arise.

1.2.1 MODELLING VERSUS EXPERIMENTATION

The results of CWM are aimed at optimising gas metal arc welding processes in terms of energy, time, strength, distortion, or whatever the constraints on the process may be. In order to gauge the value of modelling, its cost must be compared against the alternative of using experimentation or regression information. In many cases the cost of computational modelling is comparable with or less than experimentation. Table 1.1 shows the three main areas of weld analysis and lists whether experimentation or modelling is more cost effective. Please note that although it is generally more cost effective to do an experimental analysis for finding microstructural changes in welding, computational models have still been used effectively to solve real problems as will be shown in the literature review.

Computational modelling is most useful in terms of stress analysis since to determine stresses experimentally is complicated and costly. Problems in which development cost is high with a very small production volume to offset it are well suited to modelling. There are cases when it is virtually impossible to develop a welding procedure experimentally, for complex structures for example, or for large scale projects such as ship building. These structures require trial and error welding based on engineers' experience and may often result in the need for rework; in fact, Castener (1996) claims this can potentially cost as much as 5% of the total fabrication expense. This is a very significant amount of money which could be reduced by computational weld modelling.

Most Expedient Means of Analysis:	
Weld Bead / HAZ	Experimental / Modelling
Microstructure	Experimental
Stress & Distortion Simple Structure Complex Structure	 Experimental / Modelling Modelling

Table 1.1 Most cost effective means of weld analysis.

Assuming that there is hardware and software available for computational modelling, the cost of modelling consists of time to set up the model and time to solve the model. The solution time may be an insignificant cost if the result is not required immediately because the model can be set to solve after hours when the computer would otherwise be dormant. Welding experimentation on the other hand, generally requires human input for the duration of the experimentation period. Having a computer model of the welded component is useful in the development phase of product design: it is relatively quick to make modifications to the model as the product is developed and modified. If the designer were dependant on experimentation, a complete new set of experiments may be required for each change to the product. A similar argument applies to developing new welding processes such as the dual arc welding process of Murthy *et al.* (1994) in which there are many parameters to be modified and optimised.

There are many researchers who have done a great deal of work in developing regression formulae for weld analysis, however these are always limited in their applicability to the specific range of conditions for which the equations were generated. For example Chandel (1988) derived a set of regression equations for GMAW. These equations calculated the weld fusion and reinforcement dimensions, for a range of voltage, current, welding speed, "stick out" and electrode diameter. The limitations are that the equations are only valid for the four gas types tested, for the specific plate and electrode material, for the given plate thickness of 19 mm, for the given joint preparation namely bead on plate, welding process and welding angle, number of passes and preheat. If the complete range of possibilities were to be included in the analysis it would be an impossible task. In addition, many more features may be desired than the fusion and reinforcement dimensions such as temperature profiles at various locations and the resulting microstructure and stresses. This again would be impossible with a regression analysis yet the flexibility of a computer model allows these specifics to be accounted for.

1.3 THE PHYSICAL WELDING PROCESS

It is essential to have an understanding of the physical processes occurring during GMAW so that models can be developed which simulate reality. Knowing what impact the physical processes have on the weld pool can indicate which aspects are important to incorporate into the model.

1.3.1 GAS METAL ARC WELDING EQUIPMENT

A representation of the equipment used in GMAW based on Lancaster (1992) is given in Figure 1.2 (a). Figure 1.2 (b) shows the welding torch and arc. A potential difference is established between the weld piece and the welding wire. This induces the arc; a flow of current which jumps across the gap by ionising the gas. The gas flows from between the contact tube and the shield and has a second effect of shielding the weld piece from oxidising with the surrounding air. The contact tube is the point at which electric current is passed into the welding wire and it becomes part of the welding circuit. Hence, the "stick out" is the only part of the wire influenced by resistive heating. The welding controller can convert the power input into direct current with positive or negative electrode, or a pulsed current can be generated for use in the welding circuit. The rate of wire feed is automatically controlled to maintain the prescribed voltage.

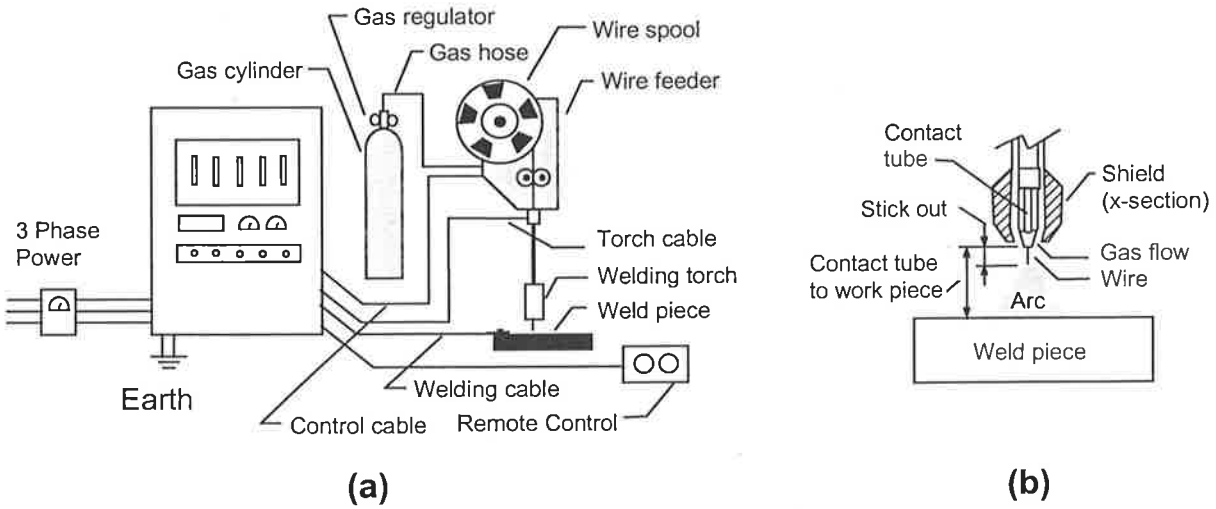

Figure 1.2 (a) Gas metal arc welding equipment **(b)** Welding torch and arc.

1.3.2 METAL TRANSFER

The melting of the electrode wire and subsequent flow of molten material from the electrode tip to the work piece is termed metal transfer. Depending on the welding conditions, different modes of metal transfer are observed in GMAW. The International Institute of Welding (IIW) designates two types of transfer for GMAW, namely bridging transfer and free flight transfer. These transfer modes together with their subclasses are summarised in Figure 1.3.

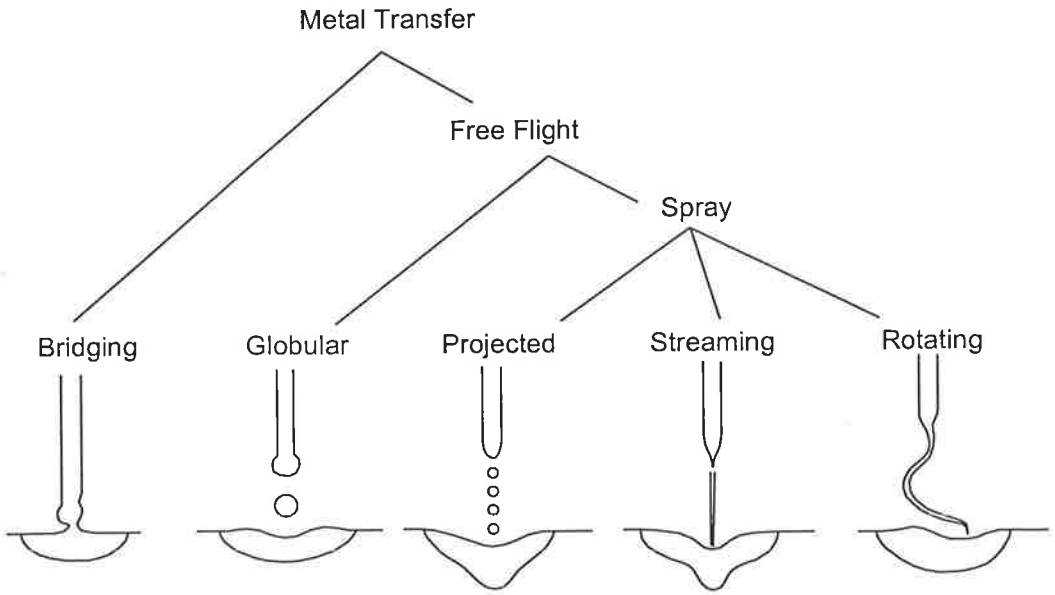

Figure 1.3 Metal transfer modes for GMAW with argon rich gas.

In bridging transfer, the molten droplet at the end of the electrode wire does not detach but is fed into contact with the molten pool surface. Electromagnetic and surface tension forces then cause the droplet to detach. In free flight transfer the droplet detaches before contact is made with the pool surface. Various modes of free flight transfer can be observed, depending predominantly on the current. At low current, elongated droplets which are slightly larger than the wire diameter form. They fall under their own weight into the pool at a rate of up to about 10 drops per second. This is termed globular transfer. At higher currents and electromagnetic intensity, the droplets reduce in size and no longer fall under their own weight, but are projected across the arc. This is the first subclass of spray transfer and is characterised by a pronounced increase in droplet frequency and a decrease in droplet size. Lesnewich (1958) reported the change to occur at about 260 A with droplet frequency changing from about 15/second to 240/second for Argon gas and 1.6 mm mild steel electrode wire. It is indicated that for the same weld with 1.2 mm diameter wire the transition would occur at about 200 A. Lesnewich also showed that there is a marked drop in the

volume of the droplets at transition. Projected transfer changes to streaming transfer at still higher currents where the electrode wire becomes tapered with essentially a continuous stream of metal flowing from the end of the taper. Streaming transfer has an affect on the resulting weld pool and fusion profile. Essers & Walter (1981) deemed streaming transfer was accountable for what is known as finger penetration which becomes apparent in GMAW at higher currents. This term describes the shape of the weld pool whereby the usual semicircular weld pool has a finger of molten material penetrating to a deeper level. This is shown in the weld pools in Figure 1.3. At extremely high currents the metal transfer mode changes again as electromagnetic effects cause the stream to rotate.

The type of gas can have a significant influence on the mode of transfer. Rhee & Kannatey-Asibu (1991) showed that for either helium or carbon dioxide shielding gas the transfer mode remains globular despite increases in current.

The mode of transfer can be controlled by using a pulsed power source. A base current heats and melts the electrode wire forming a drop. A pulse of high current elongates the drop and causes it to detach from the electrode with an acceleration towards the weld pool. In some cases the base current may be very low, or even zero so some or all of the melting of the droplet may be done by the pulse current. Pulsed GMAW has the advantages of reduced spatter loss and improved productivity (lower heat input for the same burn off rate), maintaining projected transfer and avoiding globular transfer at low currents. In addition, pulsed welding gives greater control over penetration and so it can be used for joining thin plates or tubes where high precision is needed.

1.3.3 INTERACTION OF PHYSICAL PROCESSES

There are many physical processes which interact during GMAW to generate the final resulting temperature field in the work piece. In order to develop meaningful models, it is first necessary to know what physical processes are actually occurring. These are summarised in Figure 1.4 and outlined below.

Once the arc is struck there are several processes which begin. The electrode wire is heated by its resistance to the flow of current in the wire between the contact tube and the arc. The shielding gas ionises and becomes a very hot plasma. The ionisation temperature depends on the gas type and according to Lancaster (1980) is about 10,000 to 15,000 K for Argon gas. Hsu *et al.* (1983) experimentally determined the arc temperature for GTA welding with Argon gas to be about 20,000 K near the cathode and range between 14,000

5) Linearising the problem - by considering the material properties as constant a linear mathematical model results which can be analytically solved for simple weld shapes and boundary conditions.

The development of welding models began at the base of the above list in the late 1930s. Now, sixty years on, complex flow models incorporating most of the physical processes are being built and used.

1.4.1 CONDUCTION THERMAL MODELS

As stated above, these models do not incorporate the flow of the molten pool and the associated driving forces. The weld piece is considered totally solid with internal heat transfer governed purely by conduction; the arc is represented as a moving heat source. This will be referred to as conduction based modelling. The theory of moving heat sources appears to have been developed by Wilson (1904) but was not applied to welding thermal analyses until the 1930s by Rosenthal. (Rosenthal (1941) references his initial work back to 1935).

The time dependant equation for conduction in an isotropic material with a moving heat source is given by Equation 1.1

$$\rho C_p \frac{\partial T}{\partial t} = \frac{\partial}{\partial x}\left(k \frac{\partial T}{\partial x} \right) + \frac{\partial}{\partial y}\left(k \frac{\partial T}{\partial y} \right) + \frac{\partial}{\partial z}\left(k \frac{\partial T}{\partial z} \right) + q_g \qquad \textbf{(1.1)}$$

In this equation, T is the temperature at any (x,y,z) location, t is time, ρ is the material density, C_p is the specific heat of the material at constant pressure, k is the material's thermal conductivity, and q_g is the heat generated per unit volume. The boundary conditions consist of radiative and convective heat losses and the moving heat source represents the weld heat input. The initial condition is the temperature of the material before the weld heat source is applied.

1.4.1.1 Modelling Developments

The original work by Rosenthal was based on analytically solving Equation 1.1 for a simple point or instantaneous line heat source. To achieve this, the following simplifications were made:

1) The material properties were constant rather than temperature dependant. This means that some form of average material property for the range of temperatures must be found. This can amount to a significant approximation since the latent heat of phase changes will not be captured; also, the effective conductivity changes considerably once the material exceeds the melting temperature and this cannot be accounted for.

2) The equation was made independent of the time variable. This was done by considering the heat source as stationary with the plate moving below. So, cold material passes below the arc, is heated and then the heat diffuses. If the plate is infinitely long then an effective steady state condition results, referred to in literature as quasi-steady-state (QSS), where at any coordinate *relative to the heat source* the temperature does not change. It is not steady state in the true sense of the word because *relative to the plate*, the temperature at a particular point does in fact change. If v is the velocity of the arc then the velocity of the plate below a stationary arc is -*v*. Hence $\partial x/\partial t = -v$ and this can be rearranged and substituted into Equation 1.1 to get rid of the ∂t term. Figure 1.5 shows this arrangement. In addition, this second simplification requires that the velocity and the heat source remain constant.

3) The heat source is a simple point. This causes large errors close to the heat source where the temperature tends to infinity, but is an adequate approximation some distance from the arc.

4) The plate is semi-infinite with the heat source on a flat surface, neglecting any boundaries. This means that the weld bead reinforcement is not modelled and the radiative and convective heat losses are neglected.

With the above mentioned simplifications 1) and 2), Equation 1.1 becomes:

$$-v\rho C_p \frac{\partial T}{\partial x} = k\left(\frac{\partial^2 T}{\partial x^2} + \frac{\partial^2 T}{\partial y^2} + \frac{\partial^2 T}{\partial z^2}\right) \qquad \textbf{(1.2)}$$

and including simplifications 3) and 4) the solution to Equation 1.2 was found by Rosenthal to be:

$$T - T_0 = \frac{Q}{4\pi kR} \exp^{-\frac{v\rho C_p}{2k}(\xi + R)} \qquad \textbf{(1.3)}$$

Where T_0 is the initial temperature and T is the temperature at a point $R = (x^2+y^2+z^2)^{1/2}$ from the arc heat source Q. The arc heat source $Q = \eta IV$ where IV is the welding current times the voltage which gives the welding power and η is the arc efficiency of the welding process. Here $\xi = x_0-vt$, where x_o is the distance on the x-axis from the source at $t=0$. This solution for the thermal field gave the first predictions for pool dimensions and cooling times.

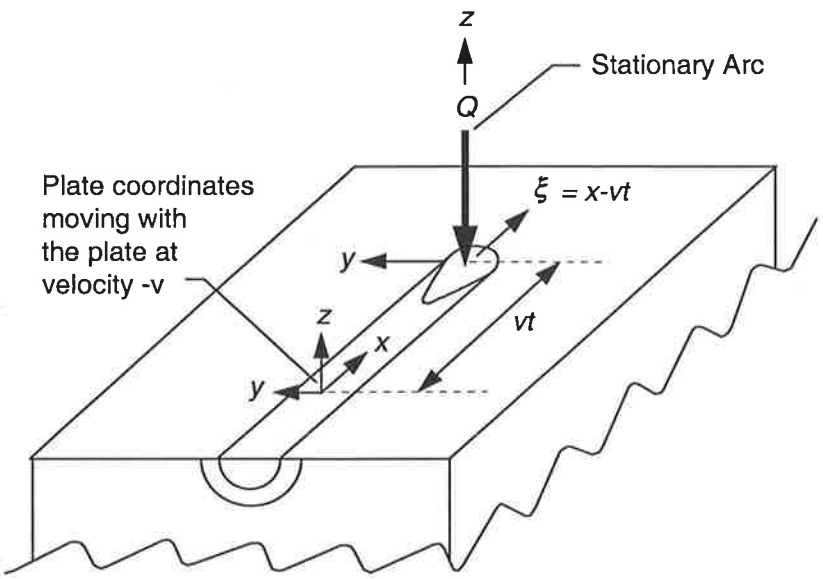

Figure 1.5 Rosenthal's QSS model.

Moore *et al.* (1985) investigated the significance of the various simplifications on predicted cooling times. It was found that constant thermal conductivity, lack of latent heat, and not modelling the weld reinforcement had the most negative effect on the predicted $T_{8/5}$ values ($T_{8/5}$ is a measure of the cooling rate and is the time it takes for the material to cool from 800°C to 500°C). Interestingly the heat source distribution did not have a significant effect on the cooling rate, however, it is clear that it does have a significant effect on the predicted temperature distribution close to the heat source, and therefore on predicted fusion zone shapes.

An obvious limitation of the above solution (Equation 1.3) is that few welding processes approximate to welding onto a plate of infinite thickness. When a plate has a finite thickness, the temperature will be somewhat higher below the arc because there is less material to conduct heat away. To model this effect, Rosenthal (1941), using the principle of superposition, introduced a series of fictitious heat sources to simulate a plate of finite thickness.

Over the following 30 years, modelling of welding revolved around application of the Rosenthal solution. Ohji (1994) presents some of the significant applications over that period such as Wells' (1952) equation relating the heat input to the weld bead width, and Christensen *et al.*'s (1965) cooling rate expression and calculations of fusion cross sectional area. With the development of computer technology and software in the 1970s, finite difference (FD) and finite element analysis (FEA) were established and employed to provide a new method of overcoming some of the short comings of the analytical methods. It should be noted that the appeal of the simplicity and instantaneous solution time for analytical models means that they are often still used in commercial software, and research work. For example the work of Kasuya *et al.* (1993) who used a complex distribution of point sources which were arbitrarily placed to match the results to experiment. Even more recently, Jeong & Cho (1997) used analytical methods quite successfully on a fillet weld by mapping the temperature distribution from a flat plate, using an energy equation. Other researchers such as Kumar *et al.* (1992) have investigated the idea of combining numerical and analytical methods in a single model, in an attempt to get the best of both worlds.

Early numerical work centred around FD analysis with work by Westby (1968), Pavelic (1969), Paley & Hibbert (1975). FEA gradually replaced FD and is almost exclusively used now due to its greater flexibility in dealing with variable part geometry. The first researchers using FE models were Hibbitt & Marcal (1973), Friedman (1975), Krutz & Segerlind (1978), Andersson (1978).

Most early numerical modelling work was done in two dimensions due to limitations of computer capabilities. This 2D approximation is based on a proposal by Friedman (1975) that if the arc is travelling at a reasonable speed, the amount of heat conducted parallel to the direction of the arc's travel will be negligible compared to that conducted perpendicular to the arc's travel. As a result, the analysis can be constrained to a 2 dimensional plane as shown in Figure 1.6. As the heat source passes through the plane, it adds heat which diffuses only within the plane as time progresses. The plate is considered to be in a QSS so that the temperature at any other plane in the plate is simply a time displacement of the analysed plane. The time displacement is $\Delta t=t-\Delta x/v$ and Δx is the distance (in the positive x direction) of the plane of interest from the analysed plane, and v is the velocity of the arc.

This work allowed inclusion of radiative and convective surface heat losses, temperature dependent material properties, complex heat source distributions, non infinite weld width and depth with the option of complex surface shapes - such as including the bead reinforcement.

Andersson (1978) worked with 2D transient models and showed the approximation was acceptable except at low welding speeds. He used a varied specific heat to account for latent heat and included the weld bead in the mesh.

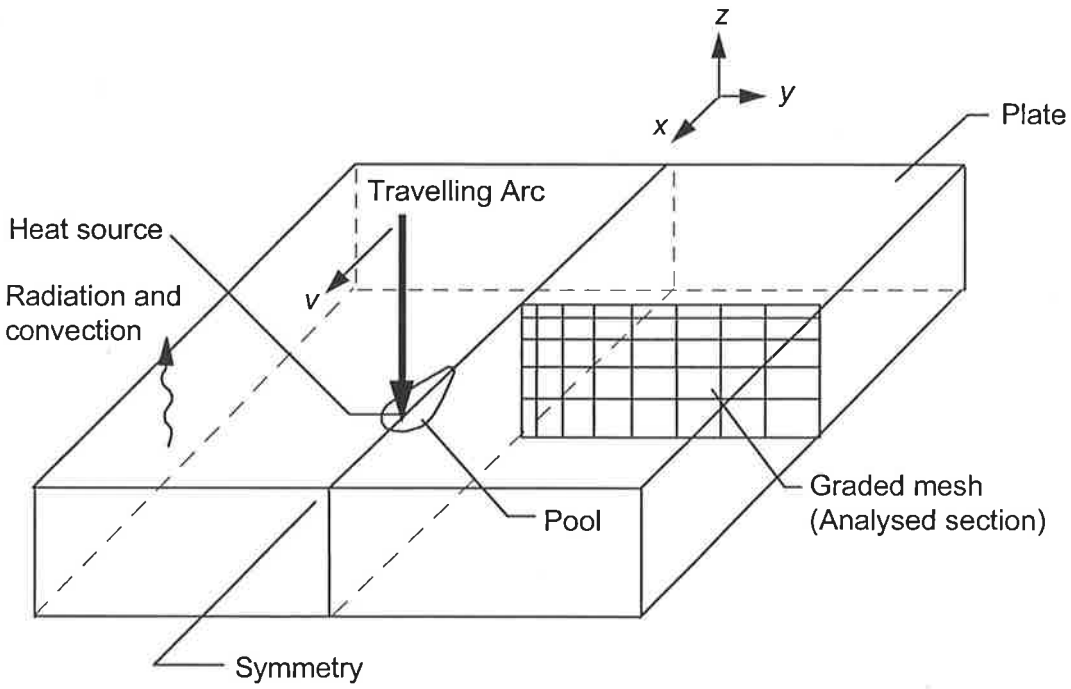

Figure 1.6 Friedman's Two Dimensional Transient FE Model.

Three dimensional models became common in the 1980s as computer technology enabled more rapid solution of the discretised equations. A few of the earliest three dimensional modellers were: Kou & Le (1983) with a QSS model of GTAW using finite difference analysis; Goldak *et al.* (1986) produced a transient model of the root pass of a girth weld and found the solution to be about 50 times more time consuming than the 2D model; Goldak *et al.* (September 1986) suggests a 3D transient mesh but which becomes 2D at a distance from the heat source where the gradient in the direction of arc travel is minimal; Tekriwal & Mazumder (1986) also generated one of the first 3D transient models, in this case of a V-joint weld; Mangonon *et al.* (1986) produced a three dimensional transient model for submerged arc welding; Na & Lee (1987) produced a 3D transient model for GTAW and reduced solution times by having a moving solution sub-domain.

The three dimensional models, although considerably more time consuming than 2D are clearly more realistic and provide good approximation of cross sectional fusion zone and heat affected zone for all welding speeds. Now in the 90s the computer potential for 3D

models is clear and there are a myriad of researchers using them. Many of these will be addressed in the following sections corresponding to the application of the 3D models.

1.4.1.2 Heat Source Developments

We have currently been discussing the development of conduction based modelling. A limitation of this kind of model is the fact that the flow of molten material within the weld pool is not calculated, even though it significantly affects the pool shape and heat distribution. The recognition of this has resulted in different techniques to compensate for the absence of fluid flow in the molten weld pool. This is achieved within the distribution of the heat source and by enhancing thermal conductivity.

As discussed above, the earliest models by Rosenthal treat the heat source as a point or line source, which is an obvious physical error since the heat applied to the weld piece is spread over an area below the arc. This caused problems with the temperature tending to infinity at the heat source location, and a lack of accuracy close to the heat source. Pavelic *et al.* (1969) were the first to propose a spatially distributed heat source, suggesting a Gaussian form of distribution. This is defined in Equation 1.4:

$$q(r) = q_0 \exp^{(-cr^2)} \tag{1.4}$$

where $q(r)$ is the heat flux at a radius, r from the source centre, q_0 is the maximum heat flux and C is an adjustable parameter which defines the spread of the heat source. The Gaussian form has experimental backing for a flat surface and is discussed in more detail in Section 3.2. Friedman (1975) applied Pavelic's Gaussian distribution to FEA producing results which were far better than Rosenthal's in the near weld region.

Eagar & Tsai (1983) used the same modelling assumptions as Rosenthal but used a Gaussian distribution. They showed a significant improvement to "near weld" solutions and also showed that the solutions tend to Rosenthal's in the "far weld". Goldak (1985) suggests that this "far weld" region would be areas where the temperature does not exceed 20% of the melting point.

Heat applied to the weld pool is not only distributed spatially on the surface, but also distributed within the pool volume by convective flow. Westby (1968) was first to apply a heat distributed within a volume, for a finite difference model while Paley & Hibbert (1975)

first included a volumetric heat source for FEA. These volumetric distributions were relatively arbitrary. Goldak *et al.* (1985) proposed a more defined distribution of heat within a volume by assuming the heat is maximum at the centre directly below the arc and decays in a Gaussian manner as the distance from the arc increases. This includes a decay in the depth of the material which is in contrast to Pavelic's heat source which is entirely constrained to the surface. The result is a distribution of heat flux in the shape of a semi-ellipsoid. Applying this source and checking against experimental results, Goldak found it necessary to define a different intensity and spread of heat flux in the leading and trailing halves of the heat source. This meant effectively the combination of two half semi-ellipsoids and hence it was named the Double Ellipsoidal heat source. It is shown in Figure 1.7 and mathematically discussed in Section 3.3. The heat source contains 6 tunable parameters which are used to tune the calculated thermal field to experimental results. Goldak demonstrated improved results using the double ellipsoidal heat source when compared with a surface Gaussian Heat source. This heat source has had a very significant impact on thermal modelling of welding and has been used extensively.

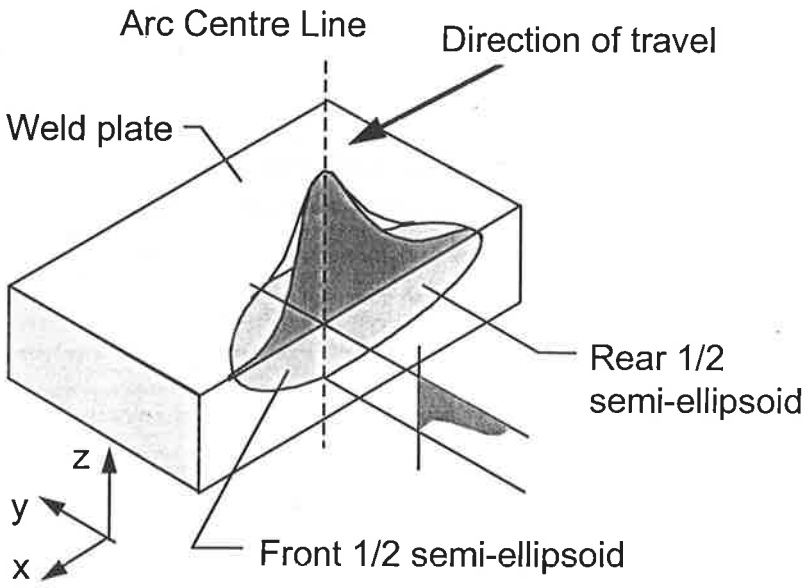

Figure 1.7 Goldak's Double Ellipsoidal Heat Source.

Goldak *et al.*'s 1985 work included an isotropic enhancement of about 4 times for the thermal conductivity of any material exceeding the melting point to account for increased conductivity in the liquid phase. Mahin *et al.* (1986) introduced the idea of anisotropically enhancing the thermal conductivity so as to produce either wider or deeper weld pool profiles. While the idea has good merit in reflecting the dominant flow pattern the enhancement was not

matched to flow, but proposed as an arbitrary means to match the model to experimental fusion profiles. Enhancement of the range of 5 to 10 times were examined.

1.4.1.3 Gas Metal Arc Welding Heat Source Models

The above heat sources were developed with GTAW in mind or without distinguishing the welding process other than by modifying the tunable parameters of the heat source. The fact that flow within the molten weld pool was shown to be significant was particularly emphasised in the modelling of GMAW. The models were unable to account for pool profiles observed in GMAW where it is now apparent that the impacting droplets in streaming transfer dominate the flow in the pool and result in finger penetration as discussed in Section 1.3.2. Literature reveals two approaches to incorporate this effect in conduction model heat sources so as *to distinguish them from a GTAW heat source definition.* These are:

(1) to split the total applied heat into a component applied by the arc and a component applied by the molten droplet;
(2) to anisotropically enhance the thermal conductivity to reflect the transfer of heat from the dominant flow pattern.

Articles which have heat sources developed specifically for GMAW will now be summarised in chronological order. More specific details of some of them will be given in Chapter 3 on heat sources. Allum & Quintino (1985) proposed a split heat source model with two point sources for the arc and droplet as shown in Figure 1.8. This source was qualitatively proposed but has not actually been applied to weld modelling.

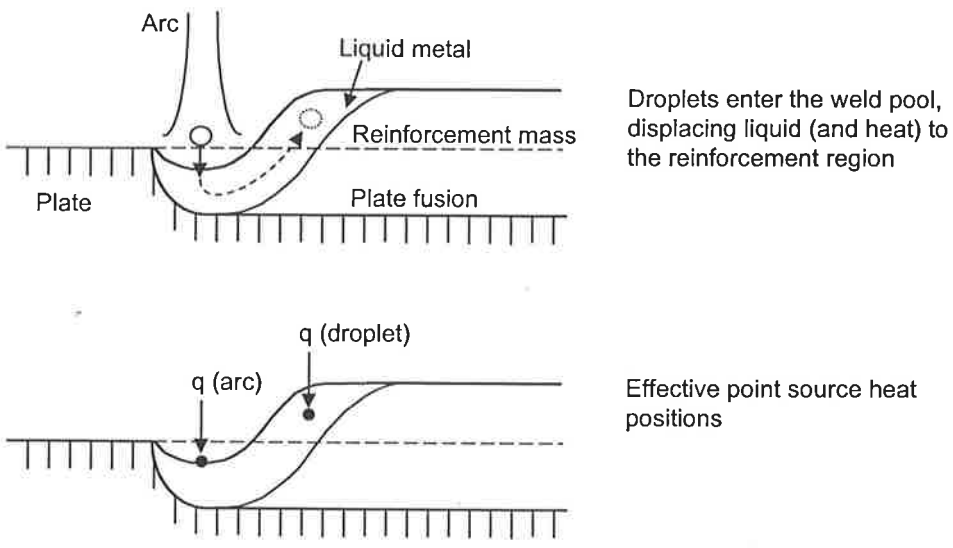

Figure 1.8 Allum & Quintino's (1985) Proposed Split Heat Source.

Tekriwal & Mazumder (1986 & 1988) modelled GMAW in a V-joint and added the droplet heat by incrementally adding a wedge of material at the droplet temperature into the groove. The remaining heat was attributed to the arc and was added as a surface Gaussian. Tsao & Wu (1988) also used a surface Gaussian to represent the arc, but the droplet heat content was added as a volumetric source distributed within the weld pool around the axis of the droplet stream. The heat was diffused in a Gaussian manner radially into the weld pool from this axis, effectively resulting in a cylindrical volumetric source. The depth of this cylinder was not specified. It should be noted that Tsao & Wu's work was in fact for a model which included convective flow and so it will be discussed in more detail in Section 1.4.3. Pardo & Weckman (May 1989) used a Gaussian surface heat source and achieved finger penetration by enhancing the thermal conductivity in the direction of the depth of the pool. The peak value was immediately below the arc and diminished with depth - it was also made to increase with increasing current. Pardo & Weckman (December 1989) used two surface Gaussian sources one for the droplet and one for the arc heat. In addition, thermal conductivity was enhanced in the depth and width of the pool by peak values of 11 and 4 respectively, decreasing with distance from the arc centre. Ortega *et al.* (1992) used a Gaussian surface flux with the heat content of the droplets added to the model in terms of the heat content of the deposited weld bead. Hong *et al.* (1993) and Dilthey *et al.* (1993) both used isotropically enhanced thermal conductivity in conjunction with separate surface Gaussian fluxes for the arc and the droplets. Liew, Wahab & Painter (1993) used a split heat source, having the arc represented by a shallow double ellipsoid and the droplet by a spherical volume source applied in the weld pool at a depth proportional to current. In the same paper a modified double ellipsoidal heat source was also trialed in which an inner portion of the distribution was made uniform to reflect the concentration of heat due to the droplet. This second approach did not show significant variation from the standard double ellipsoidal heat and as a result has not been pursued further. Results from this thesis have been published by the author in a paper, Smailes *et al.* (1995), extending Painter's work (1993) on the split heat source and applying it to V-joint welds. Kumar & Bhaduri (1994 & 1995) used a split heat source with a surface Gaussian distribution to represent the arc, and a cylindrical volume source below the arc to represent the droplet. The cylinder reached from the pool surface to a depth estimated from Lancaster's (1984) energy balance which equates the kinetic energy of the impacting droplet to the energy required to create a cavity in the weld pool. Barberis & Rebora (1996) used Tekriwal & Mazumder's (1986 & 1988) approach mentioned above but with the Gaussian heat source replaced by a uniformly distributed ellipsoidally shaped volumetric heat source.

It is clear that there are a significant number of models attempting to come to terms with the topic of this thesis, namely the modelling of GMAW. The potential value of each proposed heat source will be critically discussed in Chapter 3 which deals with heat source definitions.

The discussion on the development of heat sources shows that the accuracy of "near weld" thermal fields depends on the chosen heat source definition. This heat source definition must reflect physical features of the welding process such as the penetration characteristics for GMAW and surface heating for GTAW. The heat source will need to include features to compensate for weld pool flow.

1.4.2 CONVECTION MODELS

Convection models are those in which the flow within the weld pool and the driving forces for the flow and pool distortion are included. These models are not the focus of this thesis however they provide a useful insight into the dominant forces and flows and hence assist in defining conduction based heat sources. The time taken to solve these types of models is of the order of days to weeks and so their major attraction is that much of the information gained from them cannot be experimentally determined. At best the weld pool surface flow can be measured, but this is also difficult because any tracers used to visualise the flow can significantly affect the surface tension and resulting flow. Thus to develop further understanding of flow, numerical models need to be applied. There is an obvious difficulty in verifying the models except by showing the change in weld pool shape that can be predicted.

Initially convection models focused exclusively on GTA welding and this led to identification of the forces driving the weld pool flow listed below. The most significant outcome of convection based analysis to this work on GMAW is understanding of the additional force of the momentum of the impinging molten droplets and recognising it as the dominant force. This has assisted in developing heat source types which replicate the distribution of heat that the impingement of the droplets cause.

Literature reveals four driving forces for convective flow in GTAW:

1) Electromagnetic force (EMF) - as the current flows through the arc and into the pool and weld piece, it diverges and reacts with its own self induced magnetic field to generate the Lorentz force. This acts towards the centre line of the electric field.
2) Buoyancy force - caused by temperature gradients in the pool which induce variations in density of the molten material.

3) Surface Tension - variation in temperature, or the presence of impurities, cause a variation in surface tension over the pool surface, inducing Marangoni forces and pool flow.
4) Plasma drag and pressure - acting on the weld pool surface, it produces both a "downwards" force and radial surface shear.

Then for GMAW there is the additional force of:
5) Droplet impact - transferring kinetic and thermal energy and releasing its surface energy.

1.4.2.1 Gas Tungsten Arc Welding Convection Models

Early convection models looked at the effect of weld pool stirring, with Shercliff (1970) and Sozou (1971) analytically modelling stirring of a semi-infinite fluid by a magnetic point source. Sozou & Pickering (1976) and Andrews & Craine (1978) confined this analysis to flow within a hemispherical pool to more closely reflect the welding process. Dilawari *et al.* (1977) applied the electromagnetic flow analysis to a cylindrical region representing electroslag welding and used a finite difference method. Atthey (1980) also used a non linear numerical model for flow induced by the magnetic field; then in 1983, Oreper, Szekely & Eagar added surface tension and buoyancy forces to the electromagnetic analysis. These models showed that convective flow was the dominant means of heat transfer in the weld pool, that the surface tension had a significant effect on the flow pattern and that the electromagnetic force and heat distribution had a lesser effect.

Zacharia has been quite active in developing flow models for GTA welding. In October 1989 Zacharia *et al.* had a paper published describing a three dimensional transient model which included coupling with the arc via a free surface. Zacharia *et al.* (1989) used a convection model of stationary GTA welding to show how the action of surface active elements on the weld pool can reverse the direction of pool flow and significantly affect the resulting pool profile. Zacharia *et al.* (1991 & 1992) used a two dimensional, axisymmetric, transient convection based thermal model to investigate the effects of evaporation and surface temperature. They showed that the surface temperature for GTAW was about 2850 K with evaporation included and 3080 K without it. The peak temperature was shown to increase with power density and predictions were in good agreement with experimental measurements. The research was continued (1995) with an improvement to the model, by making all of the material properties temperature dependant.

Matsunawa (1992) included all four forces for GTAW and achieved models which showed good agreement with experimental results. They quantitatively compared the effect of the four forces and found the surface tension to be the most significant force in short arc welding and surface shear to be the most significant in long arc. He did not, however, include the deformation of the pool surface and acknowledged that the interaction between arc, pool and the surface deformation is an area which needs to be addressed.

1.4.2.2 Gas Metal Arc Welding Convection Models

Literature discussing convective modelling of GMAW is limited. Tsao & Wu (1988) were first to produce a convective model of GMAW. They included electromagnetic, buoyancy and surface tension forces. The effect of the inertia of the incoming droplets was not modelled, but accounted for by manually distributing the droplet heat in the volume of the weld pool. Heat was applied as a Gaussian surface and a cylindrical volume within the pool around the axis of the incoming droplets. Using this model Tsao & Wu were able to predict finger penetration and their results agreed well with experimental results.

Kim & Na (1991 & 1994) produced a convection model to predict bead shape, velocity field and temperature field in GMA weld pool. They included buoyancy, electromagnetic and surface tension forces. They demonstrated that the deformation of the surface of the pool is significant in convection models and that convective flow models were able to predict finger penetration. Kim & Na (1995) added the droplet impact forces to the calculation and the predicted shape of the beads and penetration were very accurate. It was concluded that the dominant forces were the electromagnetic stirring and droplet impact.

Davies (1995) modelled convective GMAW and quantitatively compared the relative magnitude of the driving forces. It was demonstrated that for spray transfer, the droplet impact is the dominant force, followed by the electromagnetic force, with surface tension driven forces becoming insignificant beyond an arc current of 150A.

After a review of current heat flow models, Bhole & Adil (1990) believed the way forward in flow modelling was to use a simplified flow model. They suggested using an approximated hemispherical flow model for which an analytical solution had been obtained by Sozou & Pickering (1976) and Andrews & Craine (1978). The quick analytical results could then be superimposed onto a FE model as a fixed boundary condition.

1.4.2.3 Free Surface

Literature shows that the deformation of the weld pool surface has a significant effect on the distribution of heat on the weld surface, on the flow within the weld pool and on the penetration of the weld. Two examples are: Rokhlin *et al.* (1993) who showed that for GTAW, pool depression has a strong effect on weld penetration and that they were linearly related; and Choo *et al.* (1990) who modelled the flow within a weld pool and showed that it is important to include the deformed surface, partly due to the deformation causing a redistribution of the heat input (see Section 3.2.1) and partly due to the physical constraint of the deformed surface affecting the internal flow.

There are seven factors shown to affect the deformation of the weld pool surface:

1) Hydrostatic force due to gravity & buoyancy.
2) Surface tension.
3) Arc plasma pressure.
4) Electromagnetic pressure.
5) Surface shear.
6) Hydrodynamic force due to Inertia of fluid flow within the pool.
7) Droplet impact.

The first two factors resist the deformation of the pool while the remainder act to increase the deformation in GMAW.

No model has been observed that incorporates all of the above forces and the early models were very simple. Friedman (1978) predicted the deformation of a pool surface for GTAW using FE computer modelling. Hydrostatic and plasma pressure forces were considered and it was shown that the surface deformation significantly affects the penetration characteristics.

Lin & Eagar (1985) equated the gravity and arc pressure with the surface tension and neglected the other forces. They demonstrated that the arc pressure was by no means strong enough to account for the level of deformation observed. A vortex flow of 10-30 revolutions per second around the arc axis was proposed to explain the deformation by a whirlpooling effect. This has not been pursued further by other researches, presumably because more recent work has demonstrated that this is not the dominant flow pattern.

In line with Lin & Eagar's work, Rokhiln *et al.* (1993) measured the arc force for GTAW to be only about 20% of the force required to counter the surface tension and metallostatic head forces for a given pool deformation. Also, the surface tension force is of the order of 8 times greater than the gravity. Rokhlin *et al.* suggested that the under prediction of the deformation may be overcome by including electromagnetic forces. Lancaster (1986) showed that electromagnetic force made some impact on the pool depression using experiments on a gallium pool. Choo *et al.* (1990) estimate that depending on the current, the surface shear may be of the same order of magnitude as the surface tension force. Hence this could be a very significant factor which has generally been neglected in surface deformation calculations.

Tsai & Kou (1989) showed that in the absence of other surface deforming forces, flow in the pool causes significant surface movement. Lee & Na (1997) on the other hand claimed that the internal flow would cause negligible effect on the pool depression. They produced a model of flow in a stationary GTAW and had the arc coupled to the pool surface and flow calculations. The calculation of the deformed pool surface only considered the arc pressure balanced by the gravitational force. They also investigated the effect of different electrode bevel angle on arc pressure and shear stress. Changing the bevel angle from 30° to 90°, reduces the surface shear stress by almost 50%. There is also a corresponding drop in peak arc pressure of 30%.

The work by Kim & Na (1991) & (1994) discussed in the previous section, demonstrated the significance of the deformation of the pool surface since it deforms the flow patterns in the pool.

1.4.3 STRESS, STRAIN AND TRANSFORMATION MODELS

In many cases interest in the thermal models is due to its application in predicting stress, strain and microstructural changes. To put the thermal analysis in the picture, a brief review will be made of how the thermal data has been applied beyond interest purely in temperature and fusion zone predictions.

Figure 1.1 showed how temperature, stress and microstructural changes were related, but as noted previously, there is a minor feed back opposing each of the arrows in the figure. Karlsson *et al.* (1991) used residual stress calculations with and without the residual stress feed back to show that the stress coupling has less than 1% influence on the thermal calculations. In terms of the microstructural coupling, the most significant effect is accounted

for by making the material properties temperature dependant in the thermal analysis so that they reflect the primary phase of the material.

Figure 1.1 is reflected in Figure 1.9, the flow chart used by Das *et al.* (1994) who have produced a comprehensive CWM model. They used ABAQUS in conjunction with user defined subroutines to calculate thermal history, microstructural transformations and residual stress using material deposition and heat flux as input.

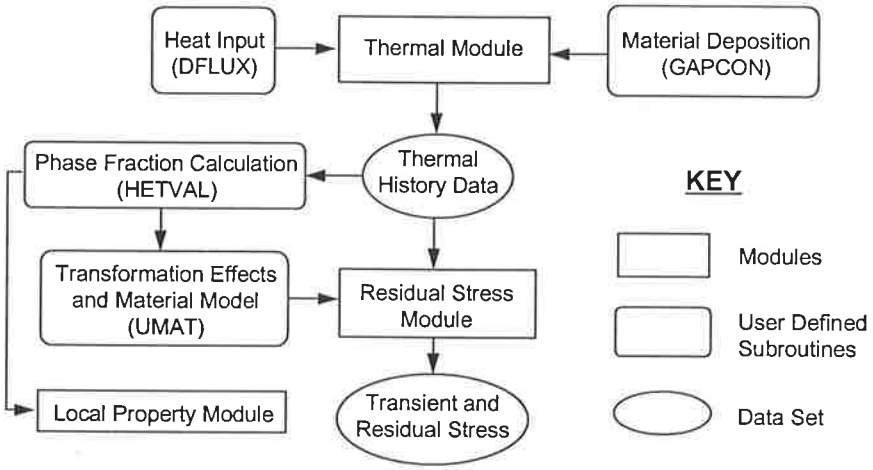

Figure 1.9 Computational Weld Mechanics model developed by Das *et al.* (1994).

Ueda *et al.* (1995) give a good summary of the establishment of CWM in Japan from the 40s to the 90s.

1.4.3.1 Microstructure

A sample of papers are discussed to illustrate that results can be extracted from the thermal models to use for microstructural analysis input:

It would appear from the literature that researchers who played a significant role in the development of models to predict microstructural changes in steels from thermal histories are Ashby & Easterling (1982) and Bhadeshia, commencing in the early 1980s. Easterling (1989) gives a review of main areas of research in modelling microstructural changes, namely calculating: the heat affected zone properties, pre and post heat treatment effects, multi-pass welding. The need for good welding thermal cycles to use as input is emphasised.

Models for microstructural changes in the HAZ: Watt *et al.* (1988) combined results from a FE heat transfer model with algorithms for the decomposition of Austenite to predict the heat affected zone microstructure. Tekriwal *et al.* (1987) used the predicted cooling rates from a three dimensional conduction QSS model to qualitatively predict dendrite arm spacings in different parts of the molten pool. Pardo, Villafuerte & Kerr (1989) used a finite element model to predict wether the grain structure in GTA welds is likely to be columnar or equiaxed. They produced a finite element model from which they extracted the two key parameters for their microstructural analysis, namely the weld pool temperature gradient and the solidification velocity. Shah *et al.* (1995) again demonstrated that the thermal cycle can be used as input to model grain growth and phase transformation in the HAZ. They use a modified Rosenthal equation for the thermal calculation. Goldak *et al.* (1995) used thermal results from **QSS** models to predict microstructural changes. Mundra *et al.* (1997) calculate the microstructure of the deposited weld metal using calculated thermal response of a convection based finite element model. A time-temperature-transformation (TTT) diagram is coupled to the cooling curves of the weld metal to find the continuous cooling transformation (CCT) behaviour. The calculated volume fractions of the different phases is compared to experimental with good correlation - slightly better than a similar conduction based model.

Applying microstructural analysis to multi-pass welding: Clark (1985) modelled the microstructural changes in multi-pass manual metal arc welds producing semi-quantitative information. Reed & Bhadshia (1989 & 1994) used thermal model of a 69 pass weld to investigate the possibility of producing a weld which has uniform high strength within the deposited material. The aim was to reduce the volume fraction of unreaustenitised material to give uniform properties in the deposited material. They used the thermal analysis to propose a means to ensure each new bead deposited will reaustenitise almost all of deposited material adjacent to it.

No papers were isolated which dealt with finite element modelling of microstructure for pre and post heat treatment.

1.4.3.2 Residual Stress & Distortion Calculations

Goldak (1989) carried out an overview of modelling thermal stress and distortion in welds. He summarised that between the early and late eighties, modelling of residual stress shifted from "cross-sectional two dimensional plane strain and axisymmetric models to models of longer welds using plane stress, shell and three dimensional elements". Apart from near the weld, these newer models give good predictions of residual stress and distortion. The

inclusion of phase transformation effects and transformation plasticity, and microstructural changes are needed to improve near weld stress calculations.

Goldak & Oddy *et al.* (1986) showed the assumption of plane strain used by many researchers to be invalid. Similarly, McDill *et al.* (1992) compared 2D and 3D residual stress calculations and show that close to the weld in the heat affected zone the 2D calculation can be considerably in error.

It has been common to include transformation effects in residual stress calculations for some time now. Transformation volume change was initially included resulting in a limited degree of success. Lindgren *et al.* (1988) improved on previous residual stress calculations by including yield strength hysteresis, however, results close to the weld were still significantly in error. Oddy *et al.* (1989) went one step further and showed that it is vital that the transformation plasticity as well as the volume change and yield strength hysteresis be included. Leaving one or more of these out resulted in longitudinal stress errors of ± 300% at the weld centre line.

Goldak (1991) discusses the coupling of thermal analysis to microstructural evolution and stress analysis. Bergheau *et al.* (1991) used SYSWELD to couple thermal analysis and microstructural changes and then used the output to calculate the residual stresses and strains. Das *et al.* (1993) used ABAQUS, generating a transient model for the residual stress for a GMA weld with careful attention to the phase fraction at each time step which they showed is significant to the calculated residual stress.

Residual stress models have been produced for a variety of welding processes: Tekriwal & Mazumder have done quite a lot of thermal modelling work and in 1991 successfully applied it to residual stress calculations for 3D GMAW and GTAW using the finite element code ABAQUS. Roelens (1995) produced impressive transverse residual stress calculations for multi-pass welds and good results for longitudinal residual stresses. A large amount of modelling of residual stress and distortion has been conducted for application in the pipe industry. To cite just one example, Winters & Mahin (1991) use PASTA 2-D to model residual stresses in pipes effectively.

Gu *et al.* (1994) predicted stress and distortion using QSS thermal input by transforming the thermal results back to the time domain. In this case care must be taken because Oddy *et al.* (1990) showed it is important that the elements for the strain analysis are consistent with

the elements of the thermal analysis. If this is not done, significant errors in near weld region where change in thermal gradient is very large do result.

Tsai *et al.* (1995) have proposed a new method of calculating welding distortion, specifically for large structures where it is infeasible to do a complete stress and distortion analysis due to complexity and time constraints. Their method involves assuming that the dominant contributor to distortion in a weld is the contraction of the weld metal. This is modelled by applying spring elements to the modelled structure with the spring contraction reflecting the weld metal contraction. The method has provided promising results in fast times. Bachorski *et al.* (1997) have taken up the method too and showed how using the actual fusion line of the molten metal as the defined shrinkage volume produced extremely accurate distortion predictions for butt welded plates of different vee preparations.

Practical stress reducing applications of thermal modelling have been observed in the field of pre or post treatment of fabrications to minimise stress and distortion. For example, Michaleris *et al.* (1997) used a finite element analysis to demonstrate how thermal tensioning can be applied when welding a stiffener on to a plate to minimise welding induced buckling. A pre-tensioned stress field is induced which opposes that which will be generated when welding commences. The resulting peak stress is 139 MPa compared to 345 MPa acting over a larger area for no pre-tensioning. This is a significant improvement and the paper illustrates how finite element analysis can be used to find the optimum thermal tensioning conditions.

On a similar vein, Namyama *et al.* (1997) are modelling a dual heating process for post treating circumferential pipe welds to control the residual stress. A finite element analysis together with dimensional analysis is used to develop a rule base for the dual heating process parameters so that the residual stress on the inside surface of the welded pipe can be reduced to a compressive stress.

1.4.4 WELDING ARC AND METAL TRANSFER

Modelling of the arc and metal transfer is outside the scope of this research, however a sample of the work done in this area is presented because the arc and metal transfer interact with thermal modelling in several ways. They determine the material flow rate and hence the reinforcement added to the welded joint; the heat content and flow rate of the transferred metal affects the way the heat is applied to the molten weld pool, as does the

temperature and pressure of the arc; the impact energy of the droplets affect the shape of the weld pool surface and the convective flow patterns within the weld pool.

1.4.4.1 Metal Transfer

The physical effects which cause the changes in transmission mode are not yet fully understood, however, work has been done to try to develop models to predict the metal transfer:

There are two theories which attempt to explain the transfer behaviour, these are the "pinch instability" theory described by Lancaster (1979) and the "pendant drop" theory proposed by Greene (1960). Both theories have only "some general agreement with experimental results and trends", (Battersby 1994). An alternative is to try to develop a complex numerical model of the arc and electrode to determine the metal transfer behaviour, and some work has been done in this area. Haidar & Lowke (1996) have produced detailed numerical models to predict the droplet size and frequency taking into account the Lorentz force, surface tension, gravity, plasma pressure, drag of the gas flow and inertia with good results. For a simpler approach, Lowke (1997) produced an analytical model approximating the droplet as a hemisphere on the end of a solid wire. By calculating the current at which the pinching effect of the Lorentz force is great enough to distort the hemisphere, good predictions were made of the change in transfer mode from globular to spray. Bozhenko *et al.* (1997) have numerically modelled the melting of an electrode wire with given boundary conditions to approximate the arc heat to show that the evaporation effects are very significant, limiting the droplet temperature to about 2500°C for GMAW with a typical heat input. This is close to experimentally measured values for the droplet temperature.

There is a considerable amount of research into developing regression equations to describe the transfer of material to the weld piece. Chandel (1988) developed a regression equation for melting rate as a function of current, voltage, stick out, and wire diameter for direct current bead on plate welds. Pilarczyk *et al.* (1994) also developed regression functions for wire feed rate as a function of gas type, voltage, current, stick out, angle of inclination of the welding torch, and welding speed using 1.2 mm diameter wire and direct current GMAW. Halmøy (1991) gives an equation relating feed rate to stick-out and current density in the electrode wire. Lesnewich (1958) derived an equation based on consideration of basic physical principles which related wire feed rate to a quadratic equation of current. The equation has been shown to be successful under moderate and high current conditions. It was also tested for pulsed welding using the mean current value but did not yield good

results. Allum (1983) extended Lesnewich's work to make it applicable to a pulsed current of square wave form by integrating the instantaneous wire feed rate over one pulse cycle. Richardson *et al.* (1994) took it one step further and derived expressions for an idealised trapezoidal pulsed wave form having a finite slew rate (Equation 1.5). Slew rate is, the rate at which the current changes from the base current value to the peak value (ie. *dI/dt*) or visa-versa.

$$W = \alpha\bar{I} + \beta L\left\{\bar{I}^2 + \frac{\left(I_p - I_b\right)^2 t_p t_b}{\left(t_p + t_b\right)^2} - \frac{\left(I_p - I_b\right)^3}{3\left(t_p + t_b\right)dI/dt}\right\} \qquad (1.5)$$

W is the wire melting rate, L is the length of electrode wire carrying current, I_p is the peak and I_b the base current, t_p is the duration for which the current rises to and remains at its peak value, t_b is the duration for which the current falls to and remains at its base value, $\bar{I}$ is the time averaged current $(I_p t_{p+} I_b t_b)/(t_p + t_b)$. For GMAW with 1.2 mm mild steel electrodes, α, the arc constant is 2.7 x10^{-4} $mA^{-1}s^{-1}$ and β, the resistive heat constant is 0.59 x10^{-4} $A^{-2}s^{-1}$. If the slew rate is infinite, Equation 1.1 reduces to Allum's afore mentioned work for a square pulse. If I_p and I_b are equal the equation reduces to Lesnewich's original quadratic for a direct current weld. Richardson found the slew rate to have a significant effect on the predicted wire feed rate for thin, high resistance electrode wire. For more common wire such as 1.2 mm mild steel, with modern electronically controlled power sources, the effect of the slew rate is small; of the order of 5%. It is also interesting that the effect of the slew rate is more significant when, for a given mean current, the difference between the peak and base current is great.

1.4.4.2 Welding Arc

An excellent and comprehensive review of early work done on understanding and modelling the electric arc in welding is provided by Lancaster (1987). Choo *et al.* (1990) modelled the arc for GTA welding, taking into account flow and ionisation of the gas, electron flow due to the current, convection and radiation from the plasma. Evaporative losses from the weld pool were not included however. The model predicted the temperature distribution in the arc, as well as the heat flux at the surface of the weld very accurately. Of great interest to this thesis was the discovery that the Gaussian form of the heat flux at the weld surface changed dramatically when the weld pool surface was deformed. This effect will be

discussed in detail in Section 3.2 on Gaussian heat sources. An implication of this work is that there should be coupling between the arc and the weld models.

Jog *et al.* (1991) modelled the arc for a GTA weld onto a flat plate. They included heat input from electron heating and convective heating, but did not account for vapour effects or for radiation. The predicted heat flux was compared to Gaussian distribution and shown to agree exceptionally well, with a peak discrepancy of 5%.

Balanovskii (1993) attempted to derive predictive equations for thermal ionisation in the column of the welding arc. The conclusion was that the equations were not sufficiently reliable because of the impossibility of taking into account the effect of the presence of ionisers and deionisers in the actual welding conditions.

Other research in modelling the arc has focussed on the force induced by the arc on the weld pool surface. This work is especially of interest in the light of the fact that deformation of the weld pool alters the heat source distribution and as will be discussed in Section 1.4.3 it also affects the flow within the weld pool. Rokhlin *et al.* (1993) have done significant work on weld pool depression using equations for the arc force which they reference to Halmoy (1979) and Converti (1981).

Chapter 2

THE MODELLING APPROACH

2.1 INTRODUCTION

This chapter presents and justifies the modelling approach taken for this work. To put this in perspective, a brief summary of the development of GMA weld modelling will be presented from its commencement in about the early 1940s, up to the present day. For details of this historical background, refer to Section 1.4.

The earliest model can be attributed to Rosenthal who developed a simple analytical model, using the theory of a moving heat source to represent the arc on a semi infinite solid plate. This model was applied and enhanced over the following three decades but retained the limitation of being applicable only to analyses having non temperature dependent material properties and very simple geometries and boundary conditions. In the 1970s FD and FE models became computationally feasible, overcoming these limitations, but being very much slower in terms of analysis time. To combat this, modellers initially concentrated on 2D analyses which introduced a new limitation that the solution became erroneous at low welding speeds. With advances in computer technology, 3D models became common in the 1980s and have yielded very good results. Both quasi-steady-state (QSS) and transient models have been produced throughout the decades, the most significant difference being that the transient models are very much more time consuming to solve. QSS models are limited to weld geometries that do not change significantly in the direction of weld travel, and welds which are long enough that run on and off effects are insignificant. The 1980s also saw the start of convection based modelling in which the molten weld pool was modelled as a liquid. These models are extremely complex and time consuming to solve and are not practical for solving welding thermal analyses, however they have provided invaluable insight into the processes occurring in the arc and weld pool.

The degree to which the physical processes are included depends on weighing the detail which is to be obtained from the model against the overall complexity of producing and solving the model. Figure 2.1 shows a rough guide on solution times versus the level of detail required from the model for different modelling approaches.

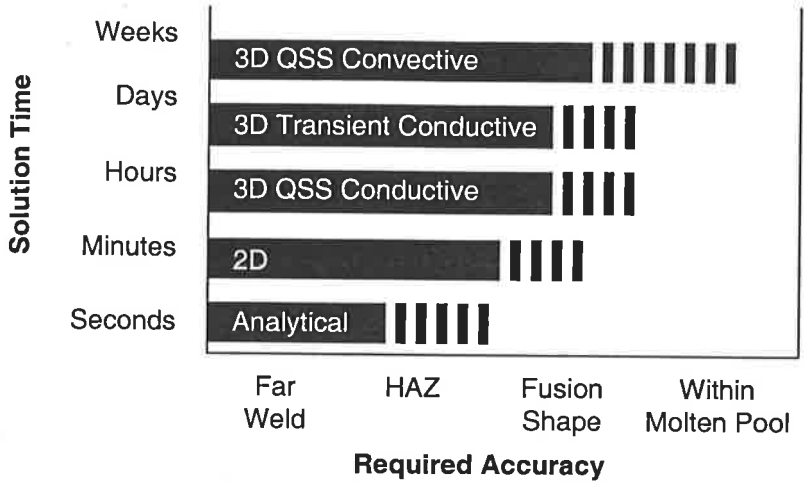

Figure 2.1 Solution time versus accuracy for different model types.

The modelling approach adopted for this research is a conduction based QSS model, based on the author's opinion that this produces good accuracy in a practical time for industrial application. In addition, a focus of this work is the development of new heat source definitions, and it is sensible to use a relatively rapid three dimensional analysis to test them. The developed heat sources can still be applied equally well to transient models if the weld configuration rules out a QSS model from being used. Other benefits of QSS analysis are in Section 2.2.4.

2.1.1 FINITE ELEMENT ANALYSIS

Finite element analysis became a useful research tool in the 1970s, being first applied to welding by Hibbitt & Marcal (1973). It has provided enormous advances in the modelling of welding, enabling complex structures governed by very non-linear processes to be modelled. It is thus the chosen means of analysis for this thesis.

In the QSS finite element analysis, the governing equation to be solved is,

$$-v\rho C_p \frac{\partial T}{\partial x} = \frac{\partial}{\partial x}\left(k\frac{\partial T}{\partial x}\right) + \frac{\partial}{\partial y}\left(k\frac{\partial T}{\partial y}\right) + \frac{\partial}{\partial z}\left(k\frac{\partial T}{\partial z}\right) + q_g \qquad (2.1)$$

this is the same as Equation 1.1 but transposed into the quasi-steady-state domain. v is the velocity of the arc in the x-direction. The boundary conditions are of the form,

$$k\frac{\partial T}{\partial n}+h(T-T_0)+S\varepsilon(T^4-T_0^4)=0 \qquad (2.2)$$

where n is the normal vector, h is the convection coefficient, ε is the emissivity, S is the Stefan-Boltzmann constant (5.67e-14 W/mm^{2}K^4) and T_o is the ambient temperature. Using finite element discretisation procedures such as detailed by Zienkiewicz (1977) a global matrix equation is derived:

$$\boldsymbol{K}\vec{T}=\vec{F} \qquad (2.3)$$

where $\boldsymbol{K}$ is the effective conductivity or global stiffness matrix, $\vec{T}$ is the vector of unknown nodal temperatures and $\vec{F}$ is an effective thermal force vector. This equation is then solved for the unknown nodal temperatures $\vec{T}$.

2.2 THE FINITE ELEMENT MODEL

2.2.1 SOFTWARE

There is a wide range of FEA software available which is suitable for weld design and analysis. Tsai (1991) reviews the major software packages outlining their capabilities. Of the listed packages, seven have an in built capability for analysing welded joints. ABAQUS would seem to be the most popular of these as it is the most commonly referenced software observed in the literature. PASTA2D is not listed, but appears regularly in literature (eg. Winters & Mahin 1991). It is especially geared to stress analysis for conduction thermal analyses and as the name suggests, it is a 2D modelling package. PHOENICS, also, appears to be quite popular for flow models and uses the finite volume approach (eg. Choo *et al.* 1990). The package "Welder" rates an occasional mention in literature and is outlined in a paper by Domey *et al.* (1992). It was set up especially for convection based thermal modelling but can also handle forced convection. Finally, SYSWELD appears quite regularly in literature for welding analysis.

The package available for this work is NISA/3D-FLUID produced by Engineering Mechanics Research Corporation, Michigan. It has several desirable features. It is, of course, capable of thermal analysis, but also has fluid capabilities so that QSS models can be produced with material "flowing" below the stationary arc. With body force and electromagnetic capabilities the software can be used to model as many features of the physical reality as desired. In addition, NISA is capable of structural and stress analysis so that the thermal results of the weld analysis can be applied directly to a model of the complete welded structure. NISA is not specifically for weld modelling but is a good general purpose FE package. Weld models developed with this software could be duplicated with many commercial packages.

2.2.2 MESH

A mesh consisting of three dimensional eight noded elements was generated. The mesh is refined around the weld pool area where the change of thermal gradient is greatest to maintain accuracy. Figure 2.2 shows a sample mesh for a T-joint weld.

It can be seen that the weld bead is meshed into the model. This is done because it has been shown by various researchers including Moore *et al.* (1985) that modelling the reinforcement can be significant to the predicted results. There could be two reasons for this significance: (1) the bead material influences the conduction paths, (2) the positioning of the heat source is related to the weld configuration and bead. This poses the apparent

contradiction that the bead dimensions must be known so that they can be predicted. Researchers such as Pardo & Weckman (1988), Hong *et al.* (1993), Liew *et al.* (1993) have assumed a parabolic reinforcement profile. They use the calculated weld pool width as input and knowing the bead cross section area from the wire feed and weld speed, the height of the bead can be found. A new fusion width is then calculated and the process is iterated. Since the actual profile of the bead is relatively insignificant compared to the cross sectional area, this iterative process is not carried out in this work, but care is taken to model the correct bead area. Figure 2.2 shows that the weld bead is meshed onto the full length of the plate rather than just to the arc location where the material is actually added. The reasoning behind this is related to the heat source definition and is addressed in Section 3.1.

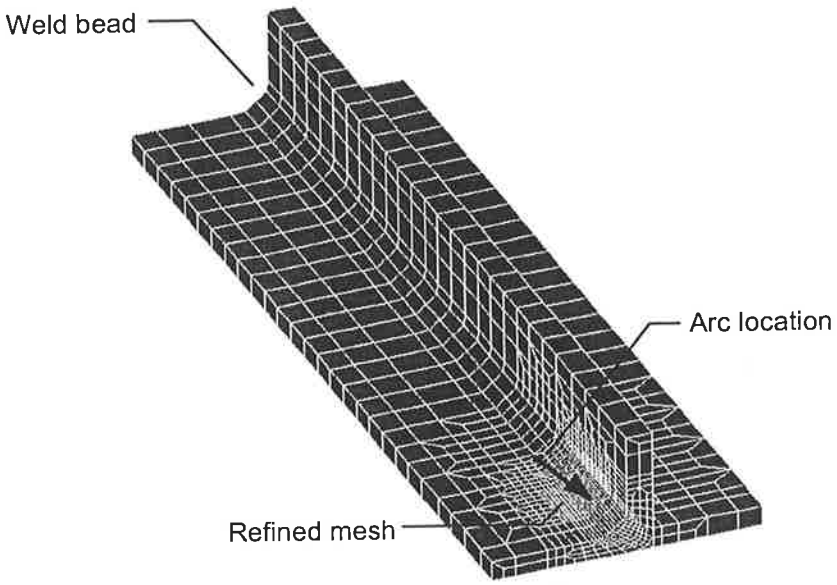

Figure 2.2 Sample mesh for a T-joint weld.

For transient models, elements are required to be added as the bead is deposited or a method of "rebirth" must be employed. Rebirth means that the element's properties are initially "turned off" which mathematically equates to them not existing. The elements are then "turned on" as the weld progresses to simulate deposition of the bead. Ortega *et al.* (1992) and Barberis *et al.* (1996) used this method.

Where welding occurs along a line of symmetry, only half the model is meshed and adiabatic boundary conditions are applied to the plane of symmetry. Details of specific meshes for weld configurations used in this research are given in Chapter 4.

2.2.3 CONDUCTION BASED MODELLING

In conduction based models the molten weld pool flow and associated driving forces shown in Figure 1.4 are not modelled but the transfer of heat within the weld piece is governed purely by conduction as shown in Figure 2.3. This is a very significant simplification as the driving forces and flow patterns within the weld pool are extremely complex to incorporate into the model. The absence of convective flow within the molten weld pool is compensated for by appropriately distributing the arc heat source and enhancing the thermal conductivity. Since we are modelling the arc and droplet as a distributed heat source, there is a further simplification that the arc itself is not modelled.

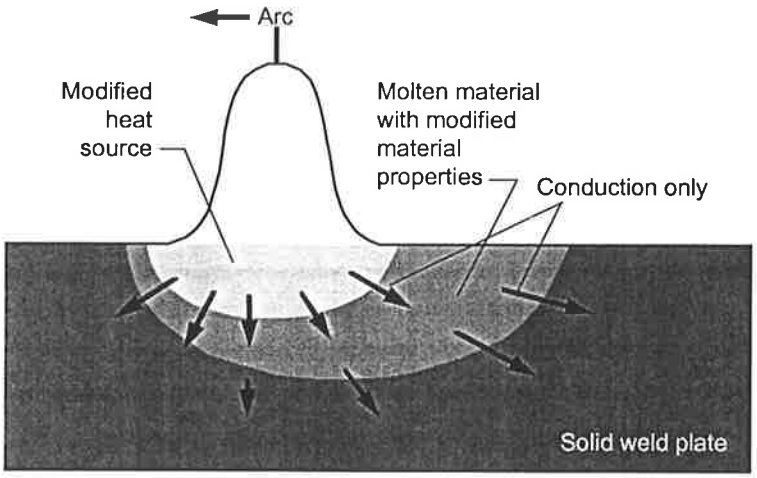

Figure 2.3 Conduction Based Model.

Conduction modelling has been tried and tested over the decades, commencing with Rosenthal's analytical work in the 1930s, described in the review Section 1.4.1.

2.2.4 THE QUASI-STEADY-STATE ASSUMPTION

The concept and history of quasi-steady-state (QSS) was introduced in Section 1.4.1. Recapping, the QSS assumption is a well established simplification which was introduced with the very earliest mathematical welding models. QSS is achieved by modelling the arc as stationary and allowing a semi-infinite plate to pass underneath the arc as shown in Figure 2.4. This is achieved by treating the plate as a fluid of extremely high viscosity which makes it effectively a solid and having it "flow" below the arc at the welding velocity v. If the plate is infinitely long then an effective steady state condition results, referred to in literature as quasi-steady-state (QSS), where at any coordinate *relative to the heat source* the temperature does not change. It is not steady state in the true sense of the word because

relative to the plate, the temperature at a particular point does in fact change. The resulting 3D QSS conduction equation for an isotropic material is given by Equation 2.1 above.

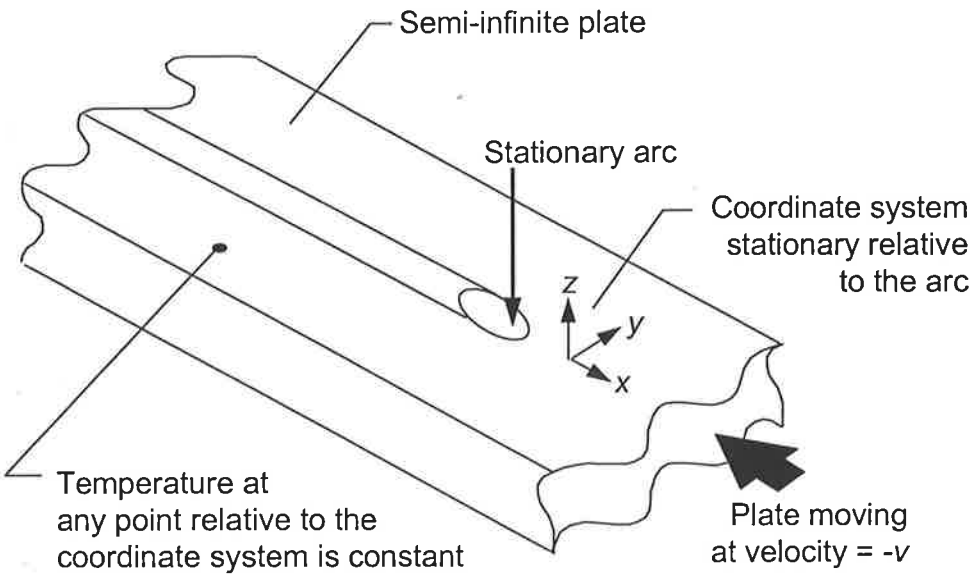

Figure 2.4 The three dimensional QSS assumption.

The QSS assumption avoids the need for a transient analysis resulting in a considerable time saving since the QSS analysis requires only one steady state solution of the matrix equations. Transient analyses, on the other hand, require the solution to be calculated approximately every 0.1 second of the weld run. A secondary advantage is that it is possible to refine the mesh in the vicinity of the weld where the change in thermal gradient is relatively high and have a more coarse mesh away from the arc to reduce the size of the matrix to be solved. In a transient analysis re-meshing is required as the arc progresses or else a fine mesh is needed along the full length of the weld. Silva & Prasad *et al.* (1996) have developed an adaptive grid technique to facilitate re-meshing in transient analyses to try to overcome this problem.

Stress, distortion and microstructure analyses are transient by nature, so to use QSS thermal results for these problems, the thermal data simply needs to be translated from distance variable to the time variable. The possibility of this has been clearly demonstrated by researchers such as: Tekriwal *et al.* (1987) who used the predicted cooling rates from a 3D conduction QSS model to qualitatively predict dendrite arm spacings in different parts of the molten pool; Goldak & Gu (1995) who demonstrated the use of thermal results from QSS models to predict microstructural changes; and Gu *et al.* (1994) to predict stress and

distortion. Goldak & Gu (1995) actually believed the results of the QSS analyses to be "more reliable" than the transient.

There are some cases in which the structure to be welded can not be approximated as a semi-infinite plate. The QSS assumption can still be a useful approximation as described in Chapter 5, dealing with complex structures. Irrespective of the QSS approximation's applicability to every welding problem, it is still useful for fast models to trial different heat sources which could then be used in the transient model.

A non-steady-state condition occurs at low currents when the mode of metal transfer is globular and there is not a constant stream of liquid metal applied to the weld pool. This would contravene the requirement for a constant heat source. Davies (1995) showed that above 150 A direct current, individual drops need not be modelled, but metal transfer can be modelled as a continuous heat and momentum source without sacrificing accuracy. All models in this work are spray transfer either due to high current or due to pulsed current and so the transfer of material does not contravene the steady state assumption. Non-steady-state is also present when the arc is first struck since the whole plate is at room temperature and takes some time to heat up. Very few researchers have done work to verify the length a weld needs to be before QSS is reached and to validify the QSS assumption, so this will be addressed in Section 2.3 by comparing transient results to an identical problem in QSS.

2.2.5 BOUNDARY CONDITIONS

The boundary conditions applied to the QSS models are summarised in Figure 2.5 for a simple flat plate. Every point in the mesh has material flowing through it at the welding velocity to simulate the plate moving below the arc. Note that the mesh itself does not move, but material passes through it. It can be observed from the figure that the meshed plate is not semi-infinite despite this being a requirement of the QSS approximation. The end conditions of the plate are formulated to simulate a semi-infinite plate. The front of the plate needs only to be meshed to a distance outside the range of the thermal effects of the arc. Hence the incoming material will all be at room temperature. At a distance behind the arc the thermal gradient becomes quite low and hence it is approximated as zero, in other words, an adiabatic boundary condition. Verification of these simplifications is given in Section 2.3.2.

The arc is represented as a heat source applied either to the surface of the elements under the arc or as a heat flux within the elements under the arc or both. Details of heat sources

are given in Chapter 3. Heat is lost from the plate through radiation and convection boundary conditions. The parameters used for these radiation and convection heat losses are: the emissivity of the material which is taken to be 0.9 as recommended for hot rolled steel and used by Goldak *et al.* (1985); the Stefan Boltzmann constant (S) which is 5.67e-14 W/mm^2K^4; and the convective heat transfer coefficient (h), taken as 1.2e-5 W/mm^2K (Andersson (1978)) on all surfaces except in the vicinity of the arc. The area below the arc has no heat losses as this is where the heat is applied. A band of 1.2 times the heat source radius has radiation and convective losses reduced by a factor of 2.5 so that there is a less abrupt change in the boundary conditions. Other researchers have used slightly different arrangements of radiative and convective losses, such as Hong *et al.* (1993) who used emissivity (ε) of 0.7 and h different on the top and bottom surfaces and ranging between 0.7 and 2.4e-5 W/mm^2K. In this work, trials of different emissivity and h indicated that the thermal results are not highly sensitive to variations in the values.

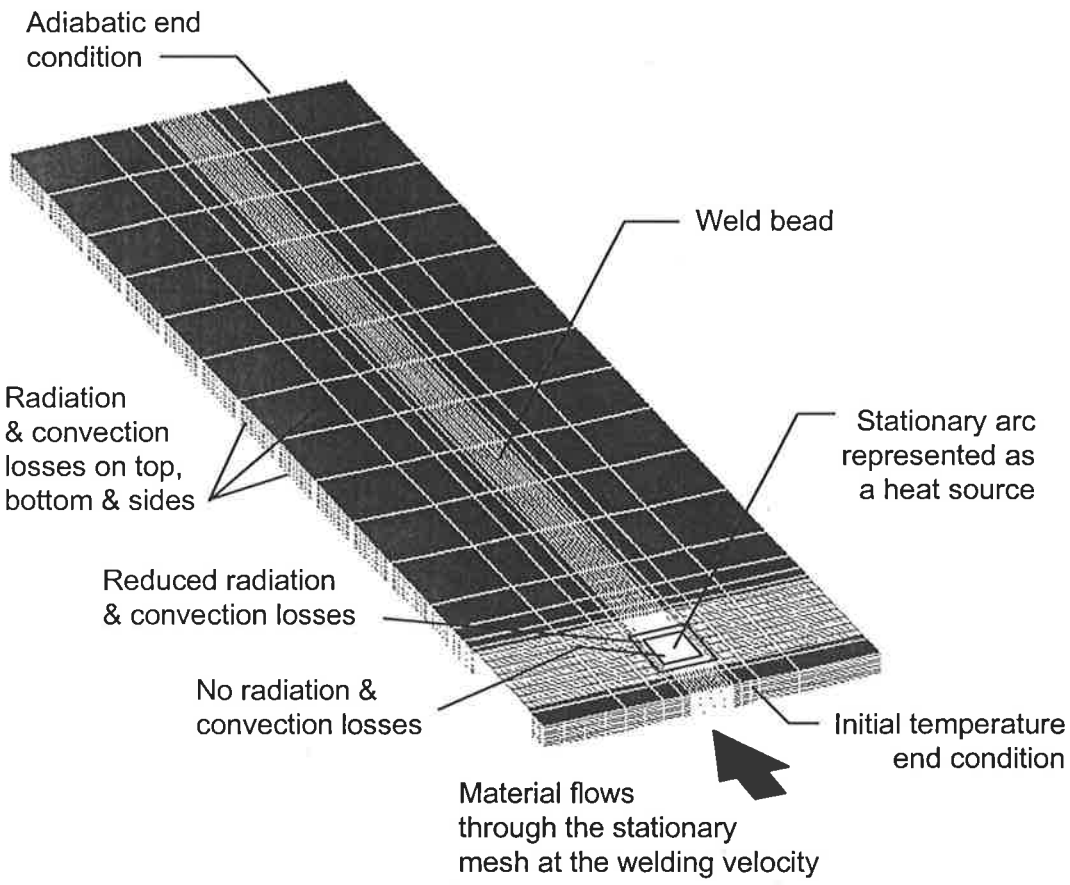

Figure 2.5 Boundary conditions for the QSS conduction model.

The boundary conditions were applied to the model by generating Fortran programs which produced heat source and boundary condition files. These files were used for loading

various joint configurations with all boundary conditions, with an option of heat source types, and simultaneously deforming the mesh to incorporate the weld bead.

2.2.6 MATERIAL PROPERTIES

The weld piece material properties defined in the finite element model are the density, thermal conductivity, viscosity and specific heat. The values of these are programmed at room temperature along with amplitude curves which describe how the properties change with temperature. The properties are in actual fact dependent not only on the temperature, but also on the cooling rate since the density, specific heat and conductivity depend on the phases present in the material. The facilities do not exist within NISA software to modify thermal properties based on thermal history, only on the current temperature, so this effect cannot be included. Miettinen *et al.* (1994), however, show that this is a small effect and so it can safely be neglected. Also, NISA software does not have the facilities to modify the thermal properties based on cooling rate, only on the current temperature, so this effect cannot be included.

The specific heat and thermal conductivity material properties are shown in Figure 2.6 (a) and (b) respectively and are based on values used by Moore *et al.* (1985). The thermal conductivity includes a step increase by a factor of 4 once the melting temperature is exceeded to reflect the enhanced conductivity due to convection. The step change is spread over 20 K so as not to cause convergence problems. Alternatives to the constant enhancement of a factor of 4 beyond the melting temperature are given by: Sudnik (1991) who used uniform thermal conductivity enhancement of (2-1773/T), no reason was given; and Winters & Mahin (1991) who increased the thermal conductivity linearly between the melt temperature and 3100 K by a factor of 6.

The effects of phase change from solid to liquid steel are included in the specific heat. This is common practice, however, some authors such as Barberis & Rebora (1996) have used the enthalpy function which has a discontinuous slope at the phase change rather than a spike and so it causes less convergence problems. At the melting temperature of 1773 K, heat is added to the material with no change in temperature and this would induce an infinite spike in the specific heat which could not be solved for in the FE model. To overcome this problem, the material properties are modified to make the phase change occur over a range of temperatures so that the spike becomes finite. The heat contained within the spike is equated to the specific heat of transformation so that the net amount of heat absorbed or released during phase change is correct. The wider the spike the more rapid convergence

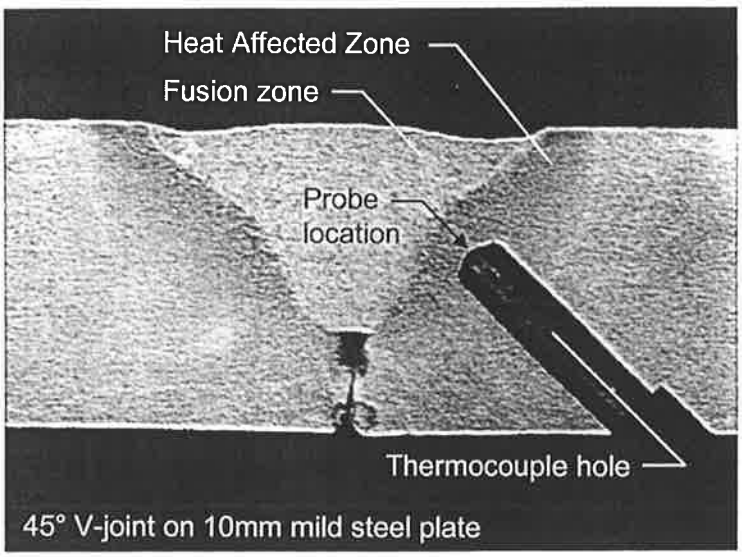

Figure 2.7 Insertion of thermocouples.

For some models, the wire feed speed is a required parameter. This was recorded directly from the welding monitor and converted to grams per second.

During welding, the test plates were raised above the welding table and supported at two edges to minimise the heat loss by conduction out of the plate. After welding, sections were taken at a number of locations along the weld to give an average fusion width and penetration. In the cases where the weld pool length was recorded, it was determined by a separate weld run with the same weld parameters, but using a "tipping device". The device holds the weld piece with high tension springs which are released part way through the weld to almost instantaneously tip and empty the molten weld material from the weld. The tipping device is described in Appendix A.

2.3.2 TESTING THE MODEL ASSUMPTIONS

The various assumptions used in the QSS conduction based FE model will be justified in this section. It will be demonstrated that the mesh size used in the models of this research is sufficiently refined; and that the analysis domain approximates a semi-infinite plate. A comparison of results from QSS and transient models will also be presented.

2.3.2.1 The Mesh Size

To start with, the question may arise as to how fine a mesh is required to give good results. Rather than derive comprehensive rules as to how fine the mesh must be, it will simply be shown that the coarseness of the meshes used in this thesis does not significantly detract

from the accuracy of the models. This is done by comparing thermal predictions from two models with identical boundary conditions, one having a refined mesh and the other a relatively coarse mesh. If the resulting prediction does not alter significantly then it is safe to say that the coarse mesh is adequate. This test was conducted for a refined mesh with elements in the fusion area being 0.125 mm^3 and for a coarse mesh with elements in the fusion area being 2.8 mm^3, as shown in Figure 2.8. A double ellipsoidal heat source was applied representing a 1.2 kJ/mm weld on 10 mm mild steel plate. The predicted weld pool dimensions, length, depth and width, for the coarse mesh were no more than 4% different form those of the refined mesh. In addition, the cooling rates differed only by about 2% in the high temperature region between 1750 K and 1050 K and by a small fraction of a percent below 1050 K. This level of discrepancy can be expected of any two finite element models which have a different mesh arrangement irrespective of whether one mesh is finer than the other. Hence, it is concluded that no significant loss of accuracy occurs by using elements in the fusion area as large as 2.8 mm^3 - possibly larger, however models within this work will remain under this 'safe' limit unless otherwise justified.

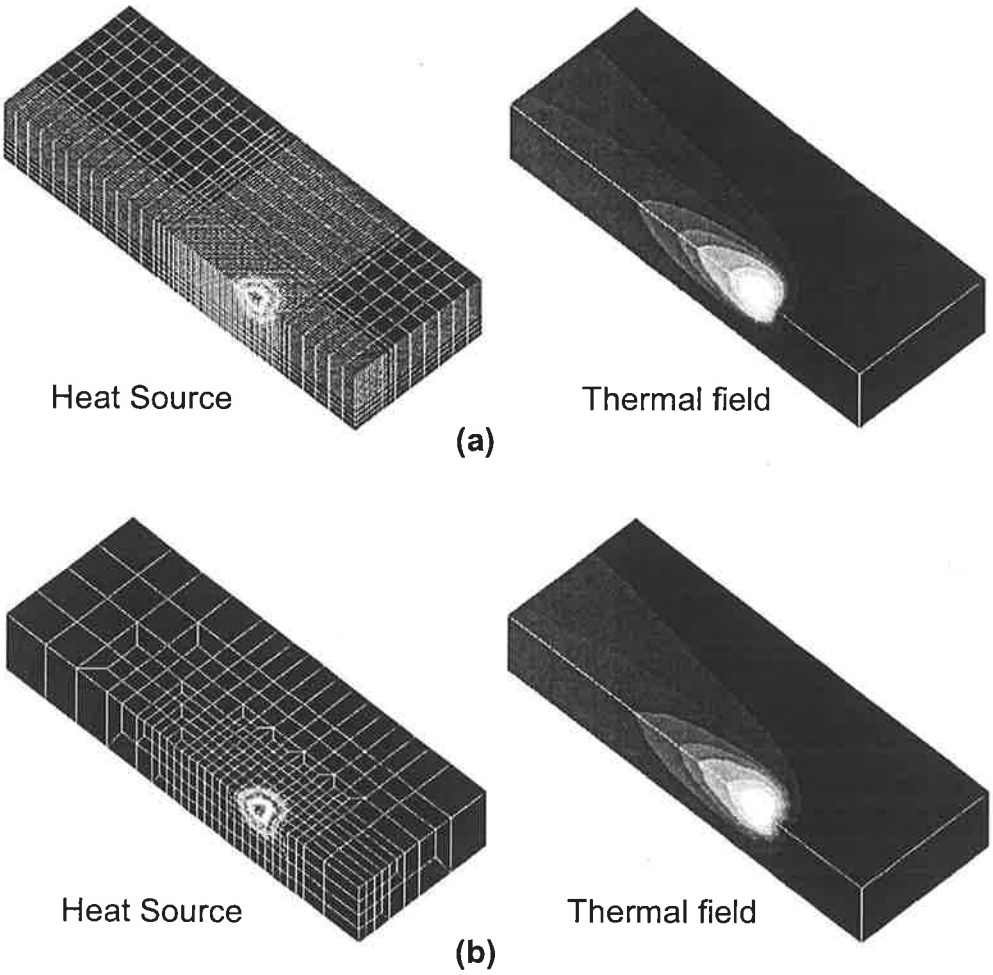

Figure 2.8 Half section meshes **(a)** refined mesh, **(b)** coarse mesh.

Goldak & Bibby *et al.* (September 1986) claim that purely for the reason of capturing the inflection of a Gaussian heat flux distribution, four quadratic elements are needed along each axis. This suggestion is also adhered to in this work.

2.3.2.2 Approximating A Semi-Infinite Plate

The models used in this work are not true QSS models because this would require a semi-infinite plate to be meshed. To simulate a semi-infinite plate, a constant temperature boundary condition is applied to the front face of the plate and an adiabatic boundary condition at the end of the plate, as explained in Section 2.2.4. FE models were produced to show that no accuracy is lost by using this approximation. Initially a model of 950 mm length was meshed so that at the end the cooling rate is 0.01 K/mm which is near enough to adiabatic. The thermal result of this mesh was used as a gauge for shorter meshes. It was found that relatively short meshes still approximated a semi-infinite plate with only a small error in temperature at the end of the plate. For example the centre line cooling curve for a relatively short mesh of 110 mm length is shown in Figure 2.9. The peak deviation from the semi-infinite result is only 3% at the adiabatic boundary, with the deviation only in the last 5 mm. This figure also shows that the effects of the heat source do not reach more than 15 mm in front of the arc centre and so whether there is infinite length of mesh in front of the arc, or only 15 mm makes no difference. All models in this thesis were meshed so that the front of the plate is well before the thermal influence of the heat source. As a result of the above discussion, it is concluded that the mesh arrangement used in this work adequately represents a semi-infinite mesh.

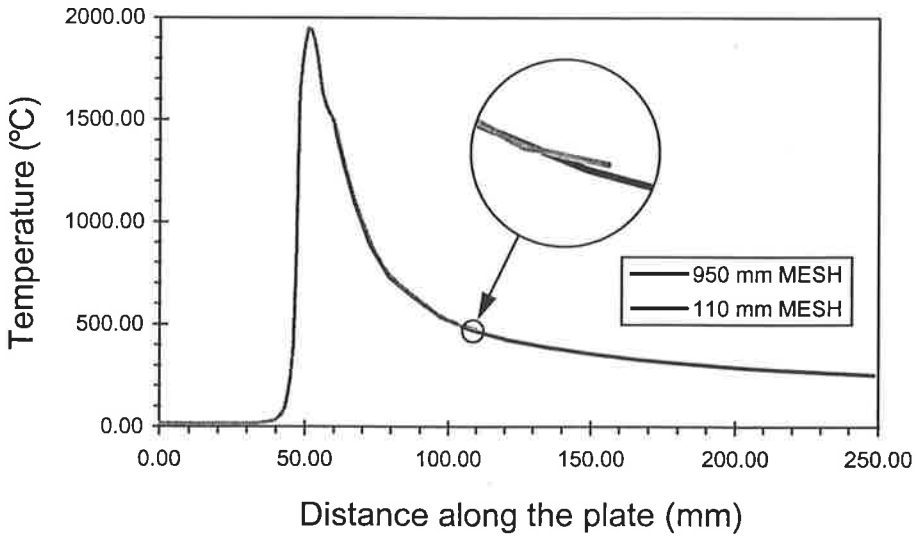

Figure 2.9 Verification of the semi-infinite plate approximation.

2.3.2.3 Validifying QSS Using Transient Models

As explained in Section 2.2.4, the plate takes a period of time to reach a quasi steady state condition. Two identical models were run, one with a QSS and one with a transient solution. By comparing the differences in the calculated temperature fields, the applicability of the QSS solution can be gauged. The weld conditions modelled were high heat input and high velocity as this is a worst case in terms of how fast the transient solution reaches steady state. It is not intrinsically obvious why high heat input takes longer to reach steady state, however it is demonstrated by Mangonon *et al.* (1986): for 1.58 kJ/mm QSS penetration is achieved after 3.5 sec; for 3.15 kJ/mm it takes 5.5 sec and for 4.72 kJ/mm it takes 7.5 sec. In terms of how far down the length of a weld before QSS is reached, high velocity is the worst case, since for a given time, the higher the velocity, the greater the distance travelled before QSS is reached. A heat input of 1.8 kJ/mm and velocity of 5 mm/sec were used on a 10 mm mild steel plate. Note that these conditions are not very high generally speaking, but in terms of the models in this thesis they are high. The heat was modelled as a line of four elements loaded with an equal share of the heat. This simple heat source definition was chosen due to the ease of replicating it identically in the transient and QSS models. The heat source and mesh are shown in Figure 2.10.

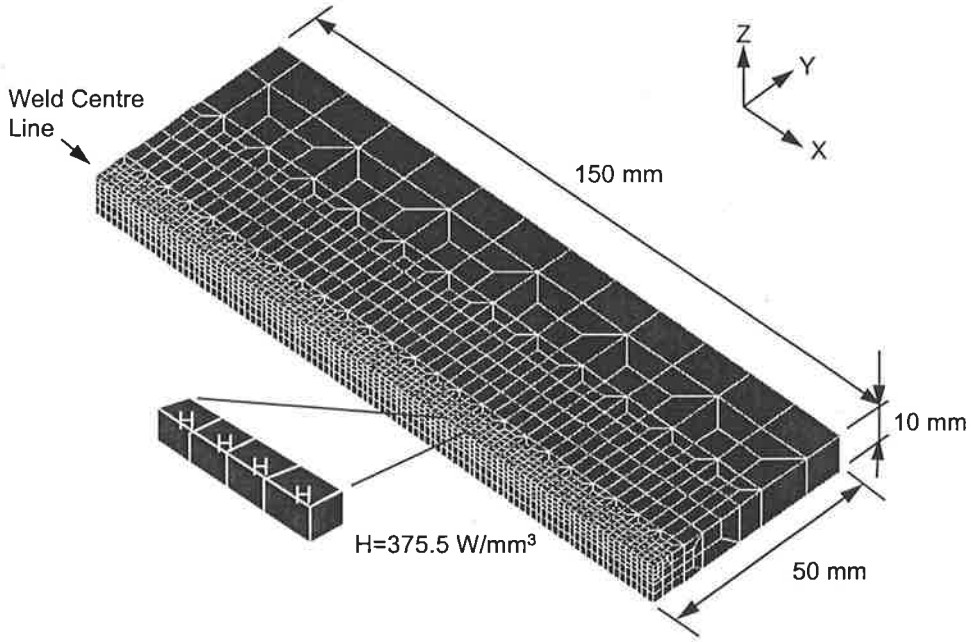

Figure 2.10 Mesh for Transient and QSS models with heat source (1/2 section).

The cooling curves calculated by the transient model at a distance of 5 mm from the weld centre line and in the middle of the plate depth-wise, are shown in Figure 2.11 (a). It can be

seen that QSS is reached before 10 seconds at this location relative to the arc. The 5th cooling curve (Figurre 2.11 (a)) which is obtained from a node located 60 mm (or 8 seconds) from the start of the weld is superimposed with the QSS cooling curve in Figure 2.11 (b) revealing a near perfect match.

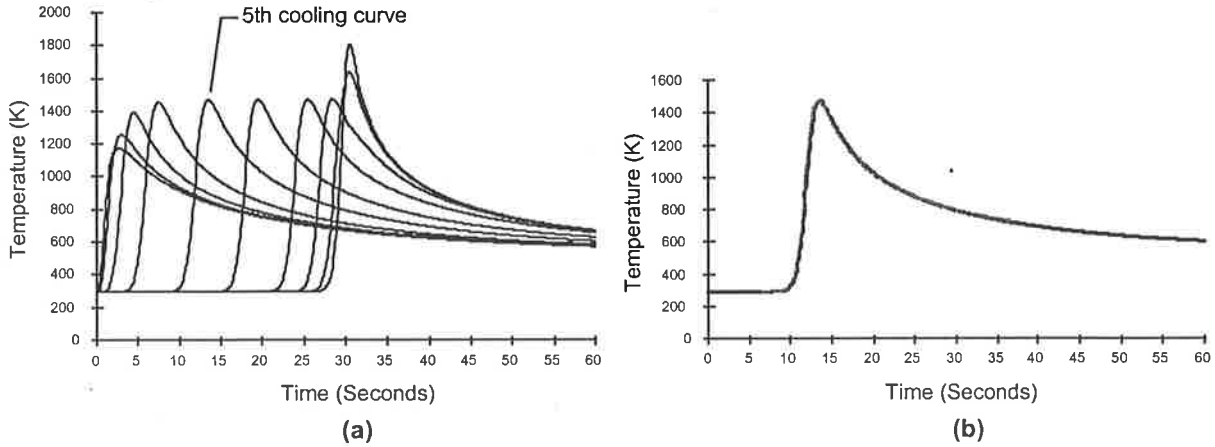

Figure 2.11 (a) Comparison of Cooling Curves at Different x-locations, **(b)** Comparison of QSS and Transient Cooling Curve for the same location.

In order to observe how the error varies with x-y location a map of the error of the transient solution relative to the QSS solution has been derived and is shown in Figure 2.12. A negative error indicates that the transient result is lower than the QSS. The error in the peak temperature is less than 5% for most of the plate and very close to zero for a very large portion. The error in the cooling rate is shown in Figure 2.12 (b). Note that the error is not calculated to the edge of the plate since the cooling rate here is very close to zero and it is difficult to get a meaningful percentage error. Besides, the cooling rate far beyond the HAZ is generally not of great interest. The error in the cooling rate, is significant in the HAZ for about the first and last 35 mm of the weld. The error is still close to zero for most of the heat affected zone.

The above results show that transient solutions do tend to the QSS solution in the HAZ except at the start and end of the weld. The most important point to be derived from this is that the results extracted from experimental welds must be taken from the pseudo-steady-state region of the weld if they are to be used to gauge the accuracy of a QSS model. If this is done then the error in the QSS results will be: negligible for the peak temperature and pool profile, and less than 3% over prediction for the $T_{8/5}$ value. All the experimental measurements taken for this work were in the pseudo-steady-state region of the weld.

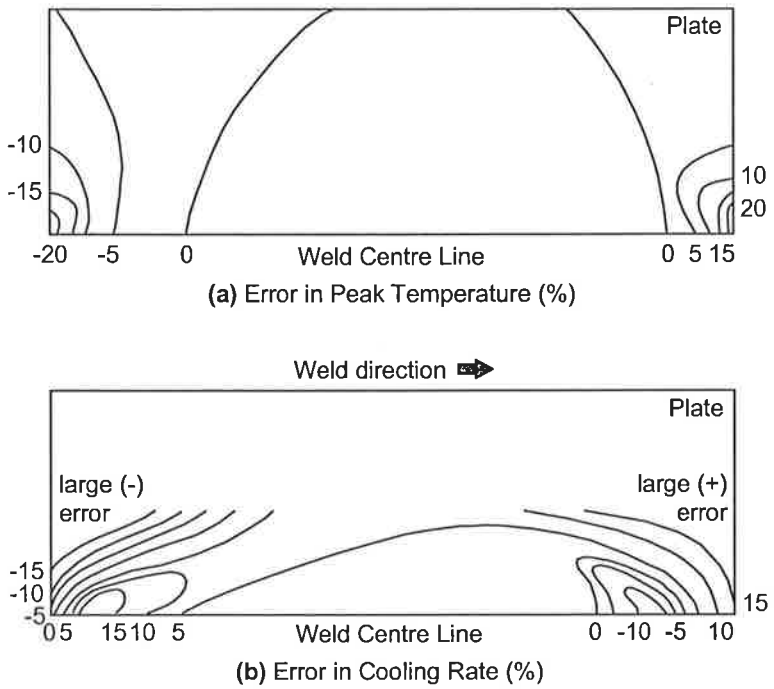

Figure 2.12 Error in transient relative to QSS solution for **(a)** Peak temperature **(b)** Cooling rate.

The above results do indicate that for short welds it is advisable to use transient models. Besides, for a short weld the duration of the weld and hence the number of time steps required is low and computationally affordable.

There are very few researchers who have done an analysis of QSS relative to transient results. Just as a means of comparison to the above discussion: Barberis *et al.* (1996) showed by FEA that pseudo-steady-state is achieved after only 15 mm of weld for 0.75 kJ/mm at 3.2 mm/s. Satonaka *et al.* (1993) investigated experimentally the time taken to reach pseudo-steady-state for GTA welding on steel 9 mm thick after a step change in velocity. When changing from 0.58 kJ/mm at 4 mm/s to 2.1 kJ/mm at 1.1 mm/s pseudo-steady-state was reached after 50 mm for peak temp, and after 25 mm for thermal gradient.

Chapter 3

HEAT SOURCES

3.1 INTRODUCTION

The energy expended in the welding process is applied to the models in terms of a heat source distribution. Deriving the most effective distribution is one of the principal aims of this thesis. This chapter revises the historical development of heat sources discussed in Section 1.4.1, proposing some adaptations as well as presenting some novel approaches. The resulting heat sources are applied and tested for various weld configurations in Chapter 4.

The earliest analytical models used point or line heat sources. This caused problems in the near weld region with temperatures tending to infinity at the source location. During the 1970s, Gaussian distributed surface heat sources were recognised as a superior heat definition, producing thermal predictions which were more accurate close to the weld. For conduction based models, this surface heat source was generally supplemented by enhancing the thermal conductivity of the molten material. This reflects the rapid convective heat transfer which is present in the molten material but not modelled in conduction models. An alternative means to ensure that the heat is rapidly spread below the surface into the molten zone is to actually place the heat within a volume below the arc. In the mid eighties, Goldak's double ellipsoidal heat source became the most common volumetric heat source.

The above heat sources did not adequately model GMAW for which the droplet heat content is significant, often resulting in finger penetration. As a result, heat sources were developed specifically for GMAW. The predominant means of achieving this was by separating the heat into two components, one from the arc and one from the droplet. Literature showed these components of heat to be added either as two surface sources, as one surface and one volumetric source, or two volumetric sources. An alternative was to use a surface heat source with an anisotropically enhanced thermal conductivity to reflect the penetration of the droplet, and hence its heat, into the material. Each of these approaches will be addressed in the following sections to come up with the favoured heat source definitions to be trialed in this work. In addition, there will be several novel approaches discussed.

The welding heat is added to the elements of the model as a boundary condition. The form of the heat source is defined within a Fortran program which produces an output file containing the boundary conditions in a format that can be read by the FE software. The value of the heat flux in the element is found by the value of the heat source function at the centre of the element. To ensure that the total heat applied is correct despite the discrete application of the heat source function, the Fortran program sums the heat applied to each element. This sum is generally a small percentage different from the specified total and so the appropriate correction factor is applied to the heat flux at each element.

3.1.3 SIMULATING CONVECTIVE FLOW

As discussed in Chapter 2, the model is conduction based. This poses the question: how do we choose a suitable heat source definition to compensate for the absence of convective flow in the weld pool?

A conduction based model will be no less accurate than a convective model if the heat within the weld pool can be distributed in the same manner that the convective flow would distribute it. This can be achieved by suitably defining the heat source and possibly enhancing the thermal conductivity, as a function of the flow in the weld pool. The flow is affected by many forces which were summarised in Figure 1.4. Davies (1995) investigated the relative magnitude of these weld pool driving forces for GMAW and the results are shown in Figure 3.2.

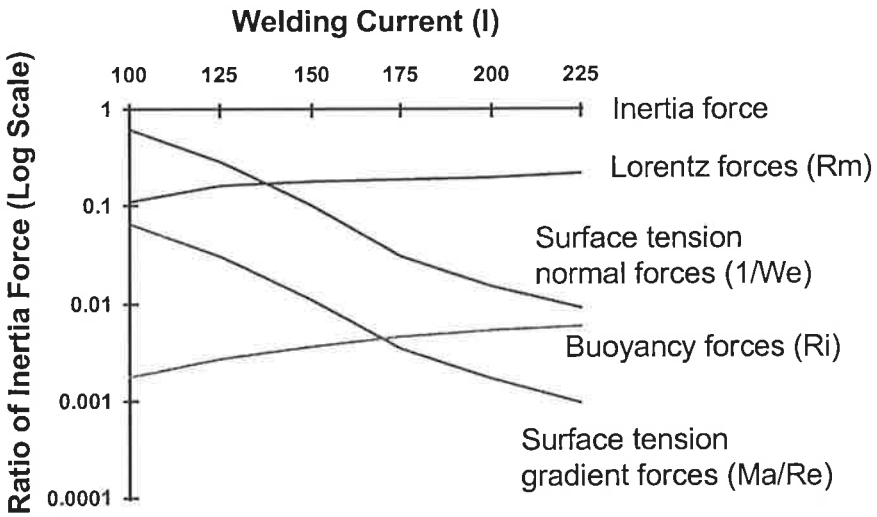

Figure 3.2 Relative magnitude of forces driving weld pool convective flow in GMAW. (Davies 1995).

This figure shows that the inertia force is dominant over most practical welding currents. At the lower scale of the currents used in this work, the surface tension normal forces due to curvature are significant. Over the range of currents used in this work, the electromagnetic force known as Lorentz force may have a small impact. The following will discuss what effect these three significant forces have on the flow and how can they be tied into the heat source definition:

The droplet inertia force has two effects: it deforms the weld pool surface making it concave; and, it induces a circulating flow pattern dominated by down flow beneath the arc as shown in Figure 3.3.

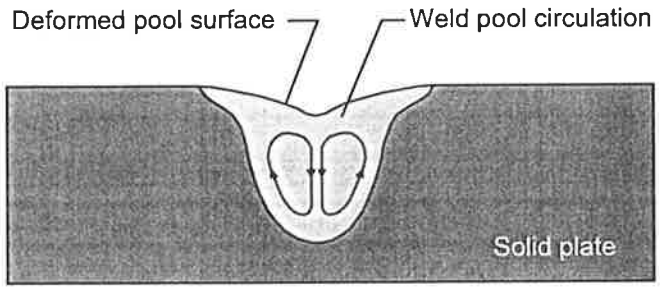

Figure 3.3 Flow pattern induced by the droplet inertia force.

The surface tension normal force acts to resist the pool deformation induced by the inertia force, while the Lorentz force adds to the flow pattern induced by the inertia force. This effect of the Lorentz force was demonstrated by Atthey (1980), since in the absence of other forces a flow pattern similar to that shown in Figure 3.3 was produced. This can be assumed to be the flow pattern occurring in GMAW since there are no other significant forces to alter it. In terms of defining a heat source distribution this result points towards a heat source which concentrates the heat input of the droplet in the region below the arc where the flow carries it. Alternatively, an enhancement of the thermal conductivity in the direction of the dominant flow could be proposed.

The effect of the deformation of the weld pool surface is to significantly alter the distribution of the arc heat source and this will be explained in detail in Section 3.2.

One check that can be carried out to indicate wether the heat in the weld pool is realistically distributed is to look at the peak surface temperature. Zacharia *et al.* (1991) and (1993) modelled GTAW and included convection and evaporation to show the peak surface

temperature was about 2850 K. This may provide a useful indicator for the successful distribution of heat in conduction models.

The following sections detail the established heat source definitions as well as proposing some modified or novel approaches to defining the heat source. A sample of the heat source definitions are trialed on the models in Chapter 4 to gauge their effectiveness.

3.2 GAUSSIAN SURFACE HEAT SOURCE

The Gaussian heat source was initially developed for GTAW by Pavelic *et al.* (1969). It is founded on the experimental observation by various researchers, such as Tsai & Eagar (1985), that the spread of heat on a flat plate for a GTAW closely approximates a Gaussian distribution. Despite the heat source having its basis in GTAW, early modellers, for example Eagar & Tsai (1983), did attempt to apply it to GMAW. It has become apparent that some form of modification is needed to account for the extra component of heat from the metal transfer in GMAW. Hence, the Gaussian source has limited applicability in this work, however, it will be outlined here as it can be a useful component of more complex heat sources which will be discussed in following sections. In addition, an important observation by Weiss *et al.* (1995) regarding the coupling of a Gaussian style heat distribution to the deformation of the weld pool will be presented here.

The components of the heat applied by the arc are the summation of convection from the hot gasses, electron flow, and radiative heat flux. These combine as shown in Figure 3.4 (a) (from Choo *et al.* 1990) to form an approximate Gaussian distribution. This distribution is represented as a heat source as shown in Figure 3.4 (b) and the heat flux q (W/mm^2), at any radius r can be expressed by Equation 3.3.

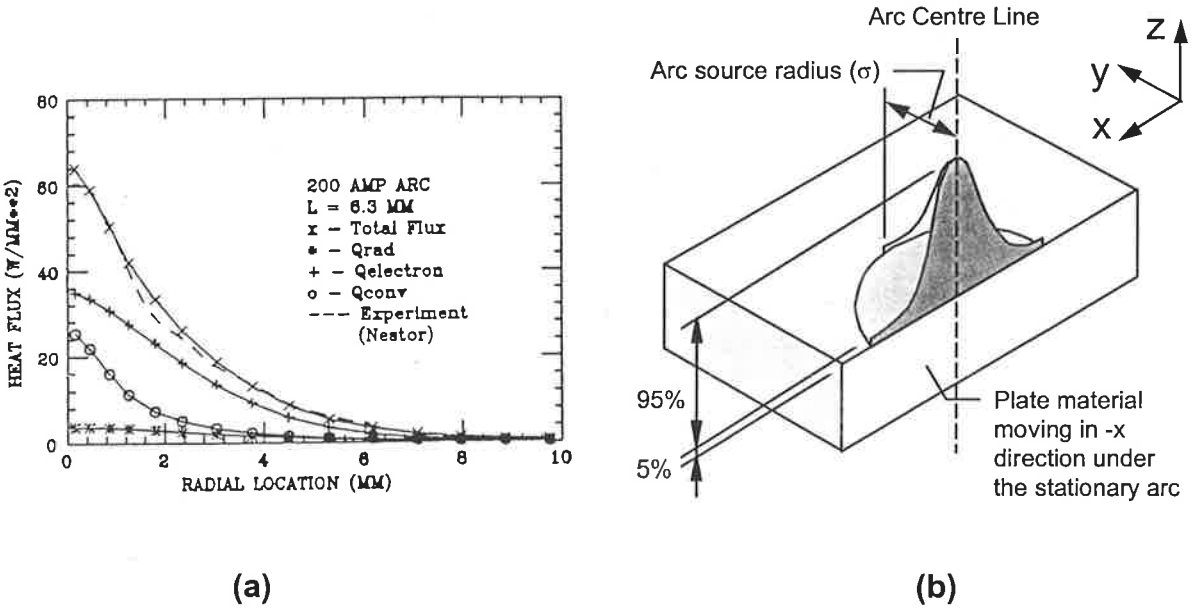

Figure 3.4 The Gaussian Distribution: **(a)** measured with its components (Choo *et al.* 1990), **(b)** represented as a heat source.

$$q(x,y) = \frac{3\eta VI}{\pi\sigma^2} e^{-3\frac{r^2}{\sigma^2}} \quad (3.3)$$

Here V is the voltage, I is the current, η is the welding process efficiency and σ is the characteristic radius of the flux distribution. The characteristic radius is defined as the radius at which the heat flux has dropped to 5% of the peak value. Any elements with their centre within this radius were loaded with a heat flux as described in Section 3.1.2.

The characteristic radius used for the surface Gaussian heat sources in this thesis is 5 mm unless otherwise specified. Work by Nestor (1962), Tsai & Eagar (1985), Lee & Na (1997) all indicates that the distribution parameter should increase with both current and arc length. Hong *et al.* (1993) however, found that the thermal prediction is not highly sensitive to the spread of the arc heat source. Presumably this is because a reduction in the radius is counteracted by an increased peak heat flux which drives the heat radially outwards. They suggest that "accurate knowledge of the value of the arc distribution parameter may not be required for GMA weld predictions". This gives some grounds for using a constant characteristic radius over a range of currents; a constant radius also prevents the introduction of too many unknown parameters into the heat source definitions. Experimental values for the characteristic radius and values used by other researchers vary somewhat, but indicate that 5 mm falls in the observed range. For example, the experimental result plotted in Figure 3.4 (b) is from Nestor (1962) who measured the distribution of heat flux for GTA welding. The characteristic radius of this approximately Gaussian experimental distribution is 6.2 mm. The result is for Argon gas at atmospheric pressure, a current of 200 A, and an arc length of 6.3 mm which are relatively typical weld conditions for the experimental work done in this thesis. For a 5.5 mm arc length and 190 A, Tsai & Eagar (1985) measure the characteristic radius to be 6.8 mm. Lee & Na (1997) showed that the characteristic radius changed from about 4 to about 6 mm as the arc length varies from 2 to 5 mm at 150 A. Hong *et al.* (1993) use 3.9 mm over a range of currents from 150 to 300 A.

3.2.1 EFFECT OF DEFORMED SURFACE

In most cases, the ideal of the arc hitting a flat surface is not a reality in GMAW. The molten pool surface on which the arc is applied is often quite concave due to a combination of the droplet impact, arc pressure and other forces mentioned in Section 1.4.2.3. In addition, with a joint which has a deep preparation such as a V-joint weld the surface which the arc strikes

is far from flat. This has a significant bearing on the distribution of heat attributed to the arc so that the heat intensity is not independent of the vertical coordinate, *z*, as in Equation 3.3.

Figure 3.4 (a) showed that the most significant source of heating is the electron flow from the current density. The convective heat input is also significant close to the arc centre and is a result of the arc temperature which again depends on the current density. Hence, if the current density distribution is found to be significantly altered by the deformation of the weld pool then it is to be expected that the approximately Gaussian heat source would also be changed significantly. The question of course is, how is it altered?

Choo *et al.* (1990) presented an excellent paper, calculating the effect a deformed weld pool has on the current density, the heat transferred to the pool and on the flow patterns resulting. It predicted that as the weld pool surface deformation increased, the distribution of current was no longer Gaussian but becomes a bi-modal distribution. An example of Choo's results are given in Figure 3.5, showing the calculated arc current distribution and the corresponding heat flux for a 1.8 mm depressed pool.

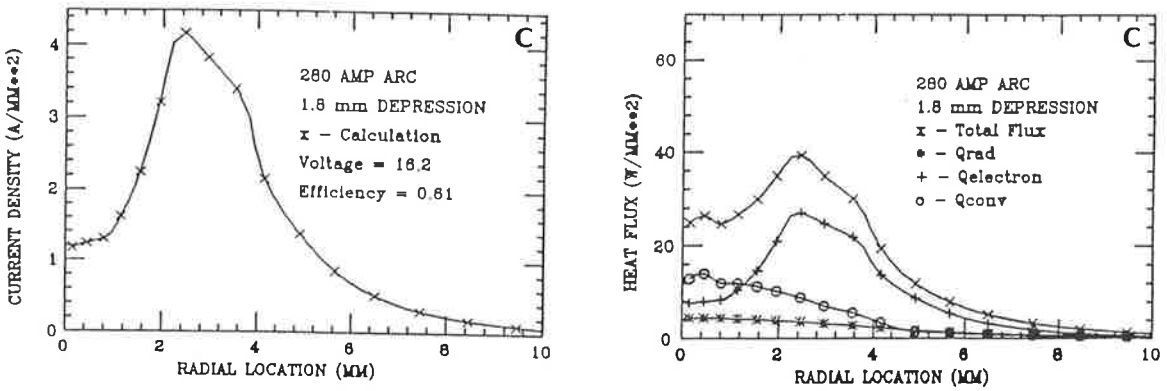

Figure 3.5 From Choo *et al.* (1990): **(a)** Current density distribution, **(b)** Heat flux distribution.

The form of the heat flux is obviously very closely related to the current density. In this thesis the heat flux will be approximated as proportional to the current density.

The next question is how is the current density found? Weiss *et al.* (1995) point out that the arc electron flow is supplied to those places with the lowest transitional resistance. The resistance is predominantly related to the distance between the electrode and the weld surface. As a result, Weiss *et al.* suggest it is possible that for a deformed surface, the heat

source intensity due to the welding arc should appear as shown in Figure 3.6 (a), which corresponds to Choo's (1990) bi-modal form of distribution. Applying the conventional flat plate intensity distribution (Gaussian) to a deformed surface would result in the distribution shown in Figure 3.6 (b).

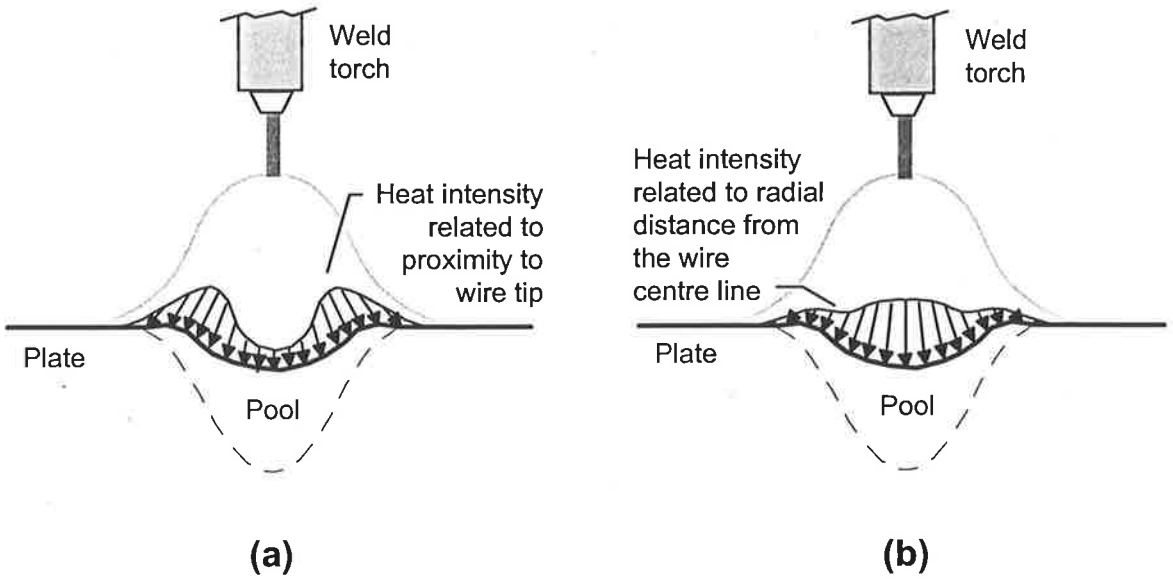

Figure 3.6 Arc heat distribution for a deformed surface: **(a)** proposed by Weiss *et al.* (1995), **(b)** conventional distribution.

There is clearly a significant difference: consider for example points A and B on Figure 3.7 (a). They are both the same three dimensional radius (r_{xyz}) from the electrode wire tip, so they have the same transitional resistance, hence the same current density, and so, the same heat flux too (if heat is assumed proportional to current). There is, however, a big difference in their two dimensional radii (r_{xy}), so according to the conventional Gaussian heat distribution, A should have close to the peak value and B close to the minimum, rather than them having the same heat flux.

Equation 3.3 representing the Gaussian heat flux will be modified to make it relevant to a deformed surface. Referring to Figure 3.7 (b), the point on the deformed surface closest to the electrode wire tip (C) should have the peak value, and the heat source will be centred around this point. The flat surface Gaussian centred around point C is superimposed on the figure. This Gaussian can be used to find the heat at every point on the deformed surface by finding a point on the flat distribution which has the same r_{xyz} from the electrode tip. For example, point D and D* have the same r_{xyz} and so D should have the heat flux value of point D* on the flat surface Gaussian (q_d). This heat flux can be found from Equation 3.3

using an effective radius equal to the distance CD*. Hence, for any point D on the deformed surface, an effective radius can be found:

$$r^2_{eff}=CD^{*2}$$
$$=OD^{*2}-OC^2$$
$$=OD^2-OC^2$$

It should be pointed out that once the heat is applied to a deformed surface in this way, it must be integrated and then scaled so that the total heat flux is correct.

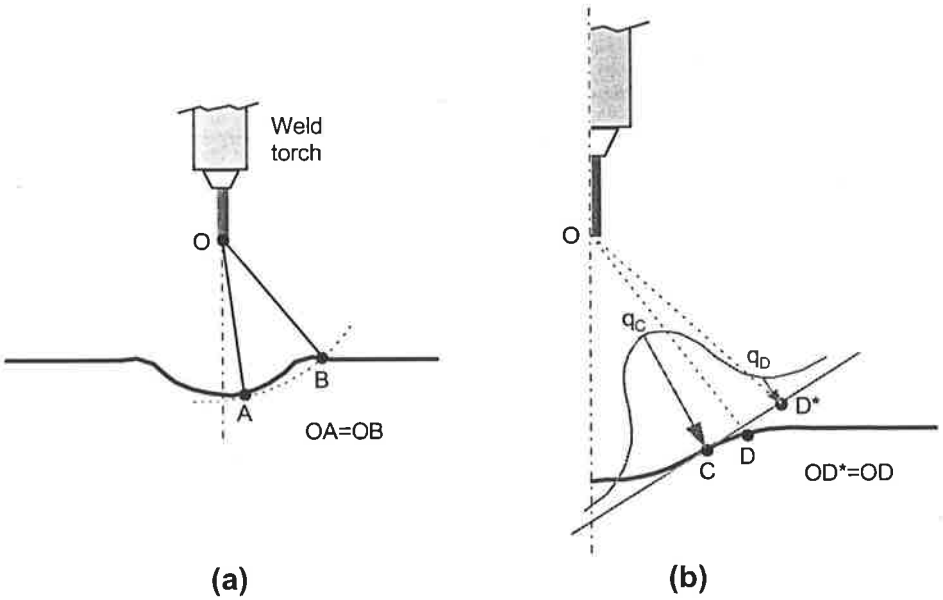

Figure 3.7 Modifying the Gaussian heat source for a deformed surface.

The above reasoning appears to yield a similar result to Weiss *et al.* (1995), but in a somewhat simpler manner. Weiss *et al.* (1995) argue that the transitional resistance is also dependent on the amount of metal vapour at different locations in the arc. This is determined by the surface temperature of the weld pool, making the heat source and pool temperature coupled. This is not accounted for in this thesis since the variation of metal vapour is a secondary effect, and besides, the temperature at the pool surface is not necessarily accurate for a conduction model.

The significant difference between the flat and the surface dependent heat source displayed in Figure 3.6 has surprisingly been disregarded in almost all work observed to date. It appears to be a major oversight which it is hoped this thesis will help to offset. The significance of the deformed pool surface heat distribution will be demonstrated in the chapter on model application.

3.3 DOUBLE ELLIPSOIDAL HEAT SOURCE

As discussed in Section 1.4.1.2, the Double Ellipsoidal (DE) heat source was developed to reflect the distribution of heat within the weld pool caused by convective flow. The heat source distribution is based on physical understanding that "the stirring velocity must decay to zero at the fusion zone boundary and rise to a maximum at the arc-weld interface" (Goldak *et al.* 1985). To reflect this, the heat is a peak at the surface of the weld pool and decays to zero at the fusion zone boundary, with a Gaussian decay. The result is an equation of the form shown below:

$$q(x,y,z) = q_0 e^{-(Ax^2+By^2+Cz^2)} \tag{3.4}$$

The constants (A,B,C) are calculated so that the total heat input is ηVI and so that the heat source decays to 5% of the peak value at the extremities, say $x=\pm a$, $y=\pm b$, $z=\pm c$ and this is outlined in Goldak *et al.* (1985). The result is shown in Equation 3.5 which is the Ellipsoidal Power Density Distribution,

$$q(x,y,z) = \frac{6\sqrt{3}\eta VI}{abc\pi\sqrt{\pi}} e^{-3\left(\frac{x^2}{a^2}+\frac{y^2}{b^2}+\frac{z^2}{c^2}\right)} \tag{3.5}$$

To become double Ellipsoidal, Equation 3.5 is simply considered separately for the front and rear sections of the heat source as illustrated in Figure 3.8. A certain fraction of the heat is added to the front of the heat source and the remainder to the back, by multiplying the heat flux by f_f and f_b respectively. Also, the value of a is different when calculating the front and back (a_f and a_b respectively).

The resulting heat source definition has 6 tunable parameters which can be used to match calculated and experimental thermal fields. The heat source was developed by Goldak *et al.* (1985) for the purpose of producing an accurate temperature field for residual stress calculations. The intention, perhaps, was not to produce a model capable of *predicting* accurate weld pool dimensions, because experimental results were needed to tune the heat source for each weld condition.

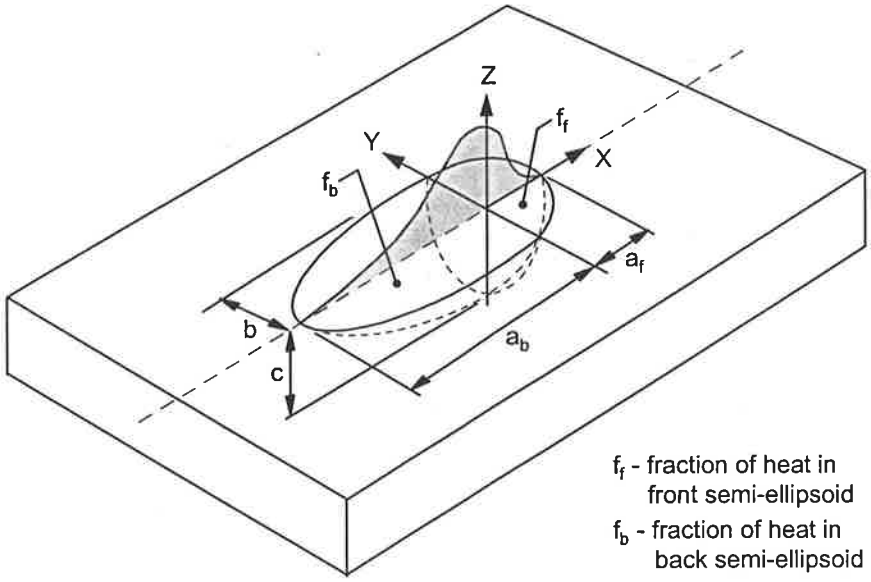

Figure 3.8 Goldak's Double Ellipsoidal heat source (1985).

Goldak *et al.* (1985) suggested appropriate values could be chosen for the DE heat source parameters by taking measurements from a weld: b=1/2 weld width, c=weld depth, a_f=1/2 weld width, a_b=2weld width, f_f=0.6, f_b=1.4. Liew *et al.* (1993) showed, using a 2D model, that it is not always possible to tune the DE heat source, even with these many parameters, since a set of parameters tuned to the best penetration prediction does not necessarily give the best $T_{8/5}$ calculation and visa versa. It would need to be a degree of compromising the results with the parameters. For this reason and since the Double Ellipsoidal heat source will be used primarily to give a gauge against which to test the more novel heat source definitions presented in this work, effort will not be expended in completely fine tuning each welding condition.

3.4 SPLIT HEAT SOURCE

The concept behind the split heat source is that the arc provides heat to the surface of the weld pool while the heat contained within the molten droplet is carried by its momentum into the molten pool below the surface. This physical effect results in what is referred to as finger penetration, as discussed in Section 1.3.2, rather than the hemispherical pool shapes observed in GTAW. As a result, the split heat source was conceived in which the arc and droplet heat are added as separate components, and located to reflect the physical arc and droplet heat distribution. Section 1.4.1.3 gives a historical background to this development. The heat content attributed to the molten droplets is added either within the volume of the weld pool as a flux or defined temperature, or as a concentrated surface heat source. The remaining heat is attributed to the arc and added as a surface heat source, or within the volume of the pool. The combinations observed in literature are summarised in Figure 3.9.

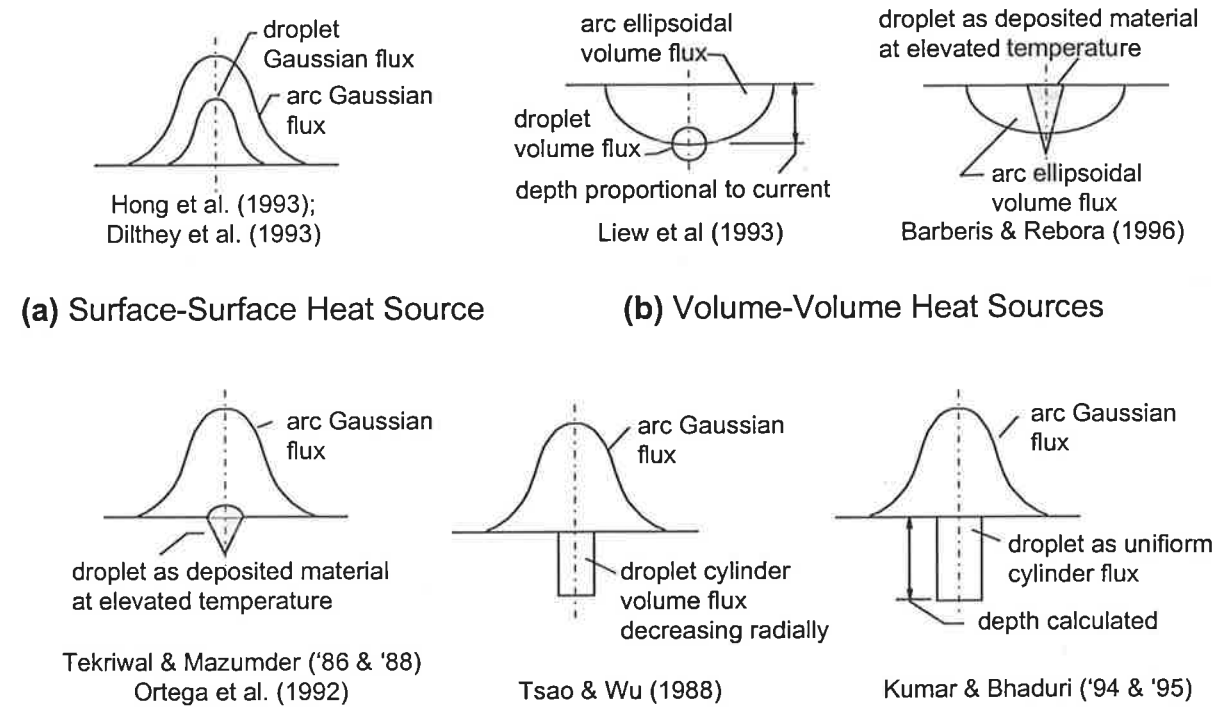

Figure 3.9 Split heat source types from literature.

The split heat sources require an estimate of the heat applied to the weld piece by the transferred material:

How much heat is in the droplet?:

There have been two approaches to answering this question:

1) Assume a set fraction of the total heat is contained within the molten droplets.
2) Assume the droplets are at a set temperature and find the heat content by the enthalpy of steel at this temperature multiplied by the material flow rate.

If the first method is used, there seems to be a range of quoted values for the fraction of heat contained in the droplet. For example, Essers & Walter (1981) attribute about 25% to the droplet while Johnson *et al.* (1991) claim about 35-40% of total is in the droplet.

Far more common, and having stronger experimental grounds is the second method of using the droplet temperature and flow rate. Jelmorini *et al.* (1977) measured droplet temperature to be about 2400°C. Waszink & Wan den Heuvel (1982) used a similar approach and estimated the droplet temperature to be 2400 ± 100°C for 1.2 mm electrode wire. Essers & Walter (1979) experimentally measured the droplet temperature to range between about 2090°C at 125 A and 2150°C at 225 A. Johnson *et al.* (1991) measured the droplet temperature to be in the range 2227-2927°C. Bozhenko *et al.* (1997) have numerically found the droplet temperature to be limited to about 2500°C by evaporation effects.

Based on the above, the droplet energy in this work is found using a droplet temperature of 2400°C. At this temperature, the energy contained within the droplets is 14.48 J/mm^3 based on the enthalpy values from Moore *et al.* (1985). With a density of 6.285e^{-3} g/mm^3 (extrapolated from Pardo & Weckman December 1989), the energy becomes 2304 J/g.

What is the metal transfer rate?:

Modelling of metal transfer is discussed in Section 1.4.4.1. Two theories put forward to qualitatively explain metal transfer are the pinch instability theory (PIT) and the static force balance theory (SFBT), but these provide only general trends. Kumar & Bhaduri (1995) used these theories to predict droplet radius, velocity and frequency to apply for their split heat source. The results predicted general trends in terms of finger penetration when the PIT was used. Numerical models to predict metal transfer, such as those by Haidar & Lowke (1996), could be used but are outside the scope of this work.

Many researchers have developed regression equations, some of which have some theoretical basis in the form of the equation. Some of these are outlined in the section on

modelling metal transfer. The regression function for wire feed rate proposed by Pilarczyk *et al.* (1994) was tested for the wire feed rates measured in this work over a range of weld conditions for direct current GMAW with Argon rich gas. The results showed the regression functions under predicted the wire feed rate by 11.1% with a 90% confidence interval of ±3.1%. This is reasonable accuracy, but shows a clear trend of under predicting the wire feed rate. The difference could possibly be due to the fact that Pilarczyk measured the wire feed by welding onto flat plate while the measurements which were made to test the function were into v-groove welds.

There was a concern that the use of PIT or regression equations for wire feed rate could introduce errors into the split heat models such that it would be unclear as to where model errors originated from. That is, wether the accuracy of the model was limited by unsatisfactory wire feed rate information or the model's own limitations. As a result, for the following research, wire feed rates were measured during welding and empirical equations derived directly from these measurements. After Liew & Painter *et al.* (1993) a linear equation between feed rate and current was generated.

3.4.1 SURFACE-SURFACE

Researchers have attempted conduction based models with a split heat source using two Gaussian surface heat sources - one to represent the arc heat and one to represent the droplet (refer to Figure 3.9 (a)).

Hong, Weckman, Strong and Pardo (1993) applied the idea of the double Gaussian heat source with a uniformly enhanced thermal conductivity factor of 10 and it was assumed that 50% of the heat input was contained in the droplet; an empirical regression equation for the efficiency as a function of welding speed, contact tube to work piece distance, voltage and current was used. They assumed that the droplet distribution parameter was equal to the wire diameter and experimented with different arc distribution parameters. The pool width and depth were both found to be about 27% over predicted when compared with experimental data in the range of 150-300 amps. By manually tuning the efficiency, these errors were reduced to about 8% over prediction of width and 8% under prediction of penetration.

Dilthey *et al.* (1993) used two Gaussian surface distributions; the spread of the distributions were empirically related to the current, stick out, gas type, wire diameter and transfer type. This resulted in the spread of the droplet heat and arc heat being over similar radii. The

proportion of heat assigned each is not explained. The results are good for the predicted width but the error is great for the predicted penetration.

Based on the above results and the reasoning that the droplet heat is actually distributed below the surface, the double surface Gaussian heat source was not used in this work. Besides, the sum of two Gaussian heat sources of a similar diameter is not significantly different from a single Gaussian with a greater peak value. Hence, the results are not expected to be much better than for a single Gaussian heat source.

3.4.2 VOLUME-VOLUME

Two examples of volume-volume split heat sources are shown in Figure 3.9 (b). Barberis and Rebora's work (1996) has the droplet heat added by filling the joint preparation with material fixed at the droplet temperature based on Tekriwal & Mazumder's work (1986 & 1988). This concept is reasonable and has shown to yield quite good results, however, the method of representing the droplet heat as a flux is chosen in preference in this work. The reason is that the fixed temperature concept works for joints with a deep penetration, where the bead material is added deep into the weld. However, for joints with little or no preparation such as butt joints, the weld bead would be added on the surface and the penetrating effects of the droplet would not be included. Also, the assumption is made that all the material within the joint preparation is at a uniform temperature. Experimental results for V-joint welds in Section 4.2 show that despite material flowing to the base of the preparation, it can be at a reduced temperature so that it does not actually fuse with the joint walls. This results in an effective penetration less than the depth of the preparation and this is impossible to predict using the fixed temperature approach.

The split heat source developed by Liew & Painter *et al.* (1993) consisted of a shallow double ellipsoid together with a uniformly distributed spherical volume source. The sphere is at a depth proportional to the welding current. This is based on experimental evidence by Essers and Walter (1979) that the penetration of a GMAW is proportional to the current. This concentration of heat below the surface fits well with the conclusion of Section 3.1.3 that the heat should reflect the dominant downward flow pattern. It works on the assumption that the droplet basically remains intact, punching its way into the pool and then dissipating its heat at a depth. The diameter of the droplet was taken as 3 times the wire diameter. It was shown to be successful in predicting finger penetration and also has the advantage that the heat source is valid over a range of currents.

The Liew & Painter heat source was investigated to some degree in this work, but yielded quite narrow weld pools. A similar concept was used but with the arc heat as a surface Gaussian, which widens the predicted weld pool somewhat, and this will be discussed in the following section.

3.4.3 SURFACE-VOLUME

The most commonly observed approach to splitting the heat source is to use a surface heat source for the arc and distribute the droplet heat within a volume (refer to Figure 3.9 (c)). This is understandable in that it represents the way the heat is physically applied, and hence, this will be the type of split heat source trialed in this work.

Tekriwal & Mazumder (1986 & 1988) and Ortega *et al.* (1992) used the concept of the bead being added at the droplet temperature, but for the reasons discussed in the previous section, this is not pursued. Tsao and Wu (1988) had the droplet heat in a cylinder below the arc centre, with the flux decreasing radially outwards. No information is given as to the radius or depth of the cylinder. The use of a cylinder for the droplet rather than a sphere such as Liew et al., reflects the idea that the droplet heat dissipates by mixing as it penetrates the pool, leaving a stream of hot material behind it. Kumar & Bhaduri (1994 & 1995) also use a cylinder for the droplet, distributing the heat uniformly within it. The diameter is defined as twice the droplet diameter, resulting in a range of 2.0 to 3.2 mm diameter cylinders. The depth of the cylinder is calculated using an energy balance developed by Lancaster (1984). They derive the depth that the droplet distorts the weld pool surface by equating the kinetic energy of the droplet to the work done to create the new cavity surface and to displace the fluid. The amount the cavity flows back between droplets is calculated to find the minimum cavity depth. The droplet heat is then applied as a cylindrical volume between the plate surface and a depth of one droplet diameter below the minimum cavity depth. Although this concept has appeal in terms of calculating the depth of the heat source, it does not yield very good results compared to the Liew *et al.* (1993) method of having the droplet depth proportional to the current.

3.4.4 MODIFIED SPLIT HEAT SOURCES

Based on the discussion in the previous sections on split heat sources, the features which appear to be the most effective were selected and combined to form the two new split heat source definitions shown in Figure 3.10 (a) & (b). These will be trialed in Chapter 4.

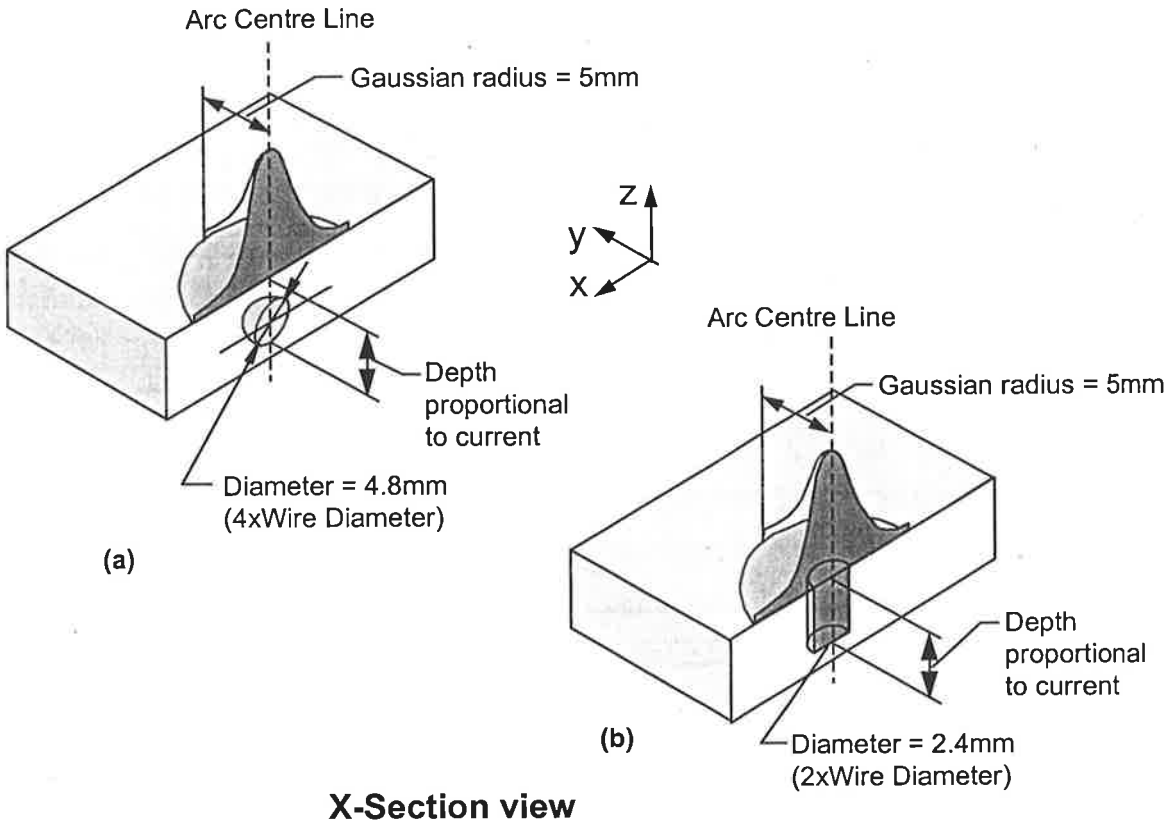

Figure 3.10 Modified split heat sources **(a)** Spherical droplet; **(b)** Cylindrical droplet.

Discussion

Both are surface-volume type heat sources, approximating as closely as possible the physical reality of where the heat is applied during welding. Both the spherical and the cylindrical distribution of the droplet heat seem reasonable and so both are tested. The depth of the droplet component was made empirically proportional to the current. The spherical diameter selected was 4 times the wire diameter which is similar to that used by Liew *et al.* (1993). In the case of the cylinder, heat is dissipated for the full depth of the droplet penetration and so a smaller diameter is expected. A diameter of two times the wire diameter is selected. This falls within the range used by Kumar & Bhaduri (1995 & 1995). The droplet heat is made to reduce radially from the wire centre line to reflect the dissipation of the heat. The content of the heat in the droplet is found from the empirical wire feed rate multiplied by 2304 J/g which is the energy level of molten steel at 2400°C. The remaining heat is applied as a surface Gaussian with a characteristic radius of 5 mm as discussed in Section 3.2.

The use of a deformed pool surface heat source in conjunction with the cylindrical split heat source above will be demonstrated in Chapter 4.

simple means of producing a closed isothermal boundary. The size of the double ellipsoid was adjusted so that the correct heat input level was achieved. Good temperature field predictions were obtained for a complex submerged arc weld consisting of two weld pools, and hence two double ellipsoidal temperature distributions. The double ellipsoidal temperature function would only be accurate for weld pools with an approximately ellipsoidal cross section. For finger penetration, an alternative temperature prescription would be needed. Goldak & Gu (1995) deformed the surface of their weld model to the shape of the fusion boundary. The shape was found from the cavity produced when a weld was stopped part way and the molten material ejected with an air jet. The temperature on the surface of this cavity was set at the melt temperature of 1500°C producing a model like that shown in Figure 3.12 (a).

It should be noted that this method is of no value in predicting a fusion profile since it is used as input, but is valuable in generating accurate temperature fields which can be used for stress and distortion analyses. The method is tested for V-joint models in Section 4.2. Due to the deep penetration of a V-joint weld it was not possible to deform the surface without excessive distortion of the elements. As a consequence, a prescribed temperature distribution was used. Unlike Gu *et al.* (1991) who used a double ellipsoidal temperature field, the distribution was matched to a measured fusion profile. The process consisted of ejecting the molten weld pool part way through a weld using the tipping device described in Appendix A. The fusion boundary was then recorded using a topographical laser scanner. An example of a fusion boundary scan is plotted in Figure 3.13.

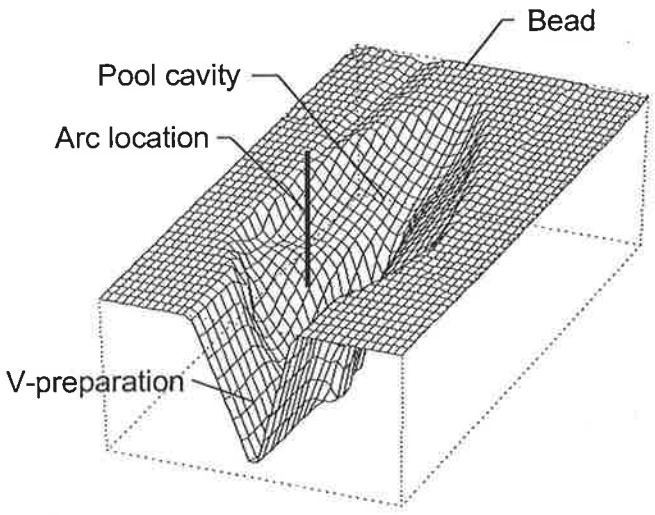

Figure 3.13 Scanned fusion boundary for a V-joint weld.

This profile is then used as input to define the weld pool as an isothermal boundary. This could be done by deforming the plate's mesh corresponding to the fusion boundary profile and applying the 1500°C isotherm as a surface boundary condition. This causes too much distortion of elements for the deep V-joint preparation so an alternative was devised: An undeformed plate mesh was used. Every node in the model was tested and if it lay within the scanned weld pool, a fixed temperature boundary condition was given to it. This temperature was calculated using the Rosenthal solution (Equation 1.3) for a moving point heat source tuned to the measured fusion boundary. The method can best be explained by referring to Figure 3.14 for a typical node (N) and its corresponding grid (G). The flux Q required to produce a temperature of 1500°C at G on the fusion boundary is calculated from the Rosenthal equation. This flux is then used to calculate the temperature at node N and this temperature is given to node N as a boundary condition. Similarly, all the other nodes within the weld pool are given a temperature which is tuned to the fusion boundary. When the model is solved numerically for nodes outside the weld pool, a relatively accurate fusion boundary results. Thus the 1500°C isotherm is indirectly prescribed by setting the temperature of nodes within the weld pool.

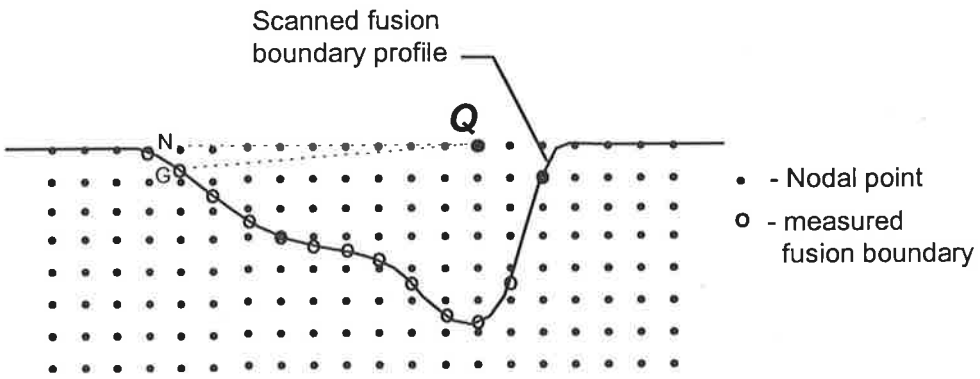

Figure 3.14 Defining the temperature at each node within the pool.

A potential application for the prescribed isotherm method which is not immediately obvious is in models which inherently require a transient analysis. By moving an isotherm through the model rather than a heat source, a less refined mesh and constant (average) material properties could be used - both of which are very helpful in reducing the transient solution's demanding computational requirements. It is reasonable to average the material properties since the large variation in properties as the temperature passes above 1500°C would not be present. A proposal is that a QSS analysis could be conducted on a small section using a

fine mesh and optimum heat source. From this the 1500°C isotherm, or a cooler one for that matter, could be extracted and used in the transient analysis without the liquid/solid phase change requirements.

3.7 INVERSE METHOD

In the physical world the welding process provides a source of heat which generates a thermal output in the weld piece. This section discusses the idea of taking this thermal "output" ie temperature measurements and using it as input to *calculate* the heat source which generated it. This is of interest as a means of developing a clearer picture of the effective form of the heat source distribution in welding. In addition, information on the internal material properties can be derived using an inverse approach. A considerable effort went into understanding the inverse process and investigating its potential for deriving heat sources. The application of inverse methods was found to be a difficult and complicated process and beyond the scope of this work. A summary of the findings will nevertheless be presented.

3.7.1 INVERSE THERMAL PROBLEM TYPES

There is much literature available on general inverse problem theory. A good text is provided by Tarantola (1987) who gives the very general definition of an inverse problem as one in which measurements of the observable parameters of a system are used to infer the values of the model parameters or functions. Observable parameters are those that define the state of the system while model parameters or functions define the system constraints. In welding, an observable parameter is the temperature; and model parameters include thermal conductivity, specific heat, while model functions could include the heat source or other boundary conditions.

The classes of inverse thermal problems are shown in Figure 3.15 and discussed below. Beck and St. Clair have done a lot of work in the area of inverse thermal problems since the 1970s. Beck (1991) classifies the inverse problem associated with welding and solidification as either estimation or design: In estimation problems *measurements* of an observable parameter are used as input whereas in design problems *desired* values of an observable parameter are used. Estimation problems are further classified as either function or parameter estimation. Beck (1991) gives an example of a parameter estimation problem in which he uses measured temperatures and a known heat input to estimate the thermal conductivity and specific heat (each of these two unknowns were parameterised as a linear function of temperature). An example of a function estimation problem is when the temperature field and the model parameters are known and a function defining the heat source is found - this is referred to as the inverse heat conduction problem (IHCP). In an early paper, Beck (1970) gives a summary of work on the IHCP and dates the earliest work

back to around 1960 by Stolz. In this paper Beck analyses a one dimensional non linear IHCP to find the time dependant surface heat flux q(0,t) from temperature measurements inside a body. He observes "a rather remarkable ability to extract information about the surface condition from experimental measurements that lag and are damped compared to the surface condition". If the flux and the temperature field are known, finding the model parameters such as conductivity is an example of a parameter estimation problem.

In the IHCP the entire mathematical domain is considered as solid with phase change accounted for in the material properties (cf. Section 2.2.3) and the heat transfer governed by conduction. A second type of function estimation problem of interest is the Inverse Stefan Problem (ISP) which includes a solid and liquid phase. The ISP accounts for latent heat by an energy balance at the fusion boundary, however, heat transfer is still purely conduction with no convective flow in the liquid region. Note that as Zabaras (1990) showed, the latent heat effects can be incorporated into an effective specific heat, essentially reducing the problem to non linear heat conduction. Zabaras appears to be a key worker in the ISP. There are two types of ISP which have potential relevance to welding: (a) finding the motion of the fusion front from measured temperatures in the solid eg. Zabaras and Ruan (1989) and (1991); and (b) finding the heat transfer boundary conditions from fusion front motion.

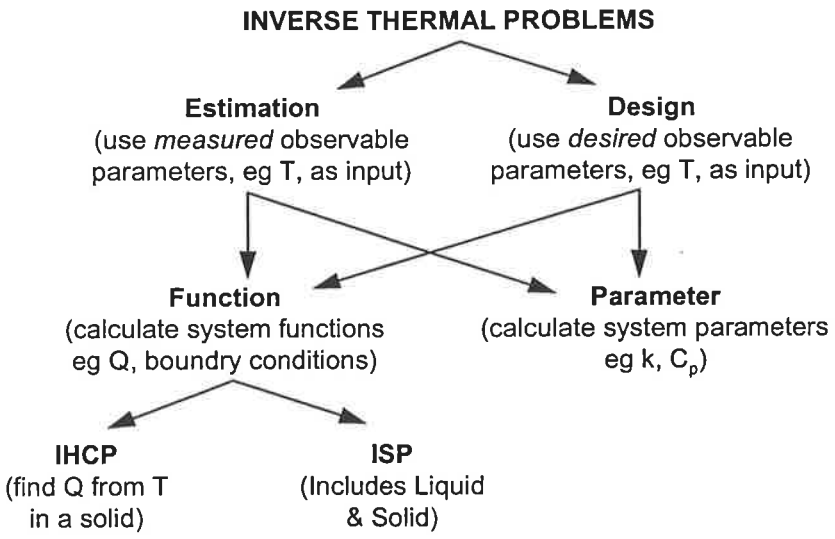

Figure 3.15 Classes of inverse thermal problems.

3.7.2 POTENTIAL USES OF INVERSE METHODS IN WELD MODELLING

There are several reasons why inverse methods may be useful for finite element modelling of GMAW:

1) Heat Source Calculation

The IHCP or the ISP type (a) mentioned above could be used to calculate the heat flux applied by the arc and molten droplets from discrete temperature measurements in the solid weld piece. By observing the shape of the heat source, a more realistic general heat source form could possibly be found. The impact of different welding conditions on the calculated heat source could be observed so that a heat source definition which is a function of the welding parameters could be derived.

2) Efficiency Calculation

By calculating the heat source, the magnitude of heat being applied to the weld is known and this gives the actual efficiency of the weld. This is considered of limited value since there are experimental means to find efficiency which appear to be reliable (see Section 3.1.1)

3) Compensation for Model Limitations

A heat source calculated using inverse methods automatically compensates for limitations in the mathematical model. For example: an experimental temperature field is used as input to an inverse heat conduction problem and a heat source calculated. This heat source, if used as input to the forward heat conduction problem, will by definition yield the exact experimental temperature field - even though it is a conduction analysis. So, the heat source has built in compensation for the lack of convection. Similarly, it can compensate for approximate material properties, or other mathematical simplifications.

4) Estimation of Material Properties

Parameter estimation problems can be used to find the specific heat or conductivity that should be used in a thermal welding model.

5) Calculation of Weld Fusion Boundary

The ISP (type b) mentioned in Section 3.7.1 could be used to calculate the weld fusion boundary from discrete temperature measurements in the solid zone. There are experimental techniques to obtain a weld fusion boundary profile upon extermination of the weld, such as the tipping device in Appendix A. Using the ISP could potentially have application for in process determination and control of weld fusion boundary dimensions.

6) Inverse Design

The inverse design problem could be used in welding in several ways. For example, there may be a maximum allowable temperature on the inside face of a weld piece. This temperature could be used as input in an Inverse design problem to find a heat flux level that would satisfy the temperature criterion. Again, a certain fusion depth and width may be required for a particular weld; a heat source can be calculated using inverse design methods to achieve this. Welding parameters can then be chosen which give this heat source and hence the weld pool dimensions.

3.7.3 REVIEW OF INVERSE METHODS APPLIED TO WELDING

There are not a very many examples in literature of inverse methods being applied specifically to welding problems. Each of the potential uses listed in Section 3.7.2 will be addressed to highlight any papers found which attempt a welding application to some degree.

1) Heat Source Calculation

A very interesting recent attempt at predicting the heat input of an arc weld, was presented by Nakatani and Ohji (1993). Their actual intention is for the calculation of the arc efficiency, however, to do this they first calculate the arc heat source distribution. They consider the inverse three dimensional quasi-steady state problem to calculate the surface heat flux distribution from temperature measurements at target points on the under side of the work piece. The heat source is divided up into discrete point sources and the Rosenthal equation is used to predict the temperature at the target points as a function of the discrete heat sources. An objective function is produced using the error between predicted and measured temperature at the target points, and by minimising this error using convex programming techniques, the point heat sources are solved for, thereby determining the heat source distribution. The calculated heat source distribution is also used to calculate the melting point isotherm in order to examine the predicted weld pool dimensions; the results were satisfactory. The inverse calculation is tested experimentally by heating a work piece with a laser of known heat distribution and trying to estimate the distribution from thermocouple measurements on the bottom surface of the work piece. The estimated total heat input was accurate, enabling the arc efficiency to be calculated, however, the distribution was not very accurate and this was put down to the inaccuracies in the measured temperature values. The effect of errors in temperature measurements was highlighted by the fact that a measurement error of just 1% had very adverse effects on the predicted heat source

distribution. The problems associated with measurement errors could be minimised by increasing the number of measurement points, and by moving the points closer to the weld pool.

2) Efficiency Calculation

Macqueene, Akau, Krutz and Schoenhals (1983) investigated the use of inverse techniques in the prediction of welding arc efficiency. They calculated the heat flux input for two different 2 dimensional cases (a) a step change in surface heat flux and (b) a ramp type surface heat flux, based on the temperature measurement at an interior point. The calculated total heat input provided welding efficiency values which were comparable to experimental results. It was claimed that if the temperature data for a number of welding conditions are measured, the method can be used in an attempt to select the most energy efficient of these conditions.

3) Compensation for Model Limitations

If the temperature field is completely known in a work piece, then the heat conduction equation can be rearranged to calculate the heat source exactly. This is in effect an inverse calculation since the thermal output is used to calculate the heat input, however the usual complexities of inverse methods are avoided since the entire temperature field is known exactly. Kamala and Glodak (1993) calculated a temperature field in a three dimensional forward model of the arc welding process. This temperature field was then applied to a two dimensional model and the heat source calculated. The form of the calculated heat flux distribution would then compensate for the two dimensional approximation.

4) Estimation of Material Properties

The inverse problem of calculating thermal conductivity is investigated by Kohn and Vogelius (1984) and Bonnet, Bui, Maigre and Planchard (1992). They used a complete measured surface temperature map resulting from a known heat input to calculate the internal thermal conductivity within a body. Bonnet et. al. claim that this measurement can be used to reconstruct unknown thermal conductivity coefficients, and information on defects and cracks.

5) Calculation of Weld Fusion Boundary

Keanini and Rubinsky (1994) developed and demonstrated a method to determine the weld pool capillary interface shape in thee dimensions for plasma arc welding using a limited

number of thermocouple measurements. They parameterise the boundary shape and then apply an iterative minimisation technique to solve for the unknown parameters.

6) Inverse Design

Thermal inverse design observed in literature is limited to solidification problems for casting and no examples were found for welding. The three papers listed below are all in the category of design ISP with a defined fusion boundary velocity (solidification front). The boundary fluxes were calculated to maintain this solidification front.

Zabaras (1990) used finite time steps to solve for the flux at each time and used a method developed by Beck *et al.* (1985) known as the "future time step method". This method helps to handle data that has significant errors, and to enable smaller time steps. Zabaras and Kang (1993) optimised the objective function for the complete time domain, using the both the steepest descent method and the adjoint conjugate gradient method. Voller (1991) aimed to extend the ISP to tackle inverse melting and solidification problems which included natural convection in the fluid. Two dimensional examples were given of calculating the surface flux required to achieve a specified phase front velocity. Instability was observed in the solution when there were high temperatures and therefore high convective velocities in the liquid.

It should be possible to apply similar analyses to welding where a desired weld pool boundary and motion is used as input to find the surface heat source (rather than a heat sink as in the solidification problems).

3.7.4 METHODS OF SOLVING INVERSE PROBLEMS

Both the IHCP and ISP are what is known as ill-posed mathematical problems. This means that a small variation in the input data causes a very large perturbation in the solution. This effect can be observed in GMAW by the fact that at any distance away from the weld, it takes a relatively large change in the heat input to produce a relatively small change in the temperature. Hence, in the inverse analysis a small error in the temperature measurement has a large influence on the calculated heat input. This explains the emphasis on error analysis which is a key component of inverse methods.

The review of literature revealed a significant input from three researchers: Beck, who has worked on the IHCP since about 1965 and has two texts (1977 & 1985); Zarabas (eg. 1989, 1990, 1993) who is currently doing much work on the ISP; and Murio (eg. 1987, 1989, 1990)

who has worked extensively with the space marching approach to solving inverse thermal problems.

There appears to be two general approaches to solving inverse thermal problems: the objective function method and the space marching method which are briefly outlined.

OBJECTIVE FUNCTION METHOD

Essentially, the general approach is:

(1) Express the unknown variable (eg heat source) as a function or as a set of parameters to be solved for.
(2) Find an equation which links the unknown variable to an observable parameter (eg temperature).
(3) Derive an objective function which is usually the least squares error between measured values of the observable parameter and values calculated from the unknown function or set of parameters.
(4) Minimise the objective function to find the optimum values for the unknown function or set of parameters.

There can be several stages within each step. If the model is implicit the optimum parameters need to be solved for iteratively. If the model is explicit, then the error can be formulated and minimisation techniques applied. There are several tools which appear regularly in the literature: Regularisation techniques -smooths the objective function so that the effect of errors in the measured observable parameters has less impact; Future Time Method - developed by Beck which uses information from a future time to indicate the present value of the unknown parameters; Sensitivity Coefficients - indicate which experimental condition is best for estimating a certain parameter; Gradient Optimisation - finding the fastest convergence of the minimisation of the objective function.

In the IHCP the model is generally implicit and so the inverse method may reduce down to a well controlled and optimised iteration of forward problems. A better method may be the space marching approach.

SPACE MARCHING METHOD

Murio has a host of papers on this method, dealing with both the IHCP and the ISP. For example: Murio (1989) & Guo, Murio & Roth (1990) - calculating the surface heat flux from

measured internal temperatures; Hinestroza & Murio (1993) - calculating the convective heat transfer coefficient at the top surface of a plate from measured temperature and flux on the bottom surface; Mejia & Murio (1993) - calculating the anisotropic thermal conductivity in a rod, knowing the initial temperature distribution and the temperature and flux at one end; Murio (1992) - solving the ISP.

The space marching process can be most simply understood with reference to the one dimensional steady state case shown in Figure 3.16 (a).

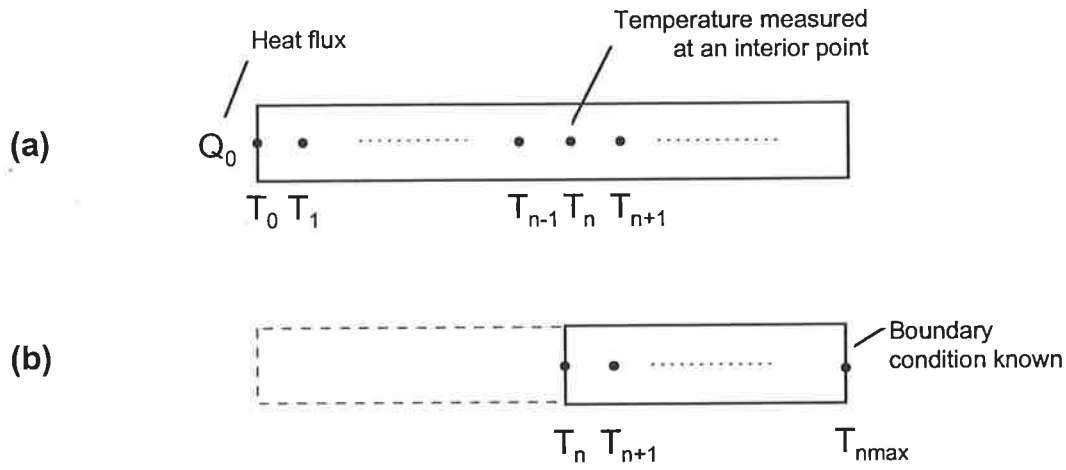

Figure 3.16 Space marching in one dimensional steady state heat conduction **(a)** using known temperature at two adjacent nodes; **(b)** using known temperature at one node and known boundary condition.

The inverse problem is to calculate the heat flux Q_0 based on the measured temperature at node n. Now in solving the forward problem with Q_0 as an input and using finite difference discretisation, the temperature at any interior node is a function of the two nodes on either side of it (Equation 3.7).

$$T_n=f_1(T_{n-1},T_{n+1}) \tag{3.7}$$

$$T_{n-1}=f_2(T_n,T_{n+1}) \tag{3.8}$$

$$Q_0=f_3(T_0,T_1) \tag{3.9}$$

This equation can be rearranged so that the temperature at a node is a function of the two nodes to its "right" (Equation 3.8). So, knowing the temperature at two adjacent nodes, the temperature at the next node to the "left" can be found. This temperature is then used to

find the temperature at the next node to the left of it and the process continues until the heat source is reached. The flux Q_0 can then be found (Equation 3.9). A problem with this is that the temperature at two adjacent nodes is needed to start the process. Murio's approach is to experimentally measure the temperature at two adjacent node locations, which is fine in a 1D problem, but means many more measurements are needed in 2D or 3D problems. The author of this thesis proposes that T_{n+1} can be found by solving the forward problem for the end part of the rod as shown in Figure 3.16 (b) if the far boundary condition is known.

Murio has, in fact, done all his work for transient analyses and the above argument is outlined for the transient equivalent in most of his papers, such as Murio & Guo (1990). Murio (1987) introduced a tool he terms the mollification method to smooth the experimental input data for inverse methods. Murio & Gu (1990) propose another method which attempts to smooth the data as the marching progresses.

3.7.5 PROPOSED INVERSE METHOD FOR HEAT SOURCE CALCULATION

Based on the above discussion, a marching scheme is proposed for discovering the welding heat source from measured temperature information. The process is to obtain a weld pool fusion boundary profile using the tipping device in Appendix A. This then provides a 1500°C isotherm to use as a starting point to march to the surface of the pool.

As shown in Figure 3.17 (a) and Equation 3.10, for a finite difference scheme, the temperature at any node is a function of the nodes surrounding it. In order to march to the surface, this equation is rearranged into Equation 3.11 to calculate T_1 as a function of the other 4 nodes.

$$T_0=f_1(T_1,T_2,T_3,T_4) \tag{3.10}$$

$$T_1=f_2(T_0,T_2,T_3,T_4) \tag{3.11}$$

In order to generate the grid of nodal temperature values for all nodes outside of the weld pool, the fusion boundary and the plate boundary conditions are used as shown in Figure 3.17 (b) - this is similar to Section 3.6. Once the temperature field is calculated, it can be transposed onto a finite element grid. The grid may be uniform as shown in Figure 3.17 or may be fitted to the fusion boundary.

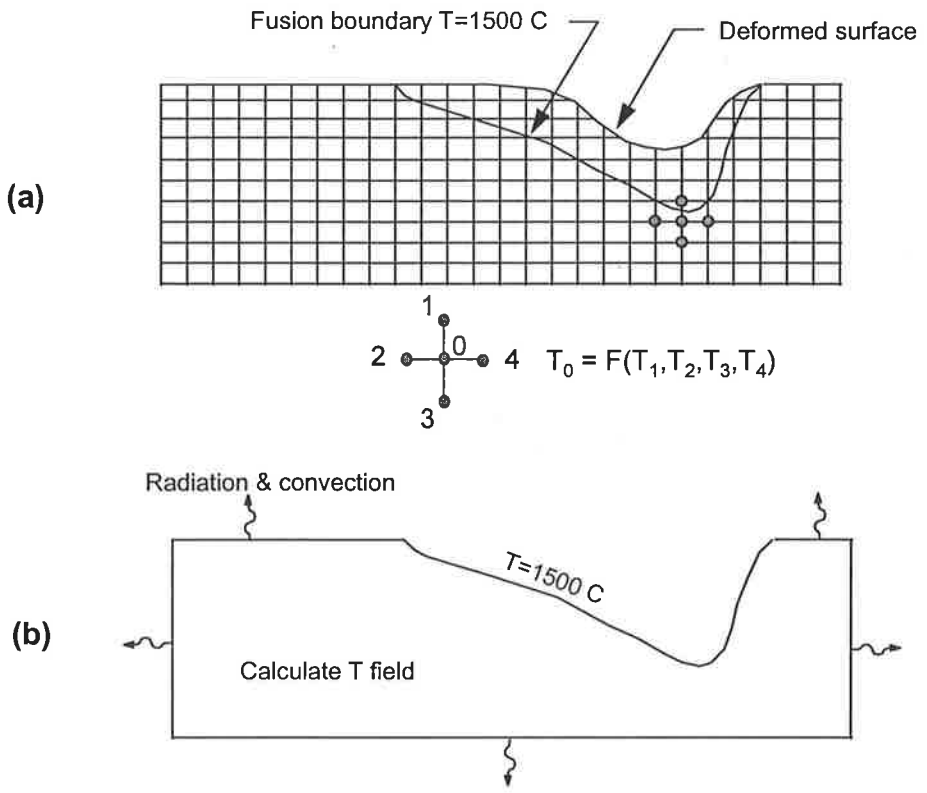

Figure 3.17 Proposed inverse method **(a)** space marching scheme, **(b)** calculation of plate temperature for input into the marching scheme.

When the above was tested for a simple case, large oscillations in the temperature of adjacent nodes were observed as marching progressed. It became apparent that the data would need special consideration to keep the solution smooth, such as Murio's mollification method (1989), Murio & Gu's method (1990) or Carasso's (1992) suggestions on schemes to ensure the error grows as slowly as possible. In addition, special consideration when marching across the fusion boundary is needed. The problem became too large and complex to incorporate into the scope of this work. The use of inverse methods for the calculation of the heat source remains as a proposal for future investigation.

Chapter 4

APPLICATION OF THE MODEL

4.1 INTRODUCTION

This chapter illustrates how the QSS conduction based model described in Chapter 2 can be combined with the heat source definitions from Chapter 3 to produce useful models for thermal prediction. It also gives comparisons of the effectiveness of the different heat source descriptions. To date, much of the work on thermal modelling of welding has been developing the theory for simple bead-on-plate welds with little specific consideration of commonly used welding joint configurations. This chapter will show how the theory can be applied to a range of joint configurations and GMA welding processes. Some relatively novel QSS conduction based models will be presented, such as: modelling of weave welding, which has never been observed in literature; the use of the deformed pool surface heat distribution; the use of QSS rather than transient analysis in multi-pass and preheat applications; the modification of heat source definitions for use on T & V-joint welds.

4.2 V-JOINT MODEL

A V-joint weld is a method of joining two pieces of material butted against each other with an edge preparation producing a 'vee' groove to be filled by the weld material. This can be seen in Figure 4.1.

Most modelling development work has been for bead-on-plate welds, with heat sources being developed and optimised for this simple welding process. These models are now being applied to real weld configurations such as V and T-joints, generally with no alteration to the heat source. Exceptions are Tekriwal and Mazumder (1986 & 1988) who's model inherently accounts for the joint configuration, because they add the bead heat by filling the joint configuration with material at an elevated molten metal temperature. Researchers dealing with multi-pass welds have also produced joint specific heat sources and this will be addressed in Section 4.4. This section deals with assessing the suitability of the heat sources discussed in Chapter 3 to V-joint welds.

4.2.1 EXPERIMENTAL DATA

The weld used in this work was anode positive pulsed GMA robotic welding. The work here applies to a single pass weld, however, a multi-pass V-joint weld is addressed in Section 4.4. The plate material was 10 mm mild steel, with a 45° V-joint preparation and 1.6 mm land as shown in Figure 4.1. The shielding gas was 82% Argon and 18% CO_2, the wire diameter was 1.2 mm with contact tube to work piece distance of 18 mm. A range of currents and welding speeds were used resulting in the experimental conditions listed in Table 4.1. Refer also to Section 2.3.1 for details of experimental procedures. Table 4.2 shows the corresponding measured results.

Run	Current (A)	Voltage (V)	Velocity (mm/min)	Power (kW)	Energy (kJ/mm)
1	245	30	300	8.80	1.8
2	184	28	220	6.40	1.8
3	128	27	150	4.40	1.8
4	130	25	220	4.36	1.2
5	190	25.5	300	6.00	1.2
6	250	28	450	8.60	1.2

Table 4.1 Experimental welding conditions (pulsed GMA robotic welding).

Run	Pool Width (mm)	Penetration (mm)	T_{85} (sec)
1	13.0	8.0	22.2
2	12.5	6.5	21.5
3	11.5	5.5	20.1
4	9.3	5.4	10.4
5	10.0	6.7	14.1
6	9.8	7.6	12.9

Table 4.2 Experimental results of the weld pool dimensions and $T_{8/5}$.

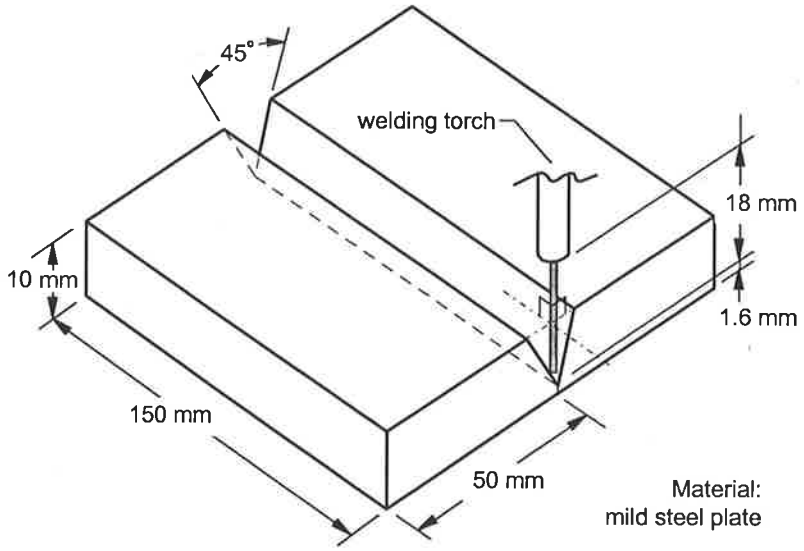

Figure 4.1 V-joint weld configuration.

It may be expected that for V-joint welds, the penetration would be at least to the base of the groove (8.4 mm in this case), however this was not observed if the penetration was carefully defined. Figure 4.2 (a) shows the experimental observation that particularly at low currents, weld material penetrates almost to the base of the groove, but satisfactory fusion to the sides of the groove occurs only to a considerably shallower depth. This is shown photographically in Figure 4.2 (b).

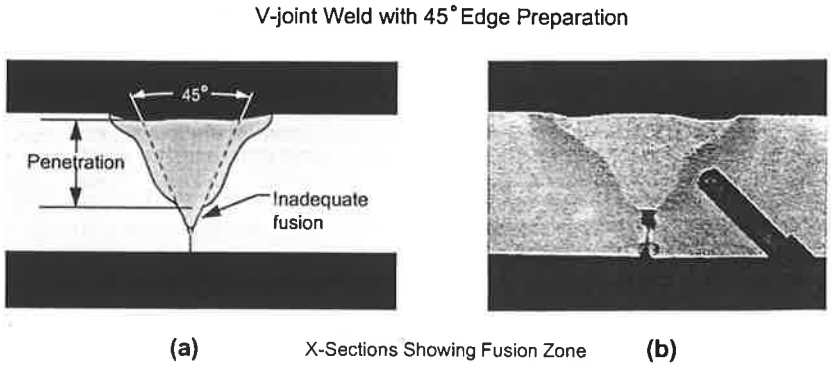

Figure 4.2 Defining penetration for V-joint welds.

4.2.2 MODEL

As explained in Section 3.1.2, the mesh should include the weld bead. In this case the bead fills the v-groove and results in a mesh which looks almost like a flat plate. There is a slight cap or under fill meshed into the plate depending on the volume of the material deposited. This bead profile is produced by calculating how full the groove would be based on empirical measurements of the wire feed rate against current; the node locations in the mesh are then adjusted using a Fortran program to fit the bead profile. The program also adds the other boundary conditions to the mesh. The resulting FE model is such as that shown in Figure 2.5 in the Chapter 2 on the modelling approach. The size of the elements in the refined region near the arc is 1 mm^3.

4.2.3 HEAT SOURCES

Six different heat source configurations were tested and these are summarised in Figure 4.3. Chapter 3 described the details of these heat sources and the reasons for their selection.

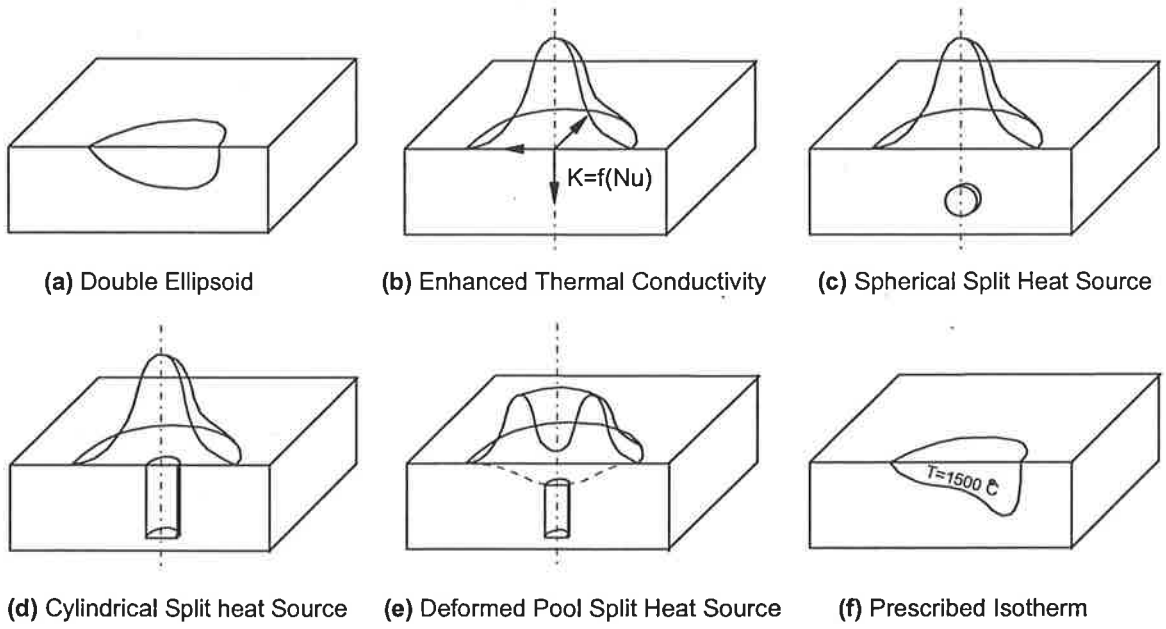

Figure 4.3 Heat sources tested for the V-joint model.

Double Ellipsoid:

The Double Ellipsoid (DE) is a very popular heat source observed regularly in literature, and so, it provides a good benchmark to gauge the effectiveness of the proposed heat sources. Initially, the parameters used to define the DE heat source were those proposed by Goldak

(refer to Section 3.3). The results obtained with these parameters provided very poor results with the width and depth of the weld bead under predicted by about 30% while the pool length was over predicted by about 30%. It was recognised that this is because the proposed ideal parameters for the DE were for a two dimensional model in which there is no conduction in the length direction and so the heat is manually spread out and weighted towards the rear of the heat source. As a result, more appropriate parameters were chosen for this 3D model. The DE width and depth were still taken directly from the experimental weld bead dimensions, but the length of the rear half ellipsoid was reduced from two times the bead width to equal the bead width. Additionally, the fraction of heat in the front and rear portions of the DE were made equal. Significantly better results were obtained with the error being halved.

Surface Gaussian with Enhanced Conductivity:

Refer to Section 3.5 for details of this heat source. The enhancement factor is determined directly from the Nusselt number which is calculated in Table 4.3 using Equation 3.6. A plot of the enhancement is given in Figure 4.4.

Run	Current (A)	Wire feed (gm/s)	Velocity (m/s)	Nu	Nu (regression)
1	245	0.954	2.23	7.5	7.8
2	184	0.702	1.32	6.1	6.1
3	128	0.471	0.53	4.4	4.5
4	130	0.515	0.55	4.5	4.6
5	190	0.894	1.42	6.6	6.3
6	250	1.273	2.30	8.1	8.0

Table 4.3 Calculated thermal conductivity enhancement factor which is equivalent to the Nusselt number.

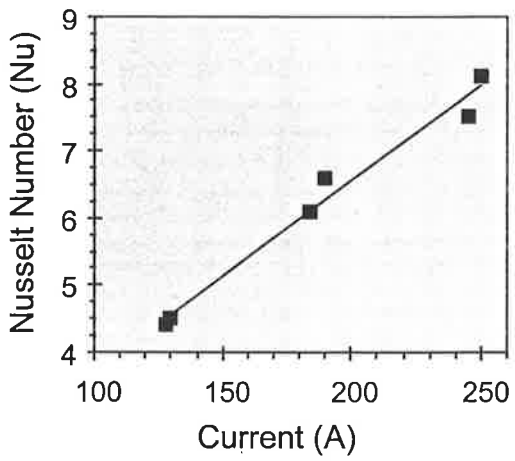

Figure 4.4 Plot of Nusselt number which is equivalent to the conductivity enhancement factor.

Software constraints required that the enhancement be applied isotropically within the molten region despite the intention that it be applied in the direction of the penetrating droplets.

Split Heat Source:

Section 3.4 provides an introduction to this type of heat source with the details given in Section 3.4.4. For both the spherical and cylindrical droplet, the wire feed rate is required to calculate the amount of heat attributed to the droplet. This is done by finding an empirical equation for the wire feed rate from experimental measurements. This is shown in Table 4.4 and Figure 4.5. It was observed that the wire feed rate was a linear function of the current, but also affected by the heat input, and so, an equation was derived for each of the two heat input levels.

Run	Current	Wire feed (gm/sec)	
	(A)	measured	Regression
1	245	0.956	0.954
2	184	0.699	0.702
3	128	0.473	0.471
4	130	0.532	0.515
5	190	0.861	0.894
6	250	1.289	1.273

Table 4.4 Measured wire feed and the resulting empirical wire feed.

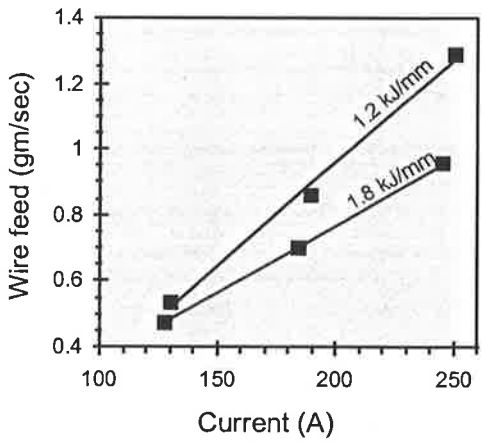

Figure 4.5 Plot of experimental (■) and empirical (solid line) wire feed.

The depth of application of the heat source is also calculated empirically from a linear equation of penetration versus current. Initially penetration was measured from the top of

the plate, but this resulted in some scatter, and the results did not appear to fit a linear relationship very well. When the penetration was measured from the top of the weld bead, however, the fit was quite good, and this is shown in Table 4.5 and Figure 4.6. Measuring from the top of the bead is in line with the notion that the depth of droplet penetration depends on its impact force and the resistance experienced once contact with is made with the molten bead.

Run	Current (A)	Penetration (mm) from:		
		top of plate	top of bead	Regression
1	245	8.0	8.0	7.8
2	184	6.5	6.5	6.5
3	128	5.6	5.5	5.4
4	130	6.5	5.4	5.5
5	190	7.2	6.7	6.7
6	250	8.1	7.6	7.8

Table 4.5 Measured penetration and the resulting empirical penetration.

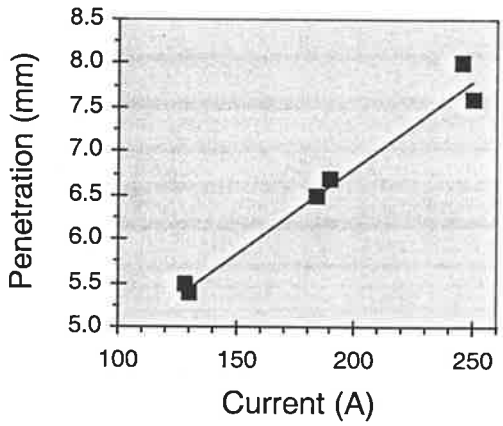

Figure 4.6 Plot of experimental (■) and empirical (solid line) penetration.

Deformed Pool Split Heat Source:

This heat source is similar to the cylindrical split heat source, but with the effects of the deformed surface incorporated. Thus the surface Gaussian is altered as described in Section 3.2.1 and the cylinder which represents the droplet is spread from the top of the depressed weld pool to the bottom of the molten pool. Note that the deformation of the weld pool surface is not actually meshed into the plate as this causes problems in QSS as outlined in Section 3.1.2, but the effects are captured in the heat source.

The calculation of the deformed pool surface heat component requires the calculation of the 3 dimensional radius (r_{xyz}) from the arc electrode wire tip to the surface of the pool and plate. This radius was found, based on the deformed pool arrangement shown in Figure 4.7 (a).

For clarity, the shaded area indicates the molten zone to distinguish it from the surface depression. To calculate the arc length, the deformation level of the pool surface (dp) and the arc length (al) shown in Figure 4.7 (b) are required. The deformation of the pool surface is assumed to be a Gaussian shape with radius of 5 mm. The 3D radius, r_{xyz}, in front of the electrode is found from the distance from the electrode tip to the bevelled face of the plate.

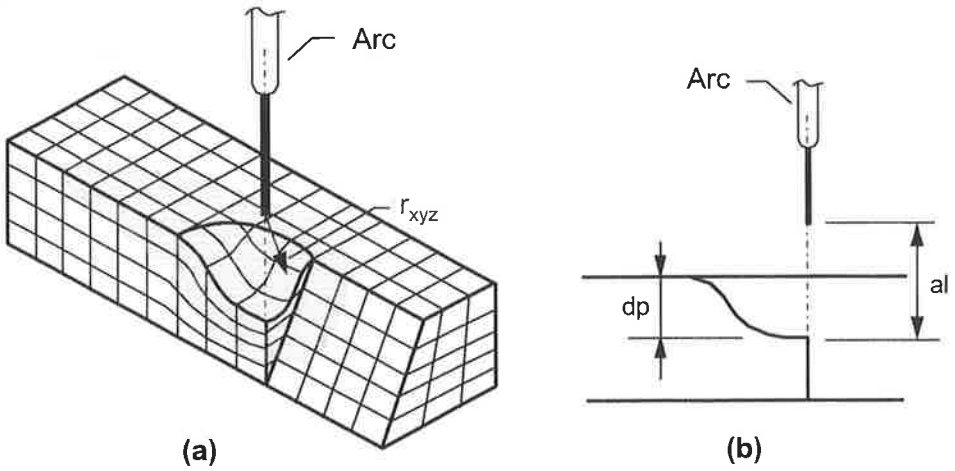

Figure 4.7 X-Section of plate and pool showing deformed pool parameters for a V-joint.

There are two approaches by which the weld pool surface position (dp) could be calculated: (I) by an equilibrium of the mechanical forces as described by Sudnik (1991) or (ii) by minimisation of the surface energy as referenced by Weiss *et al.* (1995). In both these cases the effect of the impacting molten droplets have to be added to the calculation. These methods are not straight forward and will rely on regression input for such parameters as the arc pressure, filler metal rate and velocity. Kim & Na (1995) calculated the shape and penetration of weld beads using a convective analysis which included the droplet impact forces, with good results. A convective analysis is very complex and the aim of this thesis is to achieve simple yet effective conduction models, so there would be no sense in doing a convective analysis simply to gain pool surface deformation information. What will be used in this work is an empirical equation for the depression of a weld pool developed by Rokhlin & Guu (1993):

$$dp=-1.8+560F \quad (mm) \tag{4.1}$$

This equation was derived from measured deformation during GTAW with *F* representing the arc force in Newtons. The assumption is made here that the same equation can be applied

to GMAW but with the modification that *F* becomes the sum of the arc and the droplet forces. Rokhlin & Guu measured the arc force (F_{arc}) to be proportional to the current squared as given by Equation 4.2:

$$F_{arc}=7.25e^{-8}I^2 \quad (N) \tag{4.2}$$

The component of the force attributable to the droplet is found from the rate of change in momentum of the droplet as it penetrates the pool, slowing to stationary in the vertical direction. Let the duration of the momentum transfer be *dt*; the vertical momentum is initially droplet mass times droplet velocity (*mv*) and the final vertical momentum is zero. Hence, the force induced by each impacting droplet is *mv/dt*. This force is discrete, and to find an equivalent continuous force, the droplet force must be multiplied by the duration of the force (*dt*) and divided by the period between droplets. The result is shown in Equation 4.3 where *f* is the droplet frequency:

$$F_{drop}=mvf \quad (N) \tag{4.3}$$

Essers & Walter (1979) measured *mvf* and recorded it against weld pool penetration. The results of this parameter against current were extracted from the paper and are shown in Figure 4.8 and used in the calculation of the pool depression.

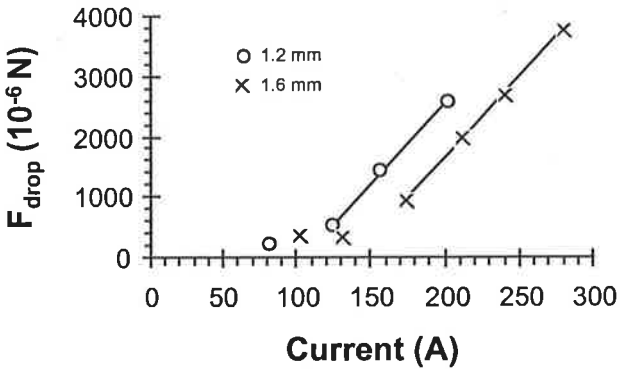

Figure 4.8 Droplet force as a function of current for 1.2 & 1.6 mm wire diameter. Extracted from Essers & Walter (1979).

It can be seen that a good linear relationship exists between the droplet force and the current for the range of currents of interest. The purpose for plotting the 1.6 mm wire was to check the linearity at higher currents and thus give confidence in extrapolating the 1.2 mm

wire to higher current values. Interestingly, the two lines are almost exactly parallel, with a gradient in Newtons/Ampere (N/A) of 26.6x10-6 N/A for the 1.2 mm wire and 26.5x10-6 N/A for the 1.6 mm wire. The weld pool depression can now be found using Equations 4.3, 4.2 & 4.1 with the results shown in Table 4.6.

Run	Current (A)	F_{drop} ($Nx10^{-3}$)	F_{arc} ($Nx10^{-3}$)	F_{total} ($Nx10^{-3}$)	dp (mm)
1	245	3.749	4.352	8.101	2.74
2	184	2.125	2.455	4.579	0.76
3	128	0.633	1.188	1.821	0.00
4	130	0.686	1.225	1.912	0.00
5	190	2.284	2.617	4.902	0.94
6	250	3.883	4.531	8.414	2.91

Table 4.6 Calculation of weld pool depression (dp).

Now, as was shown in Figure 4.7, the arc length (al) is also required for the deformed pool heat analysis. This was obtained from measurements by Zhu & Simpson (1995) of the arc length as a function of welding voltage and wire feed rate for 1.2 mm diameter wire with 20 mm contact tube to work piece distance. Some extrapolation was necessary for the results marked with an asterisk (*) in Table 4.7 below.

Run	Voltage (V)	Wire feed (cm/s)	Arc length (mm)
1	30.0	10.7	7.3
2	28.0	7.9	* 6.5
3	27.0	5.3	* 6.4
4	25.0	5.8	* 5.4
5	25.5	10.0	5.0
6	28.0	14.3	5.2

Table 4.7 Arc length, obtained from Zhu & Simpson (1995).

Using the values from Tables 4.6 and 4.7, the 3D radius r_{xyz} from the wire tip to any point on the plate can be found. The minimum value of r_{xyz} is used to find the effective radius, r_{eff}, for each point to be loaded with the deformed pool heat source, in line with the description in Section 3.2.1.

The resulting heat distributions of the surface component of the deformed pool split heat source are shown in Figure 4.9 together with a standard Gaussian for comparison. The weld runs with the greatest pool deformation, ie. runs 1 & 6 are most significantly affected. The presence of the "vee" is clearly visible. The arc tip is a lot closer to the pool surface and the

edges of the "vee", than the bottom of the groove, so these have lower transitional resistance and the heat flux is transferred to them in preference. In all cases the arc heat flux is significantly distorted from the standard Gaussian, generally with more heat being directed to the edges and the rear of the weld pool.

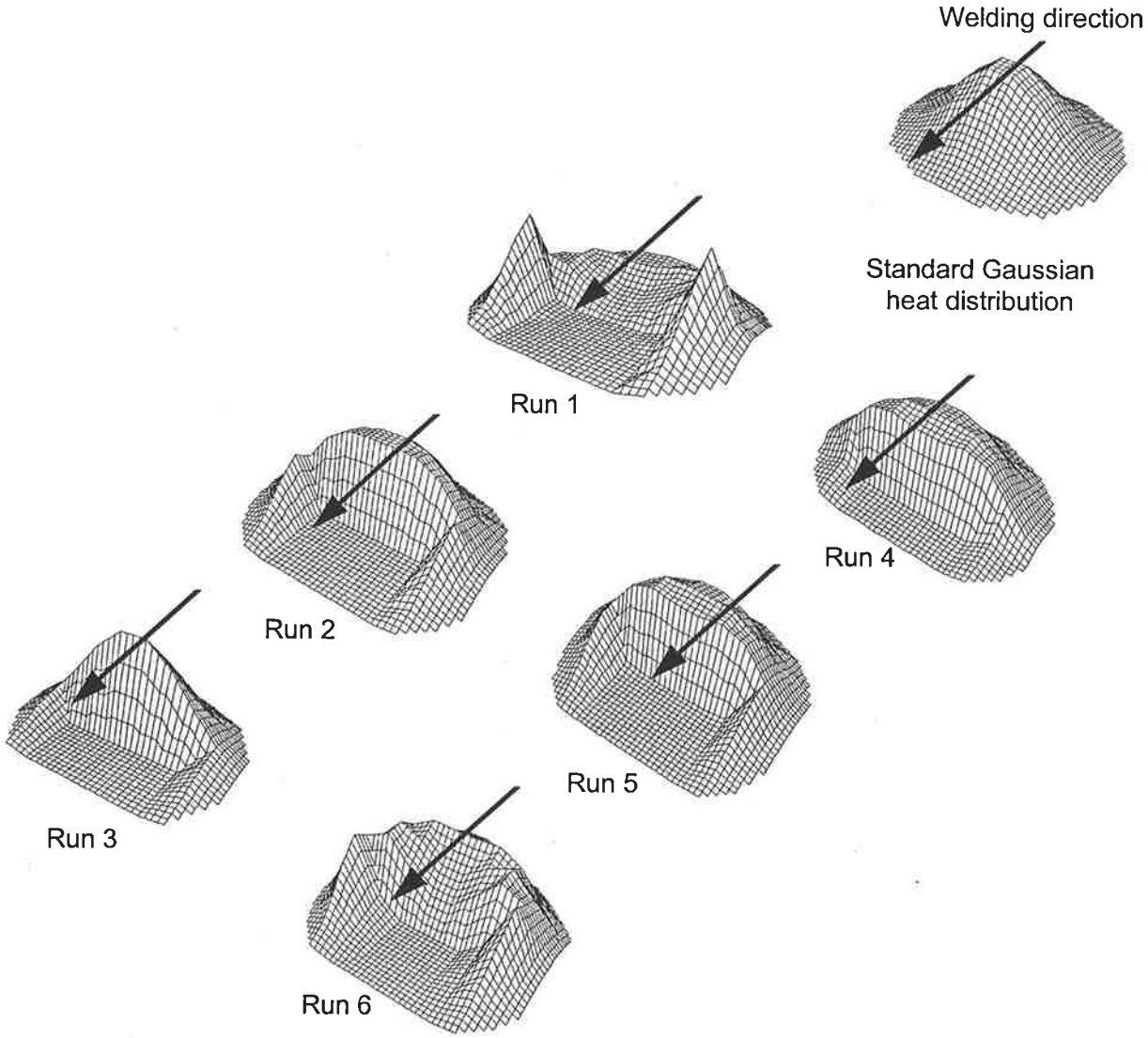

Figure 4.9 Deformed pool surface heat component for V-joint weld, compared to contemporary Gaussian form.

An experimental means for photographically mapping the pool surface was considered, but not pursued due to the unavailability of the experimental facilities. Some initial photographic work was done and the pictures shown in Figure 4.10 give some indication of the pool depression shape and arc length for a V-joint weld run. The form of the pool depression appears in agreement with that selected for the deformed pool heat calculations.

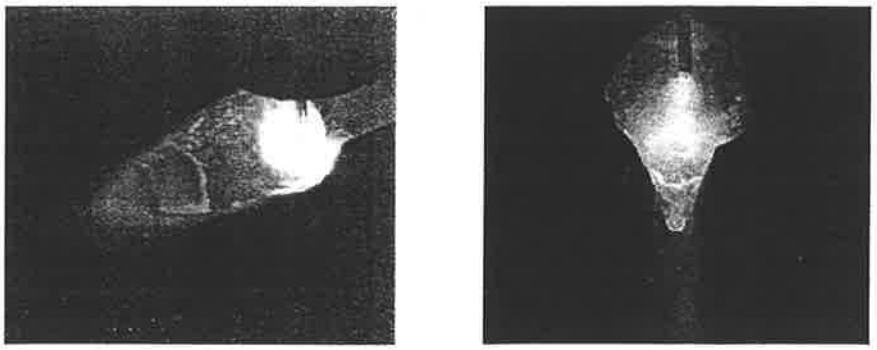

View from 45° behind the weld

View looking along the V with weld approaching

Figure 4.10 Photo of pool depression for V-joint weld.

Prescribed Isotherm:

Refer to Section 3.6 for details of this heat source definition.

4.2.4 RESULTS AND DISCUSSION

The solution time for most of these models was of the order of 45 minutes CPU time for each welding condition. The weld pool dimensions were extracted from thermal contour plots of the weld such as that shown in Figure 4.11, and the $T_{8/5}$ values from the thermal history at a point in the mesh corresponding to the thermocouple location.

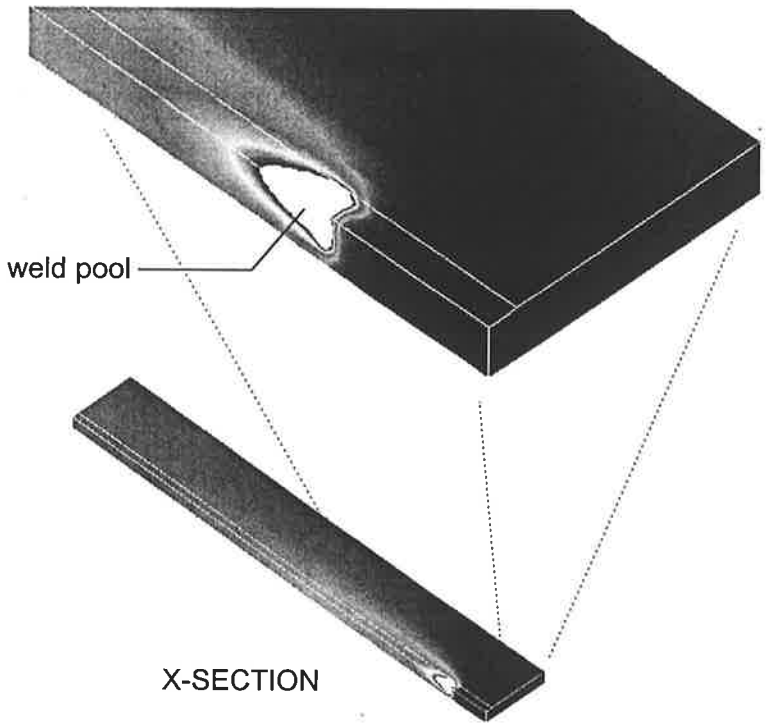

Figure 4.11 Typical thermal contour plot for a V-joint weld (run 5) with the molten region highlighted.

The results for the different heat sources and welding conditions are tabulated in Appendix B and presented graphically for a visual indication of model accuracy in Figure 4.12. The graphs are a plot of the predicted pool dimension or $T_{8/5}$ against the experimental one. Hence if the model matched the experimental exactly then the data points should fall on a straight 45° line. Note that the Tabulated results in Appendix B include also the weld length, which is not an important weld parameter and is thus not presented in the main discussion of results.

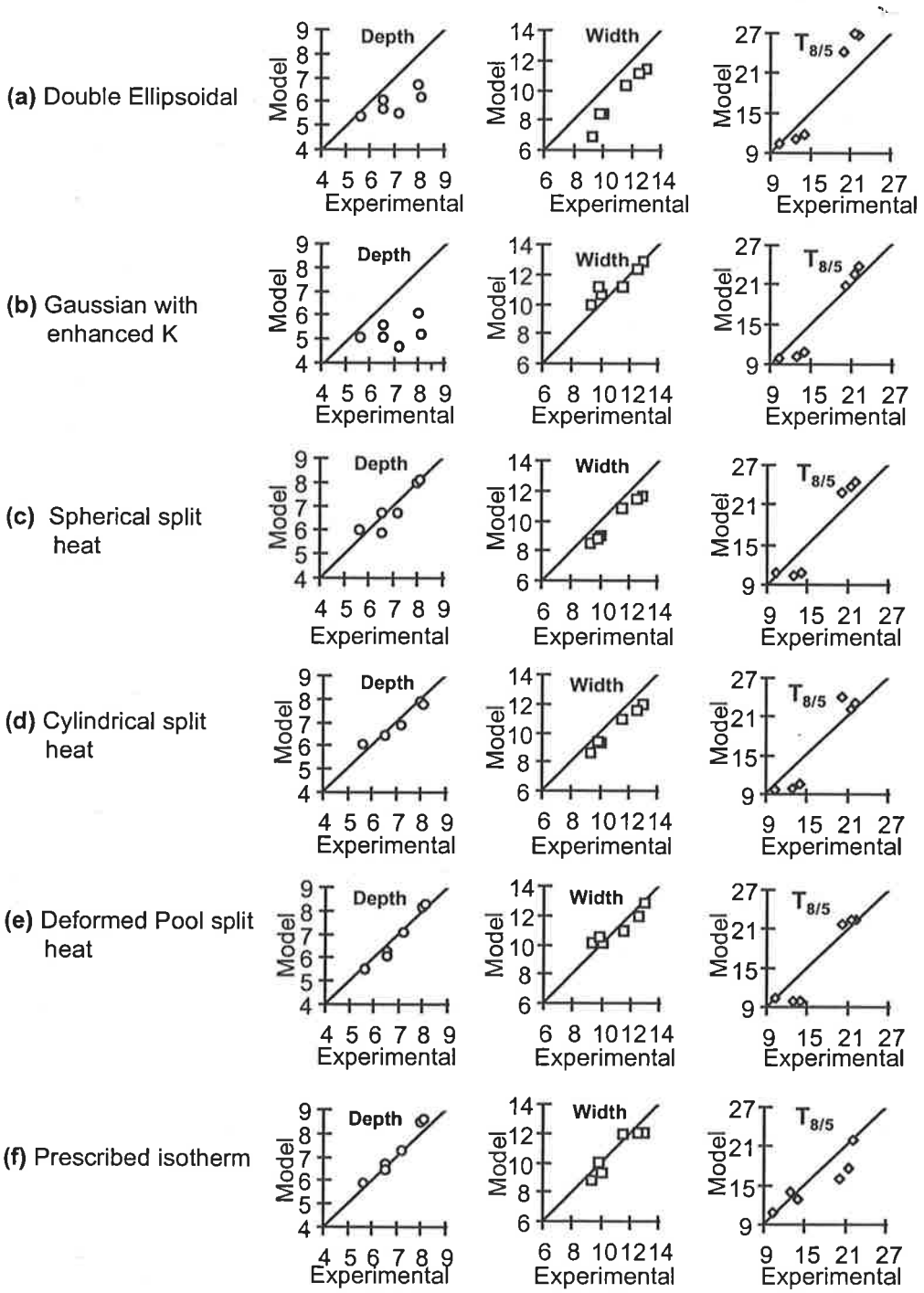

Figure 4.12 Model versus experimental results for various heat sources.

The mean error for each heat source type over the range of welding conditions is presented in Table 4.8 together with the 95% confidence interval. For example, for a model within the range of weld conditions tested, one can be 95% certain that using a Spherical split heat source, the error in the predicted penetration will be in the range -1±5% (ie. -6% to +4%).

	Error (%)		
Heat Source Type	**Depth**	**Width**	**$T_{8/5}$**
Double Ellipsoid	-14±7	-15±5	6±15
Gaussian & enhanced K	-23± 9	4±5	-6±11
Spherical split heat	-1± 5	-9±2	-1±13
Cylindrical split heat	0± 4	-6±1	-5±14
Deformed Pool split heat	-1± 3	2±5	-7±13
Prescribed isotherm	4± 2	-3±4	-6± 9

Table 4.8 Mean error of weld pool dimensions and $T_{8/5}$ for different heat source definitions over the range of weld conditions, with 95% confidence interval.

The Double Ellipsoidal model showed significant under prediction of weld pool width and depth. Generally, the deeper the experimental weld pool, the greater the error in the model's result. It seems that using a deep Ellipsoidal type distribution for a deep pool is not adequate, since the heat is spread over such a large volume that at the base there is not sufficient concentration of heat to melt the material. In the case of a shallow pool, such as bead on plate, this is not as significant since the heat source is more concentrated, and also, the base of the pool is close enough to the peak heat that heat can be driven to the bottom of the pool by the thermal gradient effects. The need to spread the heat deep into the volume of the plate in an attempt to obtain the required penetration has the effect that the concentration near the surface is also inadequate to obtain the required width of the weld pool. The surface Gaussian with enhanced thermal conductivity gives a good prediction of the weld pool width, but slightly over estimates it due to all the heat being at the surface. The depth however, is very badly under predicted and the enhanced thermal conductivity is inadequate to compensate for this. In fact, if the conductivity was enhanced further, it may increase the error in the width as it would enable a greater amount of heat transfer in this direction too. It would seem that the surface Gaussian heat source alone, would simply only be viable if anisotropic enhancement was possible, favouring conduction in the depth of the pool. As discussed in Chapter 3, this has not been possible to test in this work. The split heat source types, on the other hand, ensure that the concentration of heat at the depth of the pool is high and thus enable the penetration to be achieved. Of course, this concentration of heat at a depth, means some of the surface heat is removed and placed in the volume below the surface. This has resulted in slight under prediction of the weld pool

width for the split heat sources using the standard Gaussian surface heat source. The spherical split heat source is worse than the cylindrical in this regard since it takes the droplet heat component further away from the surface region. The deformed pool split heat source overcomes this width prediction issue because it delivers the surface component of the heat further out towards the edges of the weld pool. The result is an accurate width *and* penetration prediction which is not achieved by the other heat source definitions. The prescribed isotherm does give good results on all fronts, but this is to be expected since it is not predictive but is entirely tuned to each individual weld run.

Figure 4.13 gives an indication of how well the models predict the weld fusion shape. The results are for weld run 5 (see Table 4.1) which is a fairly typical weld condition. The model plots show the peak temperature reached at each point in the x-section plane. The "finger penetration" which is visible in the experimental result is only adequately modelled by the split heat sources, and, of course the prescribed isotherm. The finger penetration is more pronounced in the experiment than in the model results. Of the trialed heat sources, the deformed pool split heat source gives the best result due to the surface heat component widening the weld pool near the surface more than the other split heat sources.

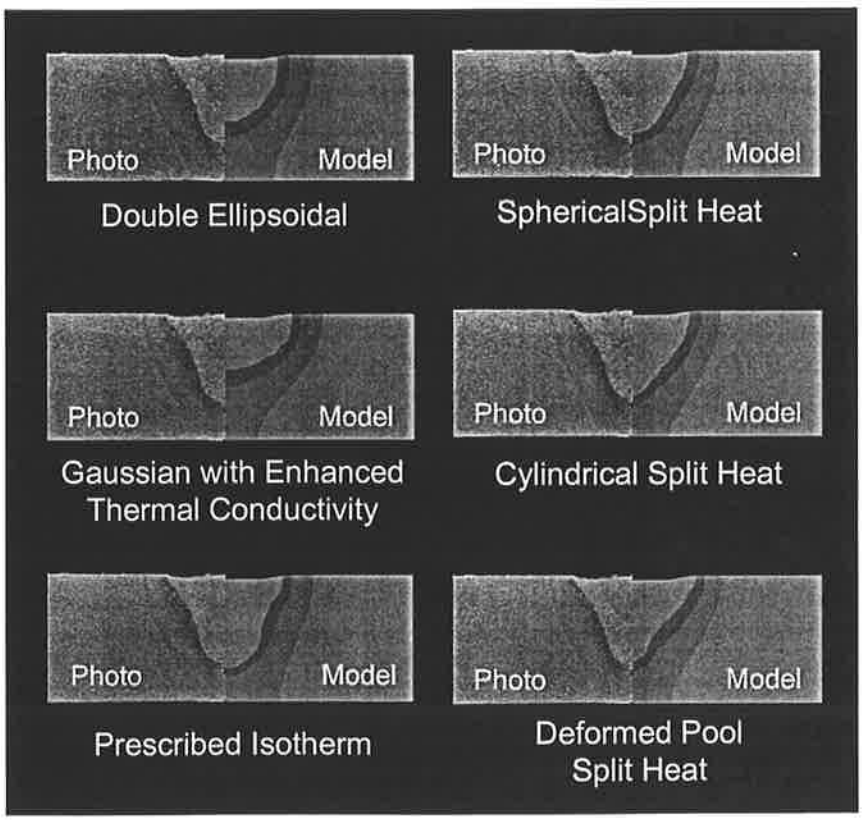

Figure 4.13 Comparison of experimental against predicted V-joint fusion profile for different heat source definitions with weld run condition 5 (ref. Table 4.1).

The error in $T_{8/5}$ is a little more difficult to discuss, as it is not clear as to the cause of these errors. Looking at the plots of experimental versus model $T_{8/5}$ in Figure 4.12, the form of the error seems to be similar for each heat source type except the prescribed isotherm. Some of the plots are offset and yield a different mean which makes it appear more accurate in Table 4.8, however, all of the tested heat sources predicted very low results for runs 5 and 6 and generally over predicted the $T_{8/5}$ for high energy input cases. In fact, if we were to consider the high and low energy cases individually, the deformed pool split heat source gives the best results for the high energy case, but the poorest results for the low energy case. The difficulty in modelling the low energy runs is an area that could receive further attention.

Further work with welds of different V-joint preparations is presented in the case study in Section 4.8.

4.2.5 CONCLUSION

The traditional DE cannot be applied unmodified to V-joint welds if prediction of the fusion profile is required. The reason for this is that it is incapable of delivering sufficient concentration of heat to the base of the weld pool to generate the deep penetration profile of V-joint welds. In addition, due to the shape of the heat source, only an elliptical shaped weld pool can be generated by the DE heat source. The Surface heat source has the same problems as the DE and the only potential for possible application is a strongly anisotropic thermal conductivity, favouring heat transfer in the depth of the pool.

The prescribed isotherm gives very good results, but the weld has to be fully measured before it can be modelled. Hence, the heat source is not predictive, but fully tuned to the experimental weld.

The split heat sources are capable of much better penetration predictions due to delivering the droplet component of the heat at a depth related to the impact force. This separation of the droplet and arc components of the heat results in less heat being applied near the surface and a slight under prediction of the weld pool width. The deformed pool heat source overcomes this problem by producing a much more realistic surface distribution, whereby the deformation of the weld pool surface, which is significant in GMAW is accounted for. It results a significant amount of heat being applied toward the edges of the pool. This gives the required increase in the weld pool width. The deformed pool split heat source is the recommended heat source for V-joint weld preparations.

4.3 T-JOINT MODEL

A very common welded joint configuration is a T-joint in which two pieces of material are butted perpendicularly against each other. There is very little work observed in literature which has gone specifically into T-joint analysis. This work not only models a T-joint, but tests heat source definitions for their effectiveness.

One interesting example of T-joint modelling worth mentioning is the work of Jeong and Cho (1997) who used *analytical* methods quite successfully on a T-joint weld. They mapped the temperature distribution from a flat plate to a T-joint, using an energy equation. The model required averaged material properties and no bead to be allowed for. The heat source parameters and the efficiency were adjusted to optimise the solution for each welding condition. It would seem that the method although it yields good results with errors of the order of 24% under prediction of width and 11% over prediction of depth, would need to be improved if the method is to be predictive over a range of conditions.

4.3.1 EXPERIMENTAL DATA

The physical welding process which was modelled in the following work is shown in Figure 4.14. In a similar manner to the V-joint models, several weld conditions were used to provide a range over which to test the heat sources. Pulsed robotic GMA welding was again used, with 82% Argon, 18% CO_2 shielding gas. The wire diameter was 1.2 mm with contact tube to work piece distance of 18 mm. The experimental conditions are listed in Table 4.9 with the corresponding measured results in Table 4.10.

Run	Current (A)	Voltage (V)	Velocity (mm/min)	Power (kW)	Energy (kJ/mm)
1	185	21	300	5.0	1.0
2	240	26	300	7.5	1.5
3	280	30	300	10.0	2.0

Table 4.9 Experimental weld conditions (pulsed robotic welding).

Run	Width (mm)	Depth (mm)	T_{85} (sec)
1	8.5	6.0	4.3
2	11.0	8.1	9.8
3	12.6	8.9	16.4

Table 4.10 Measured results of the weld pool dimensions and cooling time $T_{8/5}$.

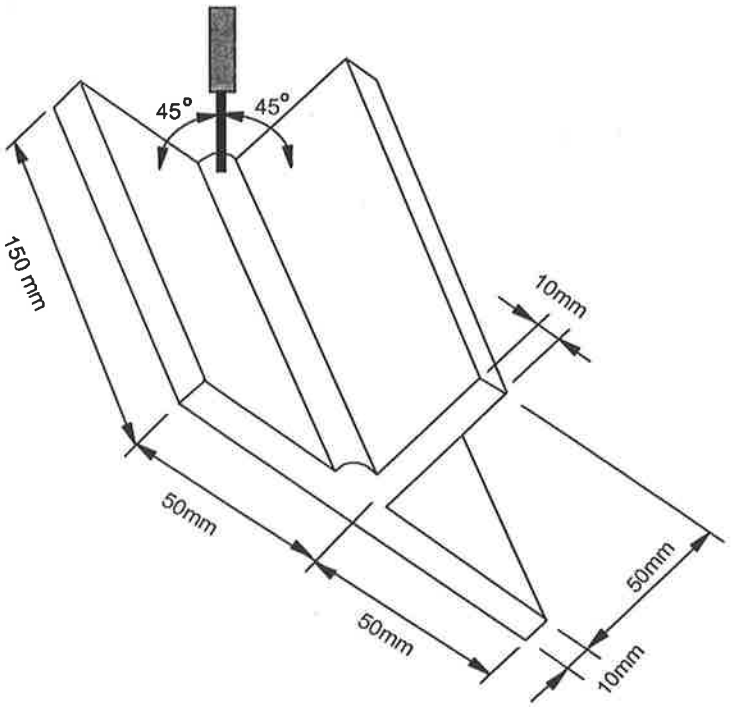

Figure 4.14 The T-joint weld configuration.

The definition of the depth and the weld pool width recorded in Table 4.10, is shown in Figure 4.15. The depth is measured from the bottom of the fusion zone to the height the bead would fill if the bead cap was flat (represented by the hashed line).

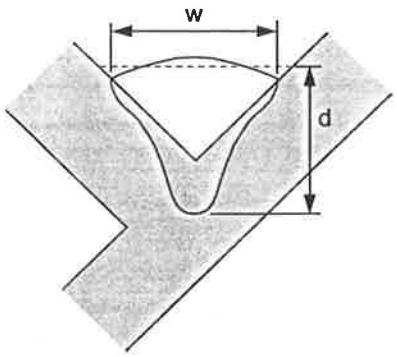

Figure 4.15 Definition of T-joint weld penetration and width.

4.3.2 MODEL

The mesh used in the modelling of the T-joint is shown in Figure 4.16. The full model was meshed since there is no line of symmetry. The bead was meshed into the plate using trend measurements of the wire feed rate. It was given a flat cap as shown by the hashed line in Figure 4.15, determined from empirical information on the wire feed rate. A mesh was

generated which could be modified by stretching the elements to any desired bead height using a Fortran program. The size of elements in the heat source region is about 1.5 mm^3. The mesh was loaded with boundary conditions as described in Chapter 2.

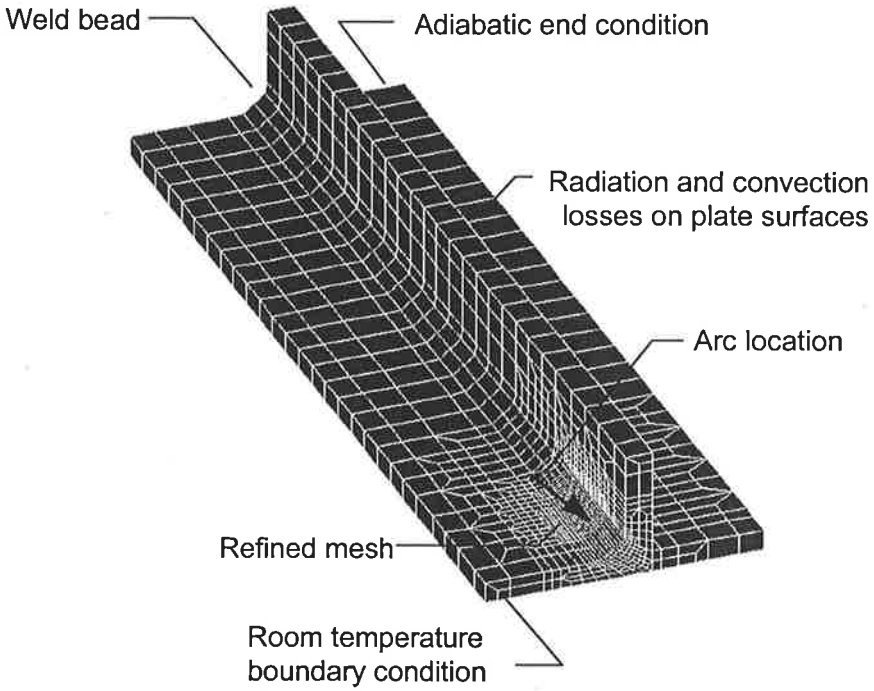

Figure 4.16 T-joint mesh.

4.3.3 HEAT SOURCES

Depositing weld metal into the vee formed between the two plates is not much different to welding into a 90° V-joint preparation so it is anticipated that similar results will be obtained to the V-joint in terms of the most effective heat source type. Those trialed in this section are the Double Ellipsoid, again primarily as a gauge, and the split heat source. The surface Gaussian was not pursued further as it is clearly a poor heat source definition without anisotropic material properties. The prescribed isotherm was also left out since it is considered to have limited application since every weld has to be laid before it can be modelled. The method of applying it and it's effectiveness was adequately demonstrated for the V-joint models. The split heat source is expected to have the best potential. Note that the deformed pool split heat source would be ideal, but it was a recent addition to the thesis and has not yet been applied for the T-joint.

Double Ellipsoidal:

The DE parameters used for this analysis were the same as those used for the V-joint. That is, the DE width and depth were taken directly from the experimental weld bead dimensions,

the length of the rear half ellipsoid was equal to the bead width, the fraction of heat in the front and rear portions of the DE were made equal.

Split heat source with cylindrical volume:

Refer to Section 3.4 for details of this heat source type. Information which is required to apply this heat source is the wire feed rate and an empirical relationship for the penetration versus current. An empirical equation for the wire feed rate is found from experimental measurements. This is shown in Table 4.11 and Figure 4.17.

Run	Current (A)	Wire Feed (gm/sec)	
		Measured	Regression
1	185	1.03	1.03
2	240	1.32	1.33
3	280	1.56	1.55

Table 4.11 Measured wire feed and the resulting empirical wire feed.

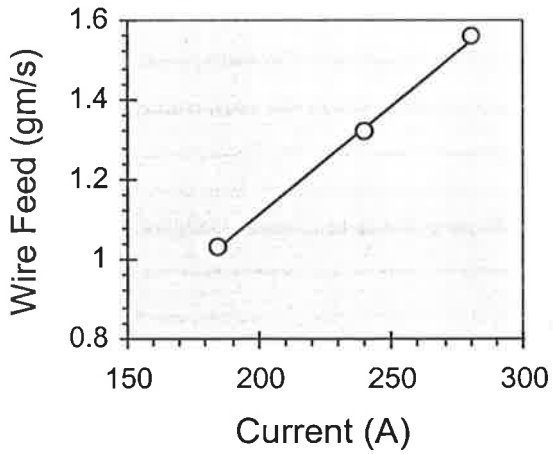

Figure 4.17 Plot of experimental (o) and empirical (solid line) wire feed.

The depth of application of the heat source is also calculated empirically from a linear equation of penetration versus current. With the penetration defined as shown in Figure 5.15, a good linear relationship was obtained between the current and penetration and this is shown in Table 4.12 and Figure 4.18.

Run	Current (A)	Penetration (mm)	
		Measured	Regression
1	185	6.0	6.1
2	240	8.1	8.0
3	280	9.3	9.4

Table 4.12 Measured penetration and the resulting empirical penetration.

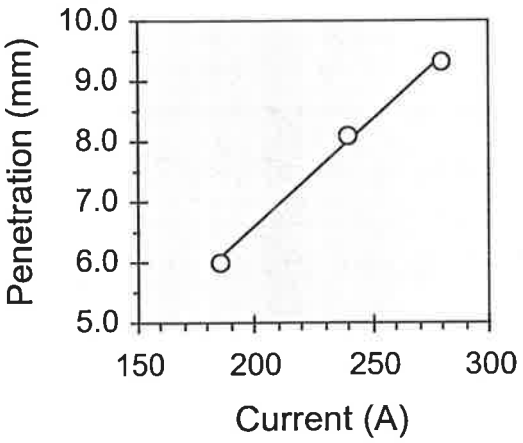

Figure 4.18 Plot of experimental (o) and empirical (solid line) penetration.

The surface component of the split heat source was a Gaussian heat distribution with a characteristic radius of 7.5 mm.

4.3.4 RESULTS AND DISCUSSION

The solution time was approximately 1 hour of CPU usage for each welding condition. The weld pool dimensions were extracted from thermal contour plots of the weld such as that shown in Figure 4.19, and the $T_{8/5}$ values from the thermal history at a point in the mesh corresponding to the thermocouple location.

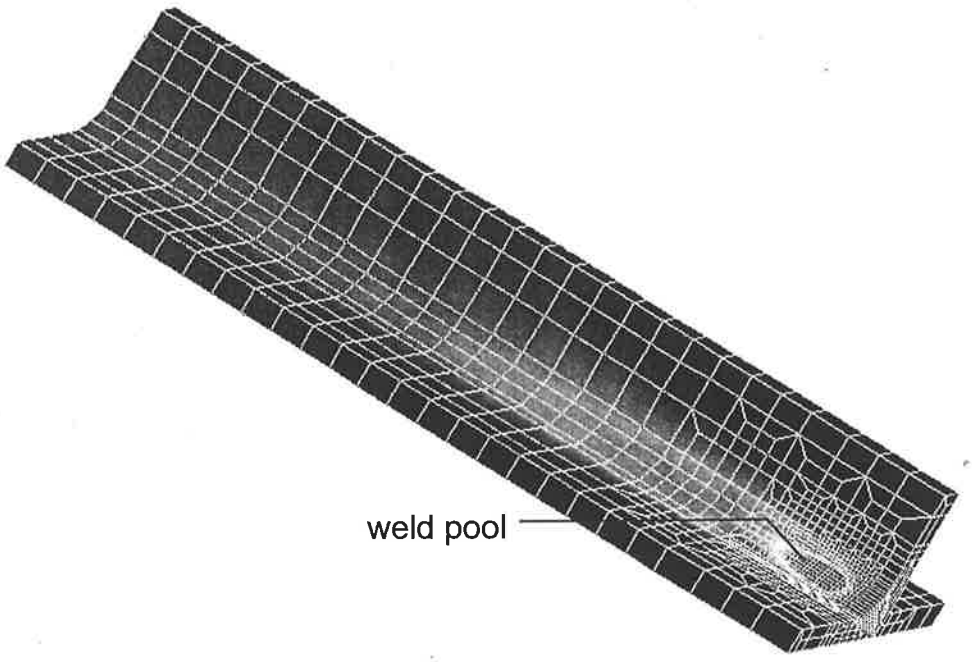

Figure 4.19 Typical thermal contour plot for a V-joint weld with the molten region highlighted.

The results for the heat sources and welding conditions are given in Table 4.13 and presented graphically in Figure 4.20. The graphs are a plot of the predicted pool dimension or $T_{8/5}$ against the experimental one. Hence if the model matched the experimental exactly then the data points should fall on a straight 45° line.

	Penetration (mm)					Width (mm)					T8/5 (sec)				
		Model		%Error			Model		%Error			Model		%Error	
Run	Expt	DE	Split	DE	Split	Expt	DE	Split	DE	Split	Expt	DE	Split	DE	Split
1	6.0	4.3	5.9	-28	-2	8.5	6.8	8.0	-20	-6	4.3	3.4	4.4	-21	2
2	8.1	5.8	8.0	-28	-2	11.0	9.1	10.0	-17	-9	9.8	6.6	8.4	-33	-14
3	9.3	6.9	9.5	-26	2	12.6	10.7	12.0	-15	-5	16.4	11.6	15.5	-29	-5
	Average Error:			-27	0	Average Error:			-17	-7	Average Error:			-28	-6

Table 4.13 Experimental and predicted results for T-joint.

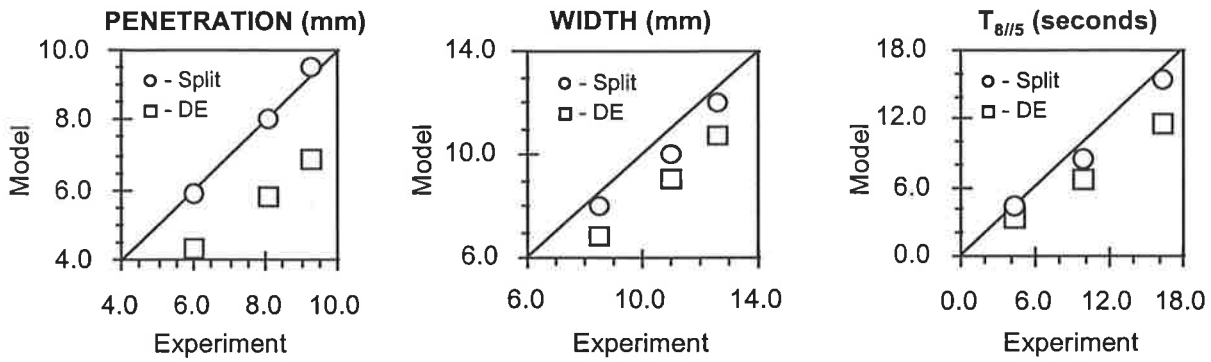

Figure 4.20 Plots of model versus experimental results for T-joint.

The DE heat source again showed the feature of under predicting the depth of the weld pool, in this case by an average of 27%. Note that it is not statistically sensible to give a 95% confidence interval since only three welding conditions are used. The width error was worse than expected, being -17% on average. Presumably this is because the DE was spread over such a large volume that there was not sufficient heat density at the surface near the edges of the source. If the details of the weld pool are not needed, but only the temperature field in the wider plate, then this would be quite adequate. The $T_{8/5}$ is also under predicted by an average of 28%.

The cylindrical split heat source was very effective in modelling the pool width and depth with average errors of -7% and 0% respectively. The width of the pool is somewhat under predicted and it is anticipated that using the deformed pool split heat source would compensate. A T-joint weld is a prime application for the deformed pool heat source since

the edges of the T-joint are quite close to the wire and would draw a considerable amount of arc current and heat. The $T_{8/5}$ predictions were better than expected when compared to the results for the V-joint, with an average under prediction of 6%.

A typical x-section plot of the peak temperature distribution for the T-joint weld is given in Figure 4.21 together with the experimental x-section. The weld condition is run number 3 (see Table 4.9) which has the greatest level of finger penetration. The split heat source is able to predict the profile with finger penetration well.

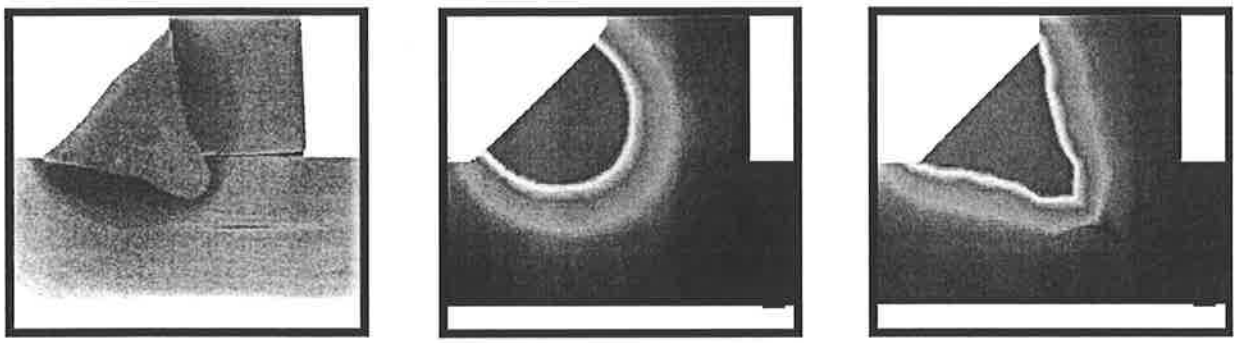

Figure 4.21 T-joint x-section of fusion zone: **(a)** Experimental; **(b)** Double Ellipsoidal Model; **(c)** Cylindrical Split Heat Model.

4.3.5 CONCLUSION

Modelling of a T-joint weld is shown to be very similar to modelling a V-joint. The split heat source that worked very well for the V-joint was also very effective for the T-joint. The cylindrical split heat source was used, but it is anticipated that the deformed pool split heat source would give still better results, reducing the under prediction of the weld pool width. The DE heat source with the given heat source parameters was unable to cope with the deep weld pool penetration.

4.4 MULTI-PASS AND PRE-HEAT MODELS

This section deals with modelling multi-pass and preheat welds using a QSS analysis, thus contributing to the reduction in the time requirements of these problems. In this section preheat and multi-pass models are both addressed because they are closely related. After any pass there is a residual temperature field in the plate so the following pass is just like laying a bead onto a preheated plate. Thus, by demonstrating the ability to use QSS models for multi-pass welds, it is also verifying its potential use for preheat models. The only example of a preheat model observed in literature was by Kasuya *et al.* (1993) who addressed the effect preheating has on the predicted $T_{15/1}$ (time to cool from 1500°C to 100°C). They used a 2D transient model where heat is actually added to the model over a specified width for a specified duration to achieve the initial, non uniform temperature distribution.

There are many researchers who have worked with modelling of multi-pass welds, however none have been observed using a QSS model. The major setback of modelling multi-pass welds is that there may be many passes and in a transient model this would greatly increase an already time consuming approach. As a result, all of the transient work observed has used 2D analysis with the exception of Tekriwal & Mazumder (1988) who only modelled two passes for a one inch weld length. Other than simplifying the problem to 2D, another common approach has been to lump the passes together.

Perhaps some of the earliest work on lumping passes in multi-pass welds was presented in a thesis by Kin (1987). He proposed that the number of passes that needed to be modelled could be reduced by grouping weld runs together. Kin found that the process could be simplified to modelling only two passes per layer of weld deposit. All passes in a layer except for the final one were grouped and treated as one pass, then the final pass for that layer was modelled separately. This produced residual stress results which were claimed to be almost identical to modelling every pass of every layer. Note, that the abstract only of this work has been reviewed.

Shim *et al.* (1991) also investigated grouping of passes to reduce the amount of computing time required. They showed that there was little difference in the calculated residual stress when individual passes were grouped and applied as a layer at a time. For thick plate, even lumping two layers gives results close to the individual pass. This work was extended by Tsai, Lee & Shim (1994). They reduced a 38 pass, double-V, 2 inch (50 mm) weld, to 14

passes and to 10 passes with a 2D transient analysis. The results showed very little loss in accuracy of stress predictions as a result of the grouping compared to the full analysis. The heat content of each pass in the group was added and applied to the model over a period of time equal to the sum of the duration of each pass in the group. They also found that root passes and capping passes can not accurately be grouped. It would also appear from their results that the last pass of a layer is more significant than the earlier ones although this was not discussed in their work.

Das *et al.* (1994) applied the grouped pass method, in two dimensional analysis, grouping all passes of one or two layers at the expense of some accuracy. They used a single pass weld to tune the heat source and thermal conductivity enhancement to give an accurate weld pool profile. They found that having tuned the heat source for a single pass, it can then be applied with the same tuning parameters to a multi-pass weld.

Hong *et al.* (1994) showed that grouping passes has little effect on the longitudinal stress distribution, however the surface transverse stress within about 15 mm of the weld toe was under predicted by between about 2 and 5 times.

An example of a 2D non-grouped multi-pass weld is given by Roelens (1995) who modelled multi-pass welding for 30 mm and 60 mm plates ranging from 8 to 30 passes. The thermal results at the end of each pass were used to calculate the microstructural changes and the changes in residual stress. Impressive results were obtained when comparing the calculated and model transverse residual stresses and good results when comparing longitudinal stresses.

Most of the above literature paints a fairly rosy picture of the lumped pass method and in fact, it is probably suitable for most stress analyses, however, there are times when individual passes may be required. For example, Reed & Bhadeshia (1989 & 1994) (refer to Section 1.2.3) produced a thermal model of a 69 pass weld for the specific purpose of finding the volume fraction of unreaustenitised material. It would seem that the grouping method is not suitable for this analysis as the volume fraction is dependant on the thermal effect of individual passes on each other. Even for cases where grouping is possible, quite a few passes are often still needed and using a QSS model could save considerable time. Given that most multi-pass models are concerned with calculating the residual stress which depends on the transient temperature field, it is worth noting that QSS thermal results can be easily translated into time dependant temperature values (refer to Section 2.2.4).

4.4.1 EXPERIMENTAL DATA

The test case examined in this work consisted of a 60° vee butt joint in 20 mm plate with 3 mm land which was filled with 5 passes as shown in Figure 4.22. Direct current GMAW with Argon rich shielding gas and 1.2 mm wire were again used. The contact tube to work piece distance was 33 mm for the root pass and 20 mm for the others. The experimental weld conditions for each pass are given in Table 4.14.

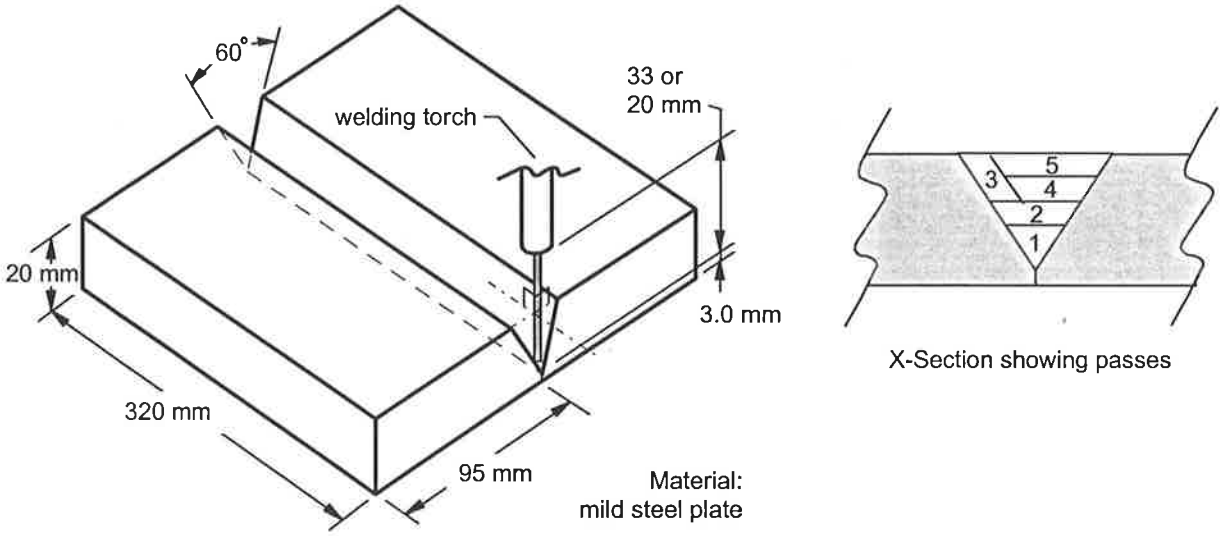

Figure 4.22 Multi-pass joint configuration.

Pass	Current (A)	Voltage (V)	Velocity (mm/min)	Wire Feed m/min	Power (kW)
1	290	34.6	400	13.2	10.0
2	320	33.5	400	9.3	10.7
3	320	33.0	400	9.0	10.6
4	320	34.6	400	11.2	11.1
5	320	34.5	400	11.1	11.0

Table 4.14 Weld conditions for each pass of the weld.

In a multi-pass weld, the profile of the weld bead of the individual passes are not easily defined. Measurements that can be taken to gauge the effectiveness of a model are the $T_{8/5}$ for each pass, the change in the overall plate temperature after each pass, and the final fusion profile of the combined passes. These will all be addressed in testing the model, however it should be pointed out that it is the approach of QSS multi-pass modelling that is being demonstrated and optimising the heat source to obtain accurate model results has not been pursued. Experimental results are listed in Table 4.15; no $T_{8/5}$ value was obtained for pass number 5 due to poor location of thermocouples.

Pass	T_{av} after the pass (K)	$T_{8/5}$ (sec)
1	365	7.8
2	400	9.6
3	426	9.5
4	463	9.8
5	448	-

Table 4.15 Experimental results for each pass.

4.4.2 MODEL

There are two approaches by which multi-pass welds could be modelled with a QSS analysis and these are outlined in Figure 4.23 (a) and (b). In the first case, the solution to a multi-pass weld could be obtained in a single calculation even though each pass is individually modelled. It would consist of a long mesh with a series of heat sources applied along its length, corresponding to the heat applied by each pass. The distance between the heat sources is given by the duration between commencement of passes (t). Thus the plate would be heated by the first pass, cool down over the duration between passes; the residual temperature feeds into the second pass which would add more heat and so forth. The model would only need to be refined around each heat source, but it would still require a very long & large model which may not always be practical. The second option divides this first suggestion into individual passes making the model a more practical size. The length of the mesh is determined by the duration between passes so that the temperature at the end of the plate would correspond to the plate temperature at the start of the next pass. This temperature distribution is applied as the boundary condition on the edge of the next pass so that the plate effectively starts off at this temperature. It can be seen that this is effectively the same as doing a preheat model, whereby the temperature of the plate is set by fixing the temperature of the incoming material at the preheat temperature. The multi-pass solution can be automated so that each pass starts automatically with the final temperature of the previous pass as a boundary condition. In addition to breaking the multi-pass model into more practical size, this second method has another advantage. In some cases, it may be specified that the plate must drop to a certain temperature between passes, rather than there being a fairly consistent time between them. This specified temperature could easily be used as the temperature boundary condition for the next pass. It would however mean that in the proposal in Figure 4.23 (a) the length of plate to be meshed between passes is not known. Another drawback of using the long model is that some of the passes may have a different welding speed which would be difficult to handle is this QSS scenario. In this work proposal (b) of Figure 4.23 will be used.

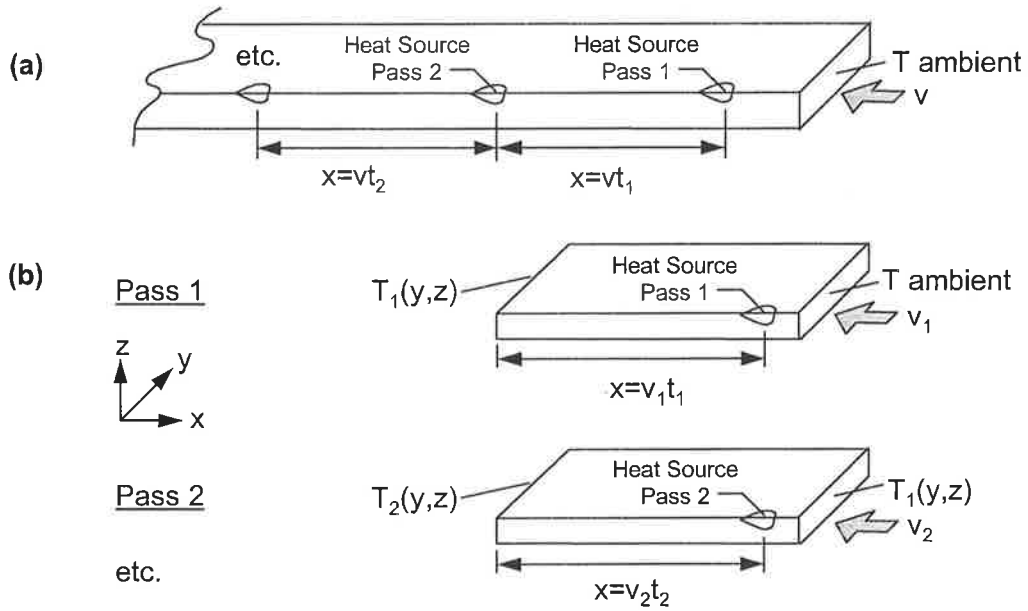

Figure 4.23 QSS multi-pass weld models **(a)** single calculation **(b)** multiple calculation.

At each pass a weld bead is added. All the weld bead passes are meshed into the model, but given material properties to "turn the material off" until the bead is deposited. These material properties are a low specific heat and low conductivity so that very little heat can be conducted into the bead and it is only capable of absorbing an insignificant amount of heat. As each pass is deposited its material properties are changed to the standard temperature dependant thermal conductivity and specific heat for steel. Boundary conditions of radiation and convection are added as per the models in previous sections.

The mesh used in this work is a very basic, coarse mesh with a simple heat source. It is shown in Figure 4.24. The material deposited in each pass is outlined in bold.

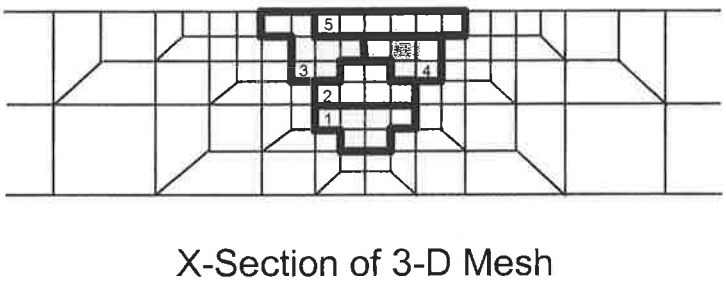

Figure 4.24 Multi-pass mesh.

The heat source was simply a uniform distribution of the heat into 12 elements for each pass. The elements loaded with heat are shown shaded in Figure 4.23 and go three elements deep into the page (hence only 4 elements per pass are shaded).

4.4.3 RESULTS AND DISCUSSION

The $T_{8/5}$ and the temperature of the plate predicted at the end of each run is given in Table 4.16

Pass	T_{av} after the pass (K)	$T_{8/5}$ (sec)
1	358	7.7
2	405	9.2
3	443	12.7
4	481	14.2
5	490	17.6

Table 4.16 Multi-pass model predictions.

The predictions are very good for the first couple of passes, but then the model begins to over predict both the $T_{8/5}$ and the residual plate temperature. Too much heat is being added to the plate in the model, or not enough is being lost. It is possible that radiation and convection coefficients should be increased. More likely the plate was not well enough insulated from the welding table. For a single pass weld, this is not very significant, but when the plate is mounted for an extended period of time such as in a multi-pass weld, a significant amount of heat may have been lost. This became more apparent as time progressed.

Looking at the resultant fusion profile at the completion of the weld runs and comparing it to the experimental profile (Figure 4.25), a surprisingly good result was obtained considering the basic model that was used. Note that the experimental profile was plotted from the test piece for clarity.

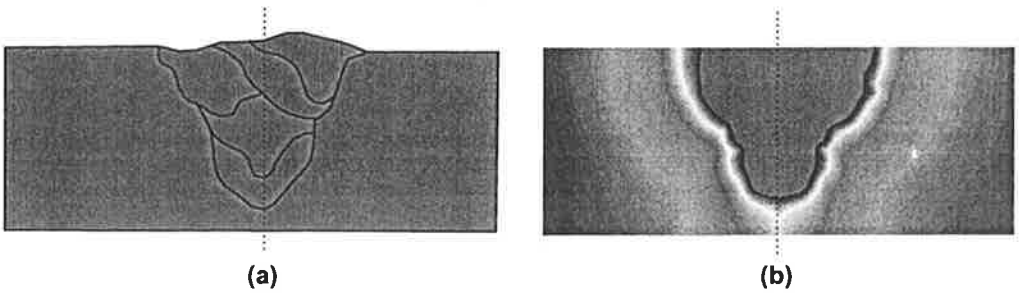

Figure 4.25 Experimental **(a)** and modelled **(b)** fusion profiles resulting from the multi-pass weld.

4.4.4 CONCLUSION

This section has demonstrated the effectiveness of using a QSS model to predict multi-pass welds. Despite a very simple model, good results were obtained. The means by which a QSS model can be used for welds with a preheat was also shown.

4.5 WEAVING

Weaving is a welding technique in which the welding torch is simultaneously moved forward in the weld direction and from side to side, forming a weaving pattern. This widens the weld pool and weld bead and allows more material to be deposited in a single pass. The technique may be used in filling a wide joint preparation, or in a capping run to neatly finish a weld and ensure there is no undercutting.

4.5.1 EXPERIMENTAL DATA

The weave weld considered in this work could exemplify a finishing run for a multi-pass weld such as the one described in the previous section. A 60° v-butt joint of the same configuration as that used in the multi-pass section was modelled. If the two passes following the root pass were laid side by side the groove would be filled to about 4.5 mm from the top of the plate. This could then be finished with a weave weld to fill the remaining cavity. In order to investigate this weaving application, the first 3 passes were not actually laid, but a groove was milled into a plate, as shown in Figure 4.26, to represent the cavity that would remain if they had been laid. By doing this, the weave fusion line is easily visible rather than being blended and possibly confused with the first passes.

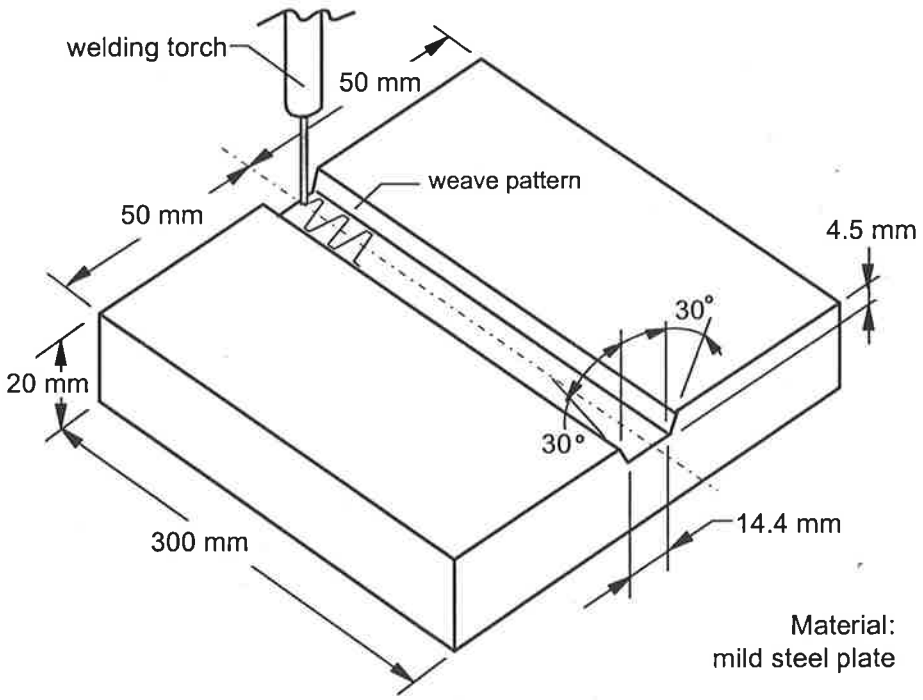

Figure 4.26 Weave weld plate configuration.

The weave used to fill the groove shown above was produced by a robotic welding machine, using the weave form shown in Figure 4.27. The wire diameter was 1.2 mm with a contact tube to work piece distance of 16 mm. The welding voltage was 37 V with a direct current of 414 A, and the shielding gas was 90% Argon and 10% CO_2. The velocity in the direction of the weld seam was 230 mm/min. A preheat of 432 K was applied to reflect the heat that would have been introduced if the first 3 passes had been laid. This is the temperature of the multi-pass weld plate after the first three passes.

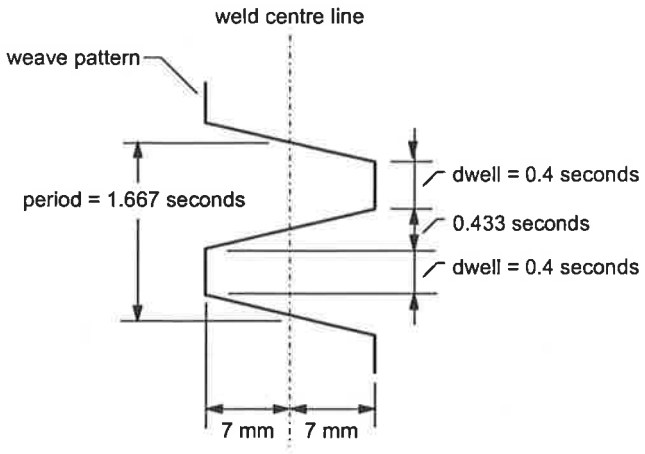

Figure 4.27 Weave form.

The weave form shown in Figure 4.27 was used in the initial experimental run and resulted in the fusion profile shown in Figure 4.28 (a).

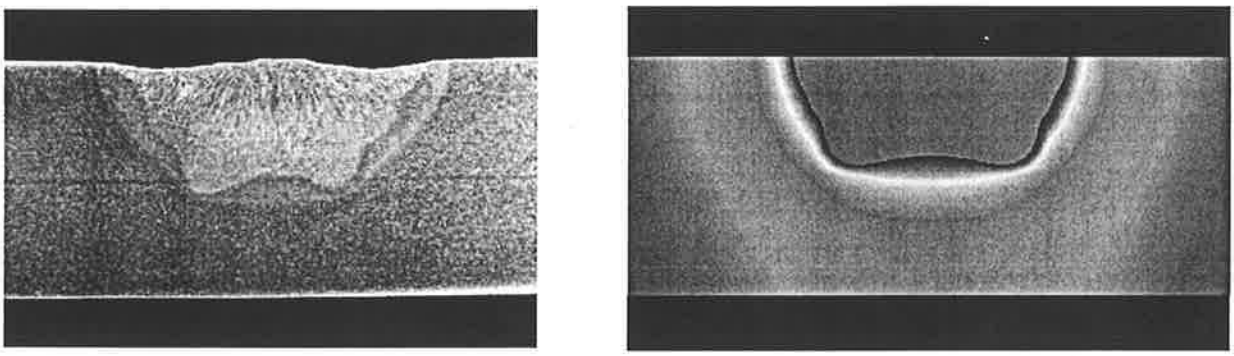

(a) **(b)**

Figure 4.28 Fusion profile of weave weld with 0.4 seconds dwell time: **(a)** experimental, **(b)** model.

4.5.2 MODEL

No published work has been found that addresses modelling of weave welding. In this section a method is presented and proven to be suitable for modelling a weave weld using a modified heat source and QSS analysis.

There are two alternative approaches by which weave modelling could be attempted:
(a) use a transient model with the heat source following the weave pattern;
(b) use a transient or steady state analysis using a heat source that does not weave, but is wide to reflect the width of the weave.

The second option is chosen for this work as it can be applied to a QSS model. If the welding problem required that a transient model be used, the second option would still be the simplest to apply, so it is certainly worthwhile proving it as a viable option. The only concern with using the wide steady heat source is that it does not capture the effect on the temperature field of the heat source being offset from side to side. For a realistic weave pattern which is quite tight such as the one used in this work, the transient effect of the heat source weaving seems to be entirely damped out. This can be observed by looking at the x-section of the weave weld in Figure 4.28 which shows symmetry about the centre line.

The heat source used in the weave model was a split heat source with a surface Gaussian representing the arc and a spherical volume source representing the droplet (refer to Section 3.4.3). The radius of the droplet was 2.4 mm and the depth of the droplet was tuned to the depth of the weave weld profile at the centre line. A Fortran program was used to integrate the heat source over a weave cycle and convert it into a steady heat source. This was done as outlined in Figure 4.29 (a). A fine array was used and the heat source was swept in a straight line from side to side with the amplitude and time duration of a single weave cycle. For each point in the array the heat was summed as the source passed through it and then divided by the duration of the cycle to obtain the average heat content at that location. The resulting form of the heat source is shown in Figure 4.29 (b). The peaks in the surface part of the source are due to the dwell at the extremities of the weave. For the same reason, the heat contained within the elongated sphere would be more concentrated at the edges too.

The weld plate was meshed with elements in the region of the weave being about 2 mm^3. The preheat was modelled by applying a temperature of 432 K as a boundary condition where the material enters the mesh.

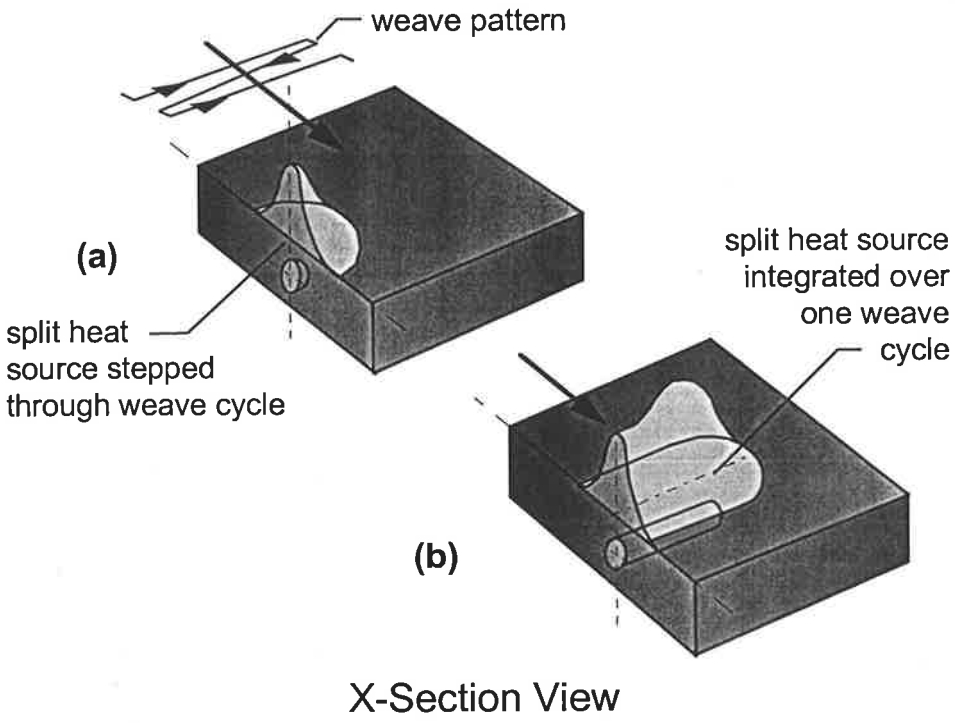

Figure 4.29 Generating a weave heat source **(a)** the base split heat source, **(b)** the integrated split heat source.

4.5.3 RESULTS AND DISCUSSION

The weave weld's fusion profile observed in the initial experimental run (Figure 4.28 (a)) was considered not to be ideal. It was assumed that an ideal weave profile would leave a relatively flat base to the fusion profile. It was decided that the model should be used to determine what weave dwell time would give the desired flat fusion profile.

To start with, the initial weave weld was modelled resulting in the fusion profile shown in Figure 4.28 (b) above. The shape of the fusion zone is good, but under predicted in its dimensions by about 13%. The reason for the under prediction is not certain since the total heat added to the weld is correct and this is what affects the overall size of the fusion zone. Despite the under prediction, the twin finger penetration effect was present, so the model was considered suitable to use for investigating the modification of the weave pattern. The dwell time was reduced from 0.4 to 0.2 seconds. This produced a model fusion profile which was quite semi-circular in shape so a dwell time of 0.3 seconds was tried. The fusion profile with this condition was close to what was intended and so an experimental verification with this new weave was done. The model and experimental fusion profiles for a dwell of 0.3 seconds are shown in Figure 4.30 (a) and (b) respectively.

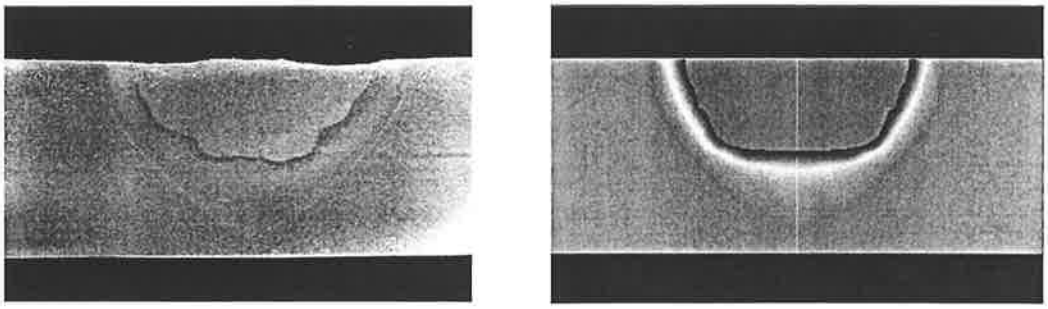

(a) **(b)**

Figure 4.30 Fusion profiles with weave having 0.3 second dwell; **(a)** experimental, **(b)** model.

4.5.4 CONCLUSION

The idea of using an integrated heat has been demonstrated and shows quite some merit. A little more work is recommended to determine the reason for under prediction of the fusion size. The integrated weave heat source is capable of capturing the effect the weave pattern has on the fusion shape.

4.6 APPLICATION FOR DISTORTION ANALYSIS

This section provides a practical application for models of the type that have been developed in this thesis for predicting the distortion of a weld.

Models of V-joint welds with varying preparation angles are produced and the predicted fusion shapes used as input for a new method of calculating weld distortion. This method was proposed by Tsai *et al.* (1995) and hinges on the assumption that the predominant cause of distortion in a weld is the shrinkage of the molten material in the weld bead as it cools. It is thus known as the shrinkage volume method and is of significant industrial relevance. It enables the distortion of complex structures to be found quickly and simply compared to the traditional modelling method which requires the entire transient thermal history, the microstructural changes and a stress analysis. The shrinkage volume method is modelled by applying spring elements to the meshed structure with the spring contraction reflecting the weld metal contraction.

Bachorski has taken up the shrinkage volume method too and used thermal fusion predictions from this thesis in his work. The results will be presented below and have been published in international conference proceedings (Bachorski, Painter, Smailes & Wahab (1997)).

4.6.1 EXPERIMENTAL CONDITIONS

Welds were made on 6 mm mild steel plates with V-joint preparations of varying angles. This is shown in Figure 4.31 and the details listed in Table 4.17. Each of the welds had full penetration as would be expected having a root gap. The width of the weld bead at the top, middle and bottom of the plate are listed in Table 4.18.

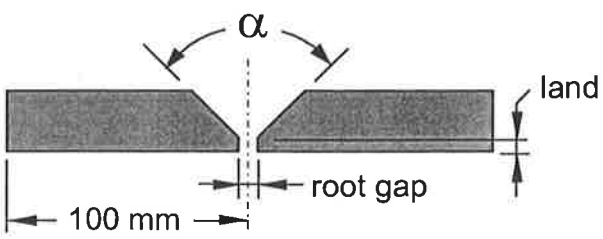

Figure 4.31 Weld set up for distortion tests.

		Current	Voltage	Power	Velocity	Root gap
Expt	α °	(A)	(V)	(kW)	(mm/min)	(mm)
1	90	340	27	9.18	450	0
2	75	340	27	9.18	470	1.6
3	60	340	27	9.18	500	1.2
4	30	340	27	9.18	550	1.6

Table 4.17 Joint details and welding conditions.

		Pool Size (mm)			Wire Feed
Expt	α °	Top	Middle	Base	(g/s)
1	90	14.4	5.1	3.9	1.9
2	75	13.4	5.3	4.6	1.8
3	60	12.4	3.6	3.2	2.0
4	30	12.0	4.1	3.5	1.7

Table 4.18 Fusion dimensions for full penetration weld runs.

4.6.2 MODEL

The models were set up in the same way as in the section on V-joints. The split heat source with a cylindrical droplet (refer to Section 3.4.3) was used. The surface Gaussian was given a radius of 7.5 mm and the cylinder radius was varied. For the case of the 90° weld which had no root gap it was 1.2 mm and for the other welds, the cylinder diameter was made equal to the root gap. This reduction in the size of the cylinder was found to be needed in order to give a high enough concentration of heat to obtain the full penetration. The cylinder radius is effectively being used, in this case, as a tuning device. A much better alternative would have been, time permitting, to gain a better understanding of the effect of the root gap so that the heat source could be modified in a more scientific manner.

4.6.3 RESULTS AND DISCUSSION

The fusion zone width for the model and experiment are compared in Table 4.19. The results are far from excellent with approximately 25% under prediction of the width at the top, 30% over prediction in the middle of the plate and reasonable predictions of the base width.

		Weld Pool Dimensions (mm)					
	α °	Top		Middle		Bottom	
Expt		Expt	Model	Expt	Model	Expt	Model
1	90	14.4	10.4	5.1	6.8	3.9	4.5
2	75	13.4	10.2	5.3	7.0	4.6	5.2
3	60	12.4	9.8	3.6	5.0	3.2	3.3
4	30	12.0	9.3	4.1	4.0	3.5	2.6

Table 4.19 Model and experimental fusion widths.

Using a deformed pool split heat source may go a long way to counteracting the lack of width at the top of the plate, but the effect of the root gap almost certainly needs to be taken into account in some way too. The results in Table 4.19 were used by Bachorski in distortion predictions using the shrinkage volume method. His results are shown in Figure 4.32 taken from Bachorski *et al.* (1997).

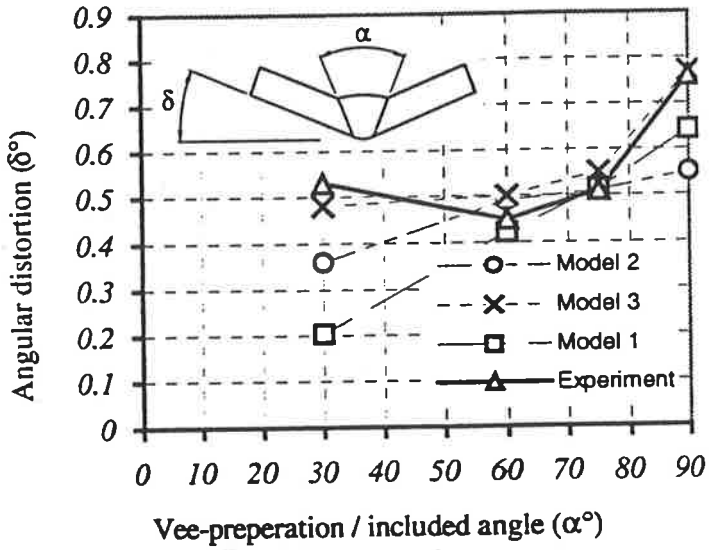

Figure 4.32 Graph comparing three different shrinkage Volume strategies to experimental results. Model 1 used the joint preparation geometry as the shrinkage volume. Model 2 used thermal modelling data to calculate the shrinkage volume and model 3 used the actual welded fusion zone of the welded samples (determined from macro-sections). - Figure taken from Bachorski *et al.* (1997).

4.6.4 CONCLUSION

The work discussed above showed that using the actual fusion line of the molten metal as the defined shrinkage volume produced extremely accurate distortion predictions for butt welded plates of different v-preparations. If the fusion profile really is the major determinant of the distortion of a weld, then this highlights the importance of the thrust of this thesis which is in producing models which are capable of predicting accurate fusion profiles.

The thermal models produced for the distortion prediction tests require further work in terms of understanding the effect of a root gap.

Chapter 5

SUMMARY AND CONCLUSIONS

5.1 SUMMARY

Thermal modelling of gas metal arc welding (GMAW) provides a tool that is being applied in an increasing range of industrial activities. Results from a thermal model can be used to find the width and penetration of a weld and it is vital input for calculating the changes in microstructure, hardness, stress and distortion. These results can often be obtained more expediently by models than by experimentation. The area in which modelling has most potential is in the stress and distortion analysis of large or complex structures, but it can also be competitive for simpler structures and for determination of the weld fusion shape and heat affected zone.

This thesis is mainly concerned with generating simple yet accurate models of GMAW to predict the thermal response of a weld piece for several different welding processes; namely: single pass V-joint and T-joint welds, multi-pass welds, weaving, preheated welds. This involves investigating and improving the heat source definition used to represent the arc and droplets in the various welds.

THE FINITE ELEMENT MODEL

To fully model all the processes occurring within a weld is too complex and computationally uneconomical to yield industrially attractive results. Models have historically been simplified by the following means: modelling the weld piece only and representing the arc and metal transfer as heat and material input boundary conditions; refraining from modelling the complex convective flow within the weld pool, so the model is governed simply by conduction heat transfer; analysing the model in the quasi-steady-state (QSS); reducing the dimension of the model to 2D; linearising the problem by using constant material properties. All but the last two tactics were employed in the models used in this work.

The models were generated using NISA/3D-FLUID finite element modelling software. Three dimensional, eight noded elements were used. The elements in the fusion zone were kept below about 2.8 mm^3 as this level of coarseness was shown to yield no significant loss of

accuracy for the models in this work. In most cases, elements of 1 mm^3 were used in the fusion region. The weld bead was meshed into the model with the dimensions determined from empirical wire feed rate. Material flows through the mesh at the welding velocity, entering at the initial plate temperature. The plate material properties were based on those used by Moore *et al.* (1985) with the latent heat of phase change included in the specific heat and a multiplication of four times the conductivity given to the material in the molten state. Radiation and convective heat losses were included as boundary conditions. The end of the plate was given an adiabatic boundary condition to approximate it being of infinite length and this was shown to be a valid simplification. For a typical set of welding conditions, the QSS model was shown to give the same results as an equivalent transient model to within 5% in the area of thermal interest (near the weld centre line) except near the start and finish of the weld run.

HEAT SOURCES

The conduction based simplification requires compensation to be made for not having flow in the molten weld pool. Appropriate choice of heat source boundary condition and an enhanced conductivity can go some way in achieving this. A major step in this direction was the development of Goldak's Double Ellipsoidal (DE) heat source definition, presented in Goldak *et al.* (1985). The DE heat source distributes heat in a semi-ellipsoidal shaped volume below the surface with the flux a maximum at the centre and reducing in a Gaussian manner to the edges. In addition, the conductivity was enhanced by a factor of four in the molten region. This heat source is very effective for modelling gas tungsten arc welding (GTAW), but has difficulty in GMAW whenever the penetration is deep or there is finger penetration caused by the impacting molten droplets. Heat sources were sought that try to deal specifically with modelling of GMAW. This revealed the emerging concept of the split heat source in which the droplet and arc heat components are applied separately. The most successful of the observed split heat sources had the droplet component applied at some depth in the weld pool, representing the penetrating effect of the impacting droplets. These became the focus of investigating suitable heat sources for the GMAW models in this work.

Two split heat sources were developed based on what appeared to be the most effective features of the split heat sources observed in literature. Both used a Gaussian surface heat source to represent the arc and had the droplet component of the heat applied within a volume at a depth proportional to current. One used a spherical volume of four times the electrode wire diameter and the other, a cylinder of two times the wire diameter. A third novel split heat source was developed using a cylindrical volume for the droplet but making

the surface arc heat component dependent on the deformation of the weld pool surface. This deformation was shown to have a significant bearing on the distribution of heat from the arc, resulting in more heat being applied away from the electrode wire centre line than in the conventional Gaussian distribution. Surprisingly, this deformed surface heat distribution effect has been almost entirely overlooked by weld modellers and it seems it should clearly be accounted for. For the split heat sources described above, the component of heat in the droplet was obtained from steel at the experimental droplet temperature of 2400°C, multiplied by the material flow rate. The flow rate was found from an empirical relationship against current. The remaining heat was applied within the arc component of the source. The split heat source models were tied to the welding power and welding current and could thus be used over a range of welding conditions.

Other heat sources tested were: a surface Gaussian with thermal conductivity isotropically enhanced, based on the Nusselt number which indicates the ratio of conductive to convective heat transfer; a prescribed isotherm representing the weld pool boundary; and finally, Goldak's DE heat source was used as a gauge to indicate the effectiveness of the heat sources tested. For all the heat sources, an efficiency of 80% was used, based on published experimental data.

A considerable effort was expended pursuing inverse methods as a means to calculate the most effective heat source definition. A method was developed and attempted, but proved to be very complicated with the mathematical approach being unstable. It was thus left open as a possible avenue for future work.

APPLYING THE MODEL AND HEAT SOURCES

All of the heat sources described above were applied to model a V-joint weld. The results were very good for the prescribed isotherm as expected. The isotherm applied to the model was experimentally determined so it is in effect, a way to optimally tune the model. If a full fusion profile is not available, the best heat source definition was clearly the split heat source type. The two split heat sources using the Gaussian surface component both showed under prediction of the weld pool width of about 5 to 10% which the deformed pool split heat source corrected. All the split heat source definitions gave very accurate penetration predictions with close to 0% mean error and small scatter. The $T_{8/5}$ results were not as good with an average under prediction of about 5% and a large scatter. Even the prescribed isotherm produced a similar under prediction of the $T_{8/5}$ and it is unclear at this stage as to the reason for this. The DE heat source under predicted the pool width and depth by about

10 to 15% and was the only heat source to over predict the $T_{8/5}$ value. The Gaussian with enhanced thermal conductivity produced very poor penetration prediction, good width prediction and a $T_{8/5}$ prediction similar to the split heat sources. It was clear that the enhancement should have been in the direction of the flow and not isotropically applied.

Several models were produced for V-joint welds with varying root gaps as part of a distortion analysis. A cylindrical split heat source was used with the diameter of the cylinder linked to the root gap. The linking was done rather arbitrarily and more exploratory work is needed to come up with a scientific means of modelling welds which contain a root gap.

T-joint welds were modelled for which the cylindrical split heat source and the DE heat source were tested. The success of the split heat source was the same as for the V-joint, and it is anticipated that introduction of the deformed pool split heat source would have made further improvements by correcting the under predicted width. The DE results were worse than expected with width and depth being under predicted by an average of about 20% and in contrast to the V-joint model, the $T_{8/5}$ being significantly under predicted.

Several approaches were identified in literature to simplify the very time consuming analysis of multi-pass welds. No researchers, however, have been observed to attempt the significant simplification of making the analysis QSS. A simple model was generated, demonstrating the viability of using a QSS analysis. Reasonable accuracy was obtained considering the model's simplicity. Modelling a QSS multi-pass weld inherently demonstrated the use of QSS to model preheated welds.

No literature was found on the research of modelling weaving welds. It was shown that a weave weld could be modelled using a heat source which was integrated over one weave cycle. In this way, the resulting heat source could be applied to a simple QSS model. A split heat source was used with surface Gaussian and spherical volume components. The model results were sensitive to the weave pattern and changes in the pool profile were predicted for variations in the weave pattern's dwell time.

5.2 CONCLUSIONS

By investigating and extending the current state of knowledge on thermal modelling of GMAW and generating models for common and novel welding applications, the following conclusions were reached:

- Thermal modelling has growing industrial and scientific relevance and value.
- Complicated convection models are adding to our understanding of welding processes, but are not currently viable for industrial application.
- Conduction based models are industrially attractive but convection flow needs to be accounted for. This is done by enhancing the thermal conductivity and distributing the heat to reflect the convective flow.
- For GMAW the modelling direction is to use a split heat source considering the arc and droplet components separately.
  - The arc component is sensitive to the pool deformation which causes more heat to be applied away from the arc centre line than for the conventional Gaussian distribution. The pool deformation should be incorporated in heat source definitions.
  - The droplet component should be applied at a depth proportional to the current, reflecting the down flow induced by the impacting droplets. This also ties the heat source definition to the current making it applicable over a wider range of weld conditions.
- QSS can be used effectively for many welding applications and the loss of accuracy compared to transient models is only evident at the start and end of the welds and away from the weld zone.
- T-joint and V-joint models are accurately modelled using the split heat source type distribution.
- The deformed surface split heat source defined and applied in this work provided excellent results and is proposed as the most suitable heat source available.
- The use of a prescribed isotherm is developed and demonstrated as an accurate alternative heat source when a complete fusion boundary is known.
- Weaving welds are modelled for the first time. Integrating the weave heat source over one weave cycle and using a QSS model, the effect of changing the weave pattern could be predicted.

- Multi-pass and preheat models were modelled using QSS for the first time, providing a new means of simplifying the time consuming transient analysis of multi-pass welds.
- Inverse methods provide an exciting scientific means of deriving an optimum heat source. An inverse approach was developed, but due to complexity, its application was beyond the scope of this thesis.
- Weld pool fusion predictions are used for a simple and effective method of calculating deformation, known as the shrinkage volume method.

The objectives of this thesis have been met, developing efficient and effective thermal FE models, advancing the current state of knowledge of heat sources and applying them to real and original welding situations.

APPENDICES

A: WELD POOL TIPPING DEVICE

The weld pool tipping device is used to eject the molten weld pool material during a weld to reveal the fusion cavity. A test piece is mounted onto the device. The entire unit is then spring loaded with the cables taking up the tension. This induces a very large torque on the device due to the cables being offset from the spring mounting point. The device is prevented from rotating by a triggered clamp. Once the weld has stabilised, the device is triggered and the device is accelerated downwards, rotating as the cables unwind. Most of the molten metal spills from the cavity and any remaining liquid is ejected as the unit hits the strike plate below.

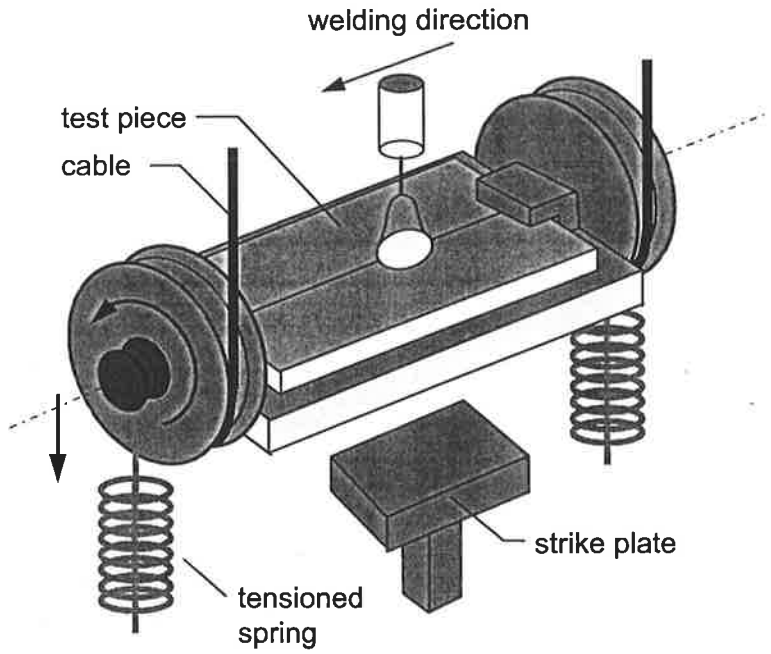

MECHANICAL EJECTION DEVICE

APPENDIX

B: TABULATED V-JOINT RESULTS

A complete table of results for the V-joint models and experiments is given below:

	Run	Experi-mental	Double Ellipsiod	Gaussian with K enhanced	Pres-cribed isotherm	SPLIT HEAT SOURCE		
						Spherical	Cylindrical	Deformed Pool
Depth	1	8	6.7	6.1	8.5	8	7.9	8.2
	2	6.5	6.1	5.6	6.7	6.7	6.5	6.3
	3	5.6	5.4	5.1	5.9	6	6.1	5.5
	4	6.5	5.7	5.1	6.5	5.9	6.5	6.1
	5	7.2	5.5	4.7	7.3	6.7	6.9	7.1
	6	8.1	6.2	5.2	8.6	8.1	7.8	8.3
Width	1	13	11.5	12.9	12.1	11.7	12	12.9
	2	12.5	11.2	12.4	12.1	11.5	11.6	12
	3	11.5	10.4	11.2	12	10.9	11	11
	4	9.3	6.9	9.9	8.8	8.5	8.6	10.2
	5	10	8.4	10.7	9.3	9	9.3	10.2
	6	9.8	8.4	11.2	10.1	8.8	9.4	10.6
T8/5	1	22.2	26.8	23.7	21.9	24.5	23.2	22.4
	2	21.5	27	22.7	17.6	23.7	22.2	22.4
	3	20.1	24.3	20.8	16.1	23	24.1	21.8
	4	10.4	10.4	10	10.8	10.8	9.7	10.3
	5	14.1	11.7	10.8	12.8	10.8	10.6	9.9
	6	12.9	11.1	10.1	14	10.3	9.8	9.8
Length	1	25.5	26.8	24	24.5	24.3	23.7	23.7
	2	20	22.7	19.8	18.8	19.5	19.3	19.4
	3	13.5	17.4	15.3	14	15.7	16	14.6
	4	12	14	13.6	14.5	13.3	12.7	11.7
	5	17	17.4	17.4	17.8	15.5	15.8	15
	6	25	20.8	21.2	24.5	18.7	19.6	19.3

Table A.1 Tabulated results of V-joint experiments and model predictions.

REFERENCES

Allum C.J.
MIG Welding - Time for a Reassessment
Metal Construction, v15, June 1983, pp347-353

Allum C.J. & Quintino L.
Control of Fusion Characteristics in Pulsed Current MIG Welding Part 1
Metal Construction, v17, April 1985, pp242R-245R

Allum C.J. & Quintino L.
Control of Fusion Characteristics in Pulsed Current MIG Welding Part 2
Metal Construction, v17, May 1985, pp314R-317R

Andersson B.A.B.,
Thermal Stresses in a Submerged-Arc Welded Joint Considering Phase Transformations
Journal of Engineering Materials and Technology, Transactions ASME, v100, October 1978, pp356-362

Andrews J.G. & Craine R.E.
Fluid Flow in a Hemisphere Induced by a Distributed Source of Current
Journal of Fluid Mechanics, v84, part 2, 1978, pp281-290

Ashby M.F. & Easterling K.E.
A First Report on Diagrams of Microstructure and Hardness for Heat-Affected Zones in Welds
Acta Metallurgica, v30, 1982, pp1969-1978

Atthey D.R.
A Mathematical Model for Fluid Flow in a Weld Pool at High Currents
Journal of Fluid Mechanics, v98, pt4, 1980, pp787-801

Bachorski A., Painter M.J., Smailes A.J. & Wahab M.A.
Finite Element Prediction of Distortion During Gas Metal Arc Welding Using the Shrinkage Volume Approach
Conference Proceedings of the AMPT'97 Conference, Portugal, September 1997, pp780-784

Balanovskii A.E.
Effective Potential of Ionisation of a Gas Mixture in a Welding Arc
Welding International, v7, n12, 1993, pp967-970

Barberis U. & Rebora A.
Finite Element Analysis of GMA (MIG) Welded Joints
Welding International, v10, n1, 1996, pp44-50

Battersby S.
Chapter 4: Metal Transfer
Internal CSIRO report: Numerical Modelling the Gas Metal Arc Welding Process: A literature Review, Division of Manufacturing Technology, South Australia, 1994, pp71-103

Beck J.V.
Nonlinear Estimation Applied to the Nonlinear Inverse Heat Conduction Problem
International Journal of Heat and Mass Transfer v13, 1970, pp703-715

Beck J.V. & Arnold, K.J.
Book: *Parameter Estimation in Engineering and Science*
pub John Wiley & Sons, 1977

Beck J.V., Blackwell B. & St.Clair C.R.Jr.
Book: *Inverse Heat Conduction Ill Posed Problems*
pub John Wiley & Sons, 1985

Beck J.V.
Inverse Problems in Heat Transfer with Application to Solidification and Welding
Modelling of Casting, Welding and Advanced Solidification Processes V, ed. M. Rappaz, M.R. Ozgu and K.W. Mahin, pub. The Minerals, Metals and Materials Society, 1991, pp503-514

Bergheau J.M. & Leblond J.B.
Coupling Between Heat Flow, Metallurgy and Stress-Strain Computations in Steels: the Approach Developed in the Computer Code SYSWELD for Welding or Quenching
Proceedings; Modelling of Casting, Welding and Advanced Solidification Processes V, ed. Rappaz M., Ozgu M.R. & Mahin K.W., pub. The Minerals, Metals & Materials Society, 1991, pp203-209

Bhole S.D. & Adil G.K.
Modelling of Heat Flow in Arc Welding: A State of the Art Survey
SAMPE Journal, v26, n2, March 1990, pp63-66

Bonnet M., Bui H.D., Maigre H. & Planchard J.
Identification of Heat Conduction Coefficient: Application to Nondestructive Testing
Iutam Symposium Tokyo japan, ed Tanaka, M. & Bui, H.D., pub Springer Verlag, 1992, pp475-487

Bosworth M.R.
Effective Heat Input in Pulsed Current Gas Metal Arc Welding with Solid Wire Electrodes
Welding Journal, v70, n5, May 1991, pp111s-117s

Bozhenko B.L., Bedenko L.I., Kovtun V.L. & Kupar R.Y.
Dissipation of Heat in a Consumable Electrode Taking the Evaporation Process into Account
Welding International, v11, n9, 1997, pp744-747

Carasso A.S.
Space Marching Schemes in the Nonlinear Inverse Heat Conduction Problem
Inverse Problems, v8, 1992, pp25-43

Cary H.B.
Summary of Computer Programs for Welding Engineering
Welding Journal, v70, n1, January 1991, pp40s-45s

Castner H.
Controlling Weld Distortion Reduces Manufacturing Costs for Shipbuilders
American Welding Society Journal, v75, n 11, November 1996

Chan B., Chandel R. & Bibby M.J
A Software System for Computing the Size and Shape of GMA (Gas Metal Arc) Welds
Welding and Joining Processes, ASME, v51, 1991, pp215-225

Chandel R.S.
Mathematical Modelling of Gas Metal Arc Weld Features
Proceedings: Modelling and Control of Casting and Welding Processes IV, ed. A.F. Giamei & G.J. Abbaschian, pub. The Minerals, Metals & Materials Society, 1988, pp109-120

Choo R.T.C, Szekely J. & Westhoff R.C.
Modeling of High-Current Arcs with Emphasis on Free Surface Phenomena in the Weld Pool
Welding Journal, v69, n9, September 1990, pp346s-361s

Christensen N., Davies V de L. & Gjermudsen K.
The Distribution of Temperature in Arc Welding
British Welding Journal, v12, n2, February1965, pp54-75

Das S., Moyer D.K., Tims M.L., Upadhya G.K. & Kleinosky M.J.
Modelling Heat Transfer, Microstructure Development, Transformation Plasticity, and Residual Stresses in GMA Mulit-Pass Butt Welds
Proceedings: Modelling and Control of Joining Processes, Orlando, December 1993, ed. T. Zacharia, pub American Welding Society, 1994, pp454-461

Das S., Upadhya G., Chandra U., Kleinosky M.J. & Tims M.L.
Finite Element Modeling of a Single-Pass GMA Weldment
Modelling of Casting, Welding and Advanced Solidification Processes VI, pub Metals & Materials Society, 1993, pp593-600

Davies M.H.
Numerical Modelling of Weld Pool Convection in Gas Metal Arc Welding
Ph.D Thesis: University of Adelaide, Australia, August 1995

Dike J., Cadden C., Corderman R., Schultz C. & McAninch M.
Finite Element Modeling of Multipass GMA Welds in Steel Plates
Proceedings: Trends in Welding Research, June 1995, ed. H.B. Smartt, J.A. Johnson & S.A. David, pub ASM International, 1995, pp57-65

Dilawari A.H. & Szekely J.
A Mathematical Model of Slag and Metal Flow in the ESR Process
MetallurgicalTransactionsB, v8B, June 1977, pp227-236

Dilthey U., Habedank G., Reichel T., Sudnik W. & Iwanow A.
Numeric Simulation of the Metal-Arc Active Gas Welding Process
Scweissen & Schneiden, v3, 1993, ppE50-E53

Domey J., Aidun D.K., Ahmadi G. & Diebold T.
Numerical Simulation of GTA Welds on Titanium Alloys with Comparison to Experimental Results
Proceedings: International Trends in Welding Science and Technology, June 1992, ed. David, S.A & Vitek, J.M., pub. ASM International, 1993, pp81-85

Doumanidis C.C
GMA Weld Bead Geometry: A Lumped Dynamic Model
Proceedings: International Trends in Welding Science and Technology, June 1992, ed. David, S.A & Vitek, J.M., pub. ASM International, 1993, pp63-67

Eagar T.W. & Tsai N.S.
Temperature Fields Produced by Travelling Distributed Heat Sources
Welding Journal, v62, n12, December 1983, pp346s-355s

Easterling K.E.
Microstructure and Properties of the Heat Affected Zone
Proceedings; Recent Trends in Welding Science and Technology, May 1989, ed. S.A. David & J.M. Vitek, pub. ASM International, 1989, pp177-188

Essers W.G. & Walter R.
Some Aspects of the Penetration Mechanisms in Metal-Inert-Gas (MIG) Welding
Proceedings: Arc Physics and Weld Pool Behaviour, pub. The Welding Institute, Cambridge, May 1979, pp289-300

Essers W.G. & Walter R.
Heat Transfer and Penetration Mechanisms with GMA & Plasma GMA Welding
Welding Journal, v60, n2, February 1981, pp37s-42s

Friedman E.
Thermomechanical Analysis of the Welding Process Using the Finite Element Method
Journal Pressure Vessel Technology, Trans. ASME, v97, August 1975, pp206-213

Friedman E.
Analysis of Weld Puddle Distortion and its Effect on Penetration
Welding Journal, v57, n6, June 1978, pp161s-166s

Fukuda S., Morita H., Yamauchi Y. & Tsuji S.
Expert System for Producing WPS: From the Project in Nagasaki Prefecture
Welding and Joining Processes, ASME, v51, 1991, pp91-97

Giedt W.H., Tallerico L.N. & Fuerschbach P.W.
GTA Welding Efficiency: Calorimetric & Temperature Field Measurement
Welding Journal, v68, n1, January 1989, pp28s-32s

Goldak J.A., Chakravarti A. & Bibby M.J.
A Double Ellipsoid Finite Element Model for Welding Heat Sources
IIW Doc 212-603-85, January 1985

Goldak J., Bibby M., Moore J., House R. & Patel B.
Computer Modeling of Heat Flow in Welds
Metallurgical Transactions B, v17B, September 1986

Goldak J., McDill M., Oddy A., House R., Chi X. & Bibby M.
Computational Heat Transfer for Weld Mechanics
Proceedings: Advances in Welding Science and Technology, 1986, pp15-20

Goldak J.A., Oddy A., McDill M., Chakravarti A., Bibby M. & House R.
Progress in Computing Residual Stress and Strain in Welds
Proceedings: Advances in Welding Science and Technology, May 1986, ed. S.A. David, pub. ASM International, 1986, pp523-527

Goldak J.A.
Keynote Address: Modeling Thermal Stresses and Distortions in Welds
Proceedings; Recent Trends in Welding Science and Technology, May 1989, ed. S.A. David & J.M. Vitek, pub. ASM International, 1989, pp 71-82

Goldak J.A.
Computational Weld Mechanics as a Coupled Problem
Proceedings; Modelling of Casting, Welding and Advanced Solidification Processes V, ed. Rappaz M., Ozgu M.R. & Mahin K.W., pub. The Minerals, Metals & Materials Society, 1991, pp85-96

Goldak J.A. & Gu M.
Computational Weld Mechanics of the Steady State
Mathematical Modelling of Weld Phenomena 2, ed H.K. Bhadeshia, pub The Institute of Materials, 1995, pp207-225

Greene W.J.
An Analysis of Transfer in Gas Shielded Welding Arcs
AIEE Transactions, Part II: Applications and Industry, v79, 1960, pp194-203

Gu M., Goldak J.A. & Bibby M.J.
Computational Heat Transfer in Welds with Complex Weld pool Shapes
Advanced Manufacturing Engineering, v3, January 1991, pp31-36

Gu M. & Goldak J.A.
Steady State Forulation for Stress and Distortion of Welds
Journal of Engineering Industry (J. Engin. Ind.), v116, November 1994, pp467-474

Guo L., Murio D.A.& Roth C.
A Mollified Space Marching Finite Differences Algorithm for the Inverse Heat Conduction Problem with Slab Symmetry
Computers & Mathematics with Applications, v19, n7, 1990, pp75-89

Haidar J. & Lowke J.J.
Predictions of Metal Droplet Formation in Arc Welding
Journal of Physics D, Applied Physics (UK), v29, n12, 1996, pp2951-2960

Halmøy E.
Current-Voltage Process Characteristics in Gas Metal Arc Welding
Welding and Joining Processes, ASME, v51, 1991, pp17-27

Hibbitt H. & Marcal P.
A Numerical, Thermo-Mechanical Model for the Welding and Subsequent Loading of a Fabricated Structure
Computers and Structures, v3, 1973, pp1145-1174

Hinestroza D. & Murio D.A.
Recovery of the Transient Heat Transfer Coefficient in the Nonlinear Boundary Value Problem for the Heat Equation
Computers & Mathematics with Applications, v25, n5, 1993, pp101-111

Hong J.K., Dong P. & Tsai C.L.
Finite Element Simulation of Residual Stresses in Multi-Pass Welds
Proceedings: Modelling and Control of Joining Processes, Orlando, December 1993, ed. T. Zacharia, pub American Welding Society, 1994, pp470-476

Hong K., Weckman D.C., Strong A.B. & Pardo E.
Prediction of Gas Metal Arc Weld Bead Geometry Using a Three-Dimensional Finite Element Thermal Model
Proceedings: Transport Phenomena in Processing, ed. Guceri, S.I., pub Lancaster, Technomic Pub, 1993, pp626-635

Hosbons R.R., Ibrahim E.F., Holden T.M. & Root J.H.
The use of Neutron Diffraction to Determine Non-Destructively the Residual Strain and Texture in Welds
Proceedings; Recent Trends in Welding Science and Technology, May 1989, ed. S.A. David & J.M. Vitek, pub. ASM International, 1989, pp103-106

Hsu K.C., Etemadi K. & Pfender E.
Study of the Free-Burning High-Intensity Argon Arc
Journal of Applied Physics, v54, 1983, pp1293-1301

Jeffus L.
Welding Principles and Applications, 3rd Edition
Delmar Publishers Inc. 1993

Jelmorini G., Tichelaar G.W. & Van den Heuvel G.J.P.M
Droplet Temperature Measurement in Arc Welding
Ilw Document 212-411-77, 1977

Jeong S. K. & Cho H. S.
An Analytical Solution to Predict the Transient Temperature Distribution in Fillet Arc Welds
Welding Journal, v76, n6, June 1997, pp223s-232s

Johnson J.A., Smartt H.B., Clark D.E., Carlson N.M., Watkins A.D. & Lethcoe B.J.
The Dynamics of Droplet Formation and Detachment in Gas Metal Arc Welding
Proceedings; Modelling of Casting, Welding and Advanced Solidification Processes V, ed. Rappaz M., Ozgu M.R. & Mahin K.W., pub. The Minerals, Metals & Materials Society, 1991, pp139-146

Jog M.A., Cohen I.M. & Ayyaswamy P.S.
Heat Transfer in Electric Arc Welding
Welding and Joining Processes, ASME, v51, 1991, pp159-173

Kamala V. & Goldak J.A.
Error Due to Two Dimensional Approximation in Heat Transfer Analysis of Welds
Welding Journal v72, n9, September 1993, pp440s-446s

Karlsson L. & Lindgren L-E.
Combined Heat and Stress-Strain Calculations
Proceedings; Modelling of Casting, Welding and Advanced Solidification Processes V, ed. Rappaz M., Ozgu M.R. & Mahin K.W., pub. The Minerals, Metals & Materials Society, 1991, pp187-201

Kasuya T. & Yurioka N.
Prediction of Welding Thermal History by a Comprehensive Solution
Welding Journal, v72, n3, March 1993, pp 107s-115s

Keanini R.G. & Rubinsky B.
An Inverse Finite Element Minimization-Based Method for Solution of Multi-Dimensional Phase-Change and Material Boundary Shapes
International Journal for Numerical Methods in Engineering v37, 1994, pp1125-1141

Kim J.W. & Na S.J.
A Study on the Three-Dimensional Analysis of Heat and Fluid Flow in Gas Metal Arc Welding using Boundary-Fitted Coordinates
Welding and Joining Processes, ASME, v51, 1991, pp159-173

Kim J.W. & Na S.J.
A Study on the Three-Dimensional Analysis of Heat and Fluid Flow in Gas Metal Arc Welding using Boundary-Fitted Coordinates
Journal of Engineering for Industry, v116, February 1994, pp78-85

Kim J.W. & Na S.J.
A Study on the Effect of Contact Tube-to-Workpiece Distance on Weld Pool Shape in Gas Metal Arc Welding
Welding Journal, v74, n5, May 1995, pp141s-152s

Kin C.
Study of Finite Element Modelling of Multipass Welds
Thesis: University of Waterloo, Canada, 1987

Kohn R.V. & Vogelius M.
Identification of an Unknown Conductivity by Means of Measurements at the Boundary
Proceedings: SIAM-AMS v14, pub American Mathematical Society, 1984, pp113-123

Kou S. & Le Y.
Three-Dimensional Heat Flow and Solidification During the AutogenousGTA Welding of Aluminium Plates
Metallurgical Transactions A, v14A, November 1983, pp2245-2253

Kou S. & Wang Y.H.
Computer Simulation of Convection in Moving Arc Weld Pools
Metallurgical Transactions A, v17A, December 1986, pp2271-2277

Krutz G.W. & Segerlind L.J.
Finite Element Analysis of Welded Structures
Welding Journal, v57, n7, July 1978, pp211s-216s

Kumar S. & Bhaduri S.C.
Three-Dimensional Finite Element Modelling of Gas Metal-Arc Welding
Metallurgical and Materials Transactions B, v25B, June 1994, pp435-441

Kumar S. & Bhaduri S.C.
Theoretical Investigation of Penetration Characteristics in Gas Metal-Arc Welding Using Finite Element Method
Metallurgical and Materials Transactions B, v26B, June 1995, pp611-624

Kumar B.V., Mohanty O.N. & Biswas A.
Welding of Thin Steel Plates: A New Model for Thermal Analysis
Journal of Materials Science v27, 1992, pp203-209

Lancaster J.F.
Metal Transfer in Fusion Welding
Proceedings: Arc Physics and Weld Pool Behaviour, pub. The Welding Institute, Cambridge, May 1979, pp135-146

Lancaster J.F.
Book: *Metallurgy of Welding. Third Edition*
Pub George Allen & Unwin Ltd, 1980

Lancaster J.F.
Book: *The Physics of Welding, 2nd Edition*
Pub New York: Pergamon Press, 1986

Lancaster J.F.
The Physics of Fusion Welding: Part 1 - The Electric Arc in Welding
Part 2 - Mass Transfer & Heat Flow
IEE Proceedings v134, pt. B, n5 September 1987, pp233-254

Lancaster J.F.
Handbook of Structural Welding - Processes, Materials and Methods used in the Welding of Major Structures, Pipelines and Process Plant
Abington Publishing, 1992

Lee S.Y. & Na S.J.
A Numerical Analysis of Molten Pool Convection Considering Geometric Parameters of Cathode and Anode
Welding Journal, v76, n11, November 1997, pp484s-497s

Lesnewich A.
Control of Melting Rate and Metal Transfer in Gas Shielded Metal Arc Welding. Part 2 Control of Metal Transfer
Welding Journal, v37, n9, September 1958, pp418s-425s

Liew C., Wahab M. & Painter M.J.
The Prediction of Temperature Distribution in Gas Metal Arc Welds
Presentation at: WTIA Fabcon/Fabfair, 41st Annual Welding Conference and National AINDT Conference, September 1993

Lin M.L. & Eagar T.W.
Influence of Arc Pressure on Weld Pool Geometry
Welding Journal, v64, n6, June 1985, pp163s-169s

Lin M.L. & Eagar T.W.
Pressure Produced by Gas Tungsten Arcs
Metallurgical Transactions B, v17B, n9, 1986, pp601-607

Lindgren L. & Karlsson L.
Deformations and Stresses in Welding of Shell Structures
International Journal of Numerical Methods for Engineering, v25, 1988, pp635-655

Liu S., Siewert T.A. & Lan H.G.
Metal Transfer Mode in Gas Metal Arc Welding
Proceedings; Recent Trends in Welding Science and Technology, May 1989, ed. S.A. David & J.M. Vitek, pub. ASM International, 1989, pp475-479

Lowke J.J.
Simple Model for the Transition Current from Globular to Spray Transfer in Gas Metal Arc Welding
Australasian Welding Journal, v42, n1, 1997, pp32-35

Macqueene J.W., Akau R.L., Krutz G.W. & Schoenhals R.J.
Development of Inverse Finite Element Techniques for Evaluation of Measurements Obtained from Welding Process
Proceedings: Numerical Properties and Methodologies in Heat Transfer, ed Shih, T.M., pub Hemisphere publishing, 1983, pp149-164

Mahin K.W., Shapiro A.B. & Hallquist J.
Assessment of Boundary Condition Limitations on the Development of a General Computer Model for Fusion Welding
Proceedings: Advances in Welding Science and Technology, May 1986, ed. S.A. David, pub. ASM International, 1986, pp215-223

Mangonon P.L. & Mahimkar M.A.
A Three-Dimensional Heat Transfer Finite Element Model of Submerged Arc Welding of HSLA Steels
Proceedings: Advances in Welding Science and Technology, May 1986, ed. S.A. David, pub. ASM International, 1986, pp35-45

Matsunawa A.
Modelling of Heat and Fluid Flow in Arc Welding
Proceedings: International Trends in Welding Science and Technology, June 1992, ed. David, S.A & Vitek, J.M., pub. ASM International, 1993, pp3-16

Matteson M.A., Franke G.L. & Vassilaros M.G.
A Simple 2-D Thermal Model for GMA Welds
Proceedings: Trends in Welding Research, June 1995, ed. H.B. Smartt, J.A. Johnson & S.A. David, pub ASM International, 1995, pp39-43

McDill J.M.J, Oddy A.S. & Goldak J.A.
Comparing 2-D Plane Strain and 3-D Analyses of Residual Stresses in Welds
Proceedings: International Trends in Welding Science and Technology, June 1992, ed. David, S.A & Vitek, J.M., pub. ASM International, 1993, pp105-108

Mejia C.E. & Murio D.A.
Mollified Hyperbolic Method for Coefficient Identification Problems
Computers & Mathematics with Applications, v26, n5, 1993, pp1-12

Michaleris P. & Sun X.
Finite Element Analysis of Thermal Tensioning Techniques Mitigating Weld Buckling Distortion
Welding Journal, v76, n11, November 1997, pp451s-457s

Miettinen J. & Louhenkilpi S.
Calculation of Thermophysical Properties of Carbon and Low Alloyed Steels for Modelling of Solidification Processes
Metallurgical and Materials Transactions B, v25B, December 1994, pp909-916

Moore J.E., Bibby M.J., Goldak J.A.
The Significance of the Point Source Model Assumptions on Weld Cooling Times
IIW Doc 212-064-85, January 1985

Mundra K., DebRoy T., Babu S.S. & David S.A.
Weld Metal Microstructure Calculations from Fundamentals of Transport Phenomena in the Arc Welding of Low-Alloy Steels
Welding Journal, v76, n4, April 1997, pp163s-171s

Murio D.A.
Automatic Numerical Differentiation by Discrete Mollification
Computers & Mathematics with Applications, v13, n4, 1987, pp381-386

Murio D.A.
The Mollification Method and the Numerical Solution of the Inverse Heat Conduction Problem by Finite Differences
Computers & Mathematics with Applications, v17, n10, 1989, pp1385-1396

Murio D.A. & Guo L.
A Stable Space Marching Finite Differences Algorithm for the Inverse Heat Conduction Problem with no Initial Filtering Procedure
Computers & Mathematics with Applications, v19, n10, 1990, pp35-50

Murio D.A.
Solution of Inverse Heat Conduction Problems with Phase Changes by the Mollification Method
Computers & Mathematics with Applications, v24, n7, 1992, pp45-57

Murthy Y.V.L.N., Venkata Rao G. & Krishna Iyer P.
Paramteric Study of Parrallel Heat Welding Process via Finite Element Simulation
Materials Science and Technology, v10, November 1994, pp981-985

Na S.J. & Lee S.Y.
A Study on the Three-Dimensional Analysis of the Transient Temperature Distribution in Gas Tungsten Arc Welding
Proceedings of the Institution of Mechanical Engineers, v201, nB3, 1987, pp149-156

Nakatani M. & Ohiji T.
An Algorithm for Inverse Heat Conduction Problem in Welding
Qurterly Journal of the Japan Welding Society v11, n2, 1993, pp167-172

Nayama M., Sakamoto N., Takano G. & Akitomo N.
Conditions for Execution of the Two Sided Heating Method ans its Control Procedure: Development of a Residual Stress Control Method for Pipe Butt-Welded Joints (2nd Report)
Welding International, v11, n6, 1997, pp442-451

Nestor O.H.
Heat Intensity and Current Density Distributions at the Anode of High Current Inert Gas Arcs
Journal of Applired Physics, v33, 1962, pp1638-1648

NISA/3D-FLUID
Engineering Mechanics Research Corporation, Michigan

Oddy A.S., Goldak J.A. & McDill J.M.J.
Transformation Effects in the 3D Finite Element Analysis of Welds
Proceedings; Recent Trends in Welding Science and Technology, May 1989, ed. S.A. David & J.M. Vitek, pub. ASM International, 1989, pp 97-101

Oddy A.S., McDill J.M.J. & Goldak J.A.
Consistent Strain Fields in 3D Finite Element Analysis of Welds
Journal of Pressure Vessel Technology, v112, August 1990, pp309-311

Ohji T., Kondo K., Nishiguchi K., Moriyasu M., Hiramoto S. & Shimada W.
An Optimal Heat Input Control of Arc Welding
Qurterly Journal of the Japan Welding Society v8, n2, 1990, pp167-172

Ohji T., Kometani Y., Yoshida Y., Nishiguchi K. & Tie G.
An Optimal Search of Arc Welding Parameters by a Numerical Model
Quarterly Journal of the Japan Welding Society v8, n2, 1990, pp173-178

Ohji T.
Physics of Welding (1) - Heat Conduction Theory and its Application to Welding
Welding International, v8, n12, 1994, pp938-942

Oreper G.M., Eagar T.W. & Szekely J.
Convection in Arc Weld Pools
Welding Journal, v62, n11, November 1983, pp307s-312s

Ortega A.R., Bertram L.A., Fuchs E.A., Mahin K.W. & Nelson D.V.
Thermomechanical Modelling of a Stationary Gas Metal Arc Weld: A Comparison Between Numerical and Experimental Results
Proceedings: International Trends in Welding Science and Technology, June 1992, ed. David, S.A & Vitek, J.M., pub. ASM International, 1993, pp89-93

Paley Z. & Hibbert P.D.
Computation of Temperatures in Actual Weld Design
Welding Journal, v54, n11, November 1975, pp385s-392s

Pardo E., Villafuerte J.C. & Kerr H.W.
A Finite Element Study of the Columnar-Equiaxed Transition in GTA Welding of Stainless Steels
Proceedings; Recent Trends in Welding Science and Technology, May 1989, ed. S.A. David & J.M. Vitek, pub. ASM International, 1989, pp159-164

Pardo E. & Weckman D.C
A Numerical Model of the Gas Metal Arc Welding Process
Proceedings: Modelling and Control of Casting and Welding Processes IV, ed. A.F. Giamei & G.J. Abbaschian, pub. The Minerals, Metals & Materials Society, 1988, pp187-195

Pardo E. & Weckman D.C.
The Interaction Between Process Variables and Bead Shape in GMA Welding: A Finite Element Analysis
Proceedings; Recent Trends in Welding Science and Technology, May 1989, ed. S.A. David & J.M. Vitek, pub. ASM International, 1989, pp 391-395

Pardo E. & Weckman D.C.
Prediction of Weld Pool and Reinforcement Dimensions of GMA Welds Using a Finite-Element Model
Metallurgical Transactions B, v20B, December, 1989, pp937-947

Pavelic V., Tanbakuchi R., Uyehara O.A. & Myers P.S.
Experimental and Computed Temperature Histories in Gas Tungsten-Arc Welding of Thin Plates
Welding Journal, v48, n7, July 1969, pp295s-305s

Pentegov I.V. & Sidorets
Force Effect of the Welding Arc with an Allowance Made for its Dynamics
Paton Welding Journal, v5, n12, 1993, pp734-738

Pilarczyk J. & Szczok E.
Properties of Gas Mixtures used in MAG Welding
Welding International, v8, n11, 1994, pp845-850

Radaj D.
Potential of Numerical Analysis of Weldability in the Design Process
Mathematical Modelling of Weld Phenomena 2, ed H.K. Bhadeshia, pub The Institute of Materials, 1995, pp245-262

Reed R.C. & Bhadeshia H.K.D.H.
Complete Reaustenitisation in Multirun Steel Weld Deposits
Proceedings; Recent Trends in Welding Science and Technology, May 1989, ed. S.A. David & J.M. Vitek, pub. ASM International, 1989, pp205-209

Reed R.C. & Bhadeshia H.K.D.H.
A Simple Model for Multipass Steel Welds
Acta Metallurgica, v42, n11, 1994, pp3663-3678

Rhee S. & Kannatey-Asibu E.Jr.
Observation of Metal Transfer during Gas Metal Arc Welding
Welding and Joining Processes, ASME, v51, 1991, pp203-213

Richardson I.M., Bucknall P.W. & Stares I.
The Influence of Power Source Dynamics on Wire Melting Rate in Pulsed GMA Welding
Welding Journal, v73, n2, February 1994, pp32s-37s

Roelens J.B.
Numerical Simulation of some Multipass Submerged Arc Welding - Determination of the Residual Stresses and Comparison with Experimental Measurements
Welding in the World, v35, n2, 1995, pp110-117

Rokhlin S.I. & Guu A.C.
A Study of Arc Force, Pool Depression, and Weld Penetration During Gas Tungsten Arc Welding
Welding Journal, v72, n8, August 1993, pp381s-390s

Rosenthal D.
Mathematical Theory of Heat Distribution During Welding and Cutting
Welding Journal, v20, n5, May 1941, pp220s-234s

Ruan Y. & Zabaras N.
An Inverse Finite-Element Technique to Determine the Change of Phase Interface Location in Two-Dimensional Melting Problems
Communications in Applied Numerical Methods v7, 1991, pp325-338

Satonaka S., Hari K. & Matsumoto Y.
Effects of Material Properties on Transient Response in TIG Welding
Welding International, v7, n8, 1993, pp607-613

Shah A.K., Kulkarni S.D., Gopinathan V. & Krishnan R.
Weld Heat-Affected Zone in Ti-6Al-4V Alloy, Part I - Computer Simulation of the Effect of Weld Variables on the Thermal Cycles in the HAZ
Welding Journal, v74, n9, September 1995, pp297s-304s

Shah A.K., Kulkarni S.D., Gopinathan V. & Krishnan R.
Weld Heat-Affected Zone in Ti-6Al-4V Alloy, Part II - Modelling and Experimental Simulation of Growth and Phase Transformations
Welding Journal, v74, n10, October 1995, pp325s-338s

Sercliff J.A.
Fluid Motions due to an Electric Current Source
Journal of Fluid Mechanics, v40, 1970, pp241-250

Shim Y., Feng Z., Lee S., Kim D., Jaeger J. & Tsai C.L.
Modeling of Welding Residual Stresses
Welding and Joining Processes, ASME, v51, 1991, pp29-41

Silva Prasad N. & Sankara Narayanan T.K.
Finite Element Analysis of Temperature Distribution during Arc Welding Using Adaptive Grid Technique
Welding Journal, v75, n4, April 1996, 123s-128s

Smailes A.J., Wahab M.A. & Painter M.J.
Finite Element Prediction of the Thermal Response of V-joint Gas Metal Arc Welds
Proceedings: Fourteenth Australasian Conference on the Mechanics of Structures and Materials, ed. A.J. Beasley, C.G. Foster & E.S. Melerski, pub. University of Tasmania, December 1995, v1, pp319-324

Sozou C. & Pickering W.M.
Magnetohydrodynamic Flow Due to the Discharge of an Electric Current in a Hemispherical Container
Journal of Fluid Mechanics, v73, part 4, 1976, pp641-650

Sozou C.
On Fluid Motions Induced by an Electric Current Source
Journal of FLuid Mechanics, v46, 1971, pp25-32

Stolz G.Jr.
Numerical Solutions to an Inverse Problem of Heat Conduction for Simple Shapes
Journal of Heat Transfer, v85C, 1960, pp20-26

Sudnik, W.
Research into Fusion Welding Technologies Based on Physical-Mathematical Models
Scweissen & Schneiden, v10, 1991, ppE216-E217

Szekely J.
The Mathematical Modeling of Arc Welding Operations
Proceedings: Advances in Welding Science and Technology, May 1986, ed. S.A. David, pub. ASM International, 1986, pp3-14

Tarantola, A.
Inverse Problem Theory: Methods for Data Fitting and Model Parameter Estimation, pub Elsevier Science Publishers, 1987

Tekriwal P., Sitt M. & Mazumder J.
Finite Element Modelling of Heat Transfer for Gas Tungsten Arc Welding
Metal Construction, v19, n10, October 1987, pp599R-606R

Tekriwal P. & Mazumder J.
Finite Element Modeling of Arc Welding Processes
Proceedings: Advances in Welding Science and Technology, May 1986, ed. S.A. David, pub. ASM International, 1986, pp71-80

Tekriwal P. & Mazumder J.
Three-Dimensional Finite Element Analysis of Multi-Pass GMA Welding
Proceedings: Modelling and Control of Casting and Welding Processes IV, ed. A.F. Giamei & G.J. Abbaschian, pub. The Minerals, Metals & Materials Society, 1988, pp167-176

Tekriwal P. & Mazumder J.
Finite Element Analysis of Three Dimensional Transient Heat Transfer in GMA Welding
Welding Journal, v67, n7, July 1988, pp150s-156s

Tekriwal P. & Mazumder J.
Transient and Residual Thermal Strain-Stress Analysis of Arc Welding Processes
Proceedings; Modelling of Casting, Welding and Advanced Solidification Processes V, ed. Rappaz M., Ozgu M.R. & Mahin K.W., pub. The Minerals, Metals & Materials Society, 1991, pp211-218

Tekriwal P. & Mazumder J.
Transient and Residual Thermal Strain-Stress Analysis of GMAW
Journal of Engineering Materials and Technology, Transactions of the ASME, v113, July 1991, pp336-343

Tsai C.L.
Using Computers for the Design of Welded Joints
Welding Journal, v70, n1, January 1991, pp47s-56s

Tsai C.L., Lee S.G. & Shim Y.L.
Modelling Techniques for Welding-Induced Residual Stress Predictions
Proceedings: Modelling and Control of Joining Processes, Orlando, December 1993, ed. T. Zacharia, pub American Welding Society, 1994, pp462-469

Tsai C.L., Cheng W.T. & Lee T.
Modelling Strategy for Control of Welding Induced Distortion
Modelling of Casting, Welding and Advanced Solidification Processes VII, pub Metals & Materials Society, 1995, pp335-345

Tsai M.C. & Kou S.
Maragoni Convection in Weld Pools with a Free Surface
International Journal for Numerical Methods in Fluids, v9, 1989, pp1503-1516

Tsai N.S. & Eagar
Distribution of the Heat and Current Fluxes in Gas Tungsten Arcs
Metallurgical Transactions B, v16B, December 1985, pp841-846

Tsao K.C. & Wu C.S.
Fluid Flow and Heat Transfer in GMA Weld Pools
Welding Journal, v67, n3, March 1988, pp70s-75s

Ueda Y., Murakawa H., Nakacho K. & Ma N.X.
Establishment of Computational Weld Mechanics
Trans. JWRI, v24, n2, February 1995, pp73-86

Venton P.
In Service Welding Valuation
Report To CRC for Materials Welding and Joining, Panel 7, 13 October 1997

Voller V.R.
Control of the Solidification and Melting of Metals
Modelling of Casting, Welding and Advanced Solidification Processes V, ed. M. Rappaz, M.R. Ozgu and K.W. Mahin, pub. The Minerals, Metals and Materials Society, 1991, pp515-522

Waszink J.H. & Van den Heuvel G.J.P.M.
Heat Generation and Heat Flow in the Filler Metal During GMA Welding
Welding Journal, v61, n8, August 1982, pp269s-282s

Watkins A.D., Smartt H.B. & Einerson C.J.
Heat Transfer in Gas Metal Arc Wleding
Proceedings; Recent Trends in Welding Science and Technology, May 1989, ed. S.A. David & J.M. Vitek, pub. ASM International, 1989, pp19-24

Watt D.F., Coon L., Bibby M.J., Goldak J.A. & Henwood C.
An Algorithm for Modeling Microstructural Development in Weld Heat Affected Zones (Part A) Reaction Kinetics
Acta Metallurgica, v36, n11, 1988, pp3029-3035

Weiss D., Schmidt J. & Franz U.
A Model of Temperature Distribution and Weld Pool Deformation During Arc Welding
Mathematical Modelling of Weld Phenomena 2, ed H.K. Bhadeshia, pub The Institute of Materials, 1995, pp22-39

Wells A.A.
Heat Flow in Welding
Welding Journal, v31, n5, May 1952, pp263s-267s

Westby O.
Temperature Distribution in the Workpiece by Welding
Department of Metallurgy and Metals Working, The Technical University, Trondheim Norway, 1968

Wilson H.A.
Procedures of Camberige Phillosophical Society, v12, 1904, pp406-423

Winters W.S. & Mahin K.W.
PASTA2D Modelling of an Axisymetric Stationary Gas Tungsten Arc Weld
Proceedings; Modelling of Casting, Welding and Advanced Solidification Processes V, ed. Rappaz M., Ozgu M.R. & Mahin K.W., pub. The Minerals, Metals & Materials Society, 1991, pp97-104

Zabaras N.
Inverse Finite Element Techniques For the Analysis of Solidification Processes
International Journal for Numerical Methods in Engineering v29, 1990, pp1569-1587

Zabaras N. & Kang S.
On the Solution of an Ill-Posed Design Solidification Problem Using Minimisation Techniques in Finite- and Infinite-Dimensional Function Spaces
International Journal for Numerical Methods in Engineering v36, 1993, pp3973-3990

Zabaras N. & Ruan Y.
A Deforming Finite Element Method Analysis of Inverse Stefan Problems
International Journal for Numerical Methods in Engineering v28, 1989, pp295-313

Zacharia T., David S.A., Vitek J.M. & DebRoy
Modelling the Effect of Surface Active Elements on Weld Pool Fluid Flow, Heat Transfer and Geometry
Proceedings; Recent Trends in Welding Science and Technology, May 1989, ed. S.A. David & J.M. Vitek, pub. ASM International, 1989, pp25-30

Zacharia T., David S.A. & Vitek J.M.
Effect of Evaporation and Temperature-Dependent Material Properties on Weld Pool Development
Metallurgical Transactions B, v22B, April 1991, pp233-241

Zacharia T., David S.A. & Vitek J.M.
Understanding Heat and Fluid Flow in Linear GTA Welds
Proceedings: International Trends in Welding Science and Technology, June 1992, ed. David, S.A & Vitek, J.M., pub. ASM International, 1993, pp27-31

Zacharia T., David S.A., Vitek J.M. & Kraus H.G.
Surface Temperature Distribution of GTA Weld Pools on Thin-Plate 304 Stainless Steel
Welding Journal, v74, n11, November 1995, pp353s-362s

Zacharia T., Eraslan A.H., Aidun D.K. & David S.A.
Three-Dimensional Transient Model for Arc Welding Process
Metallurgical Transactions B, v20B, October 1989, pp645-659

Zhu P. & Simpson S.W.
Theoretical Study of a Consumable Anode in a Gas Metal Welding Arc
Proceedings: Trends in Welding Research, June 1995, ed. H.B. Smartt, J.A. Johnson & S.A. David, pub ASM International, 1995, pp371-376

Zienkiewicz O.C.
The Finite Element Method
McGraw-Hill, New York, 1977